Title
Respiratory Mechanics and Gas Exchange: The Effect of Surfactants

Author
Jbaily, Abdulrahman

Publication Date
2017

Peer reviewed|Thesis/dissertation

Respiratory Mechanics and Gas Exchange: The Effect of Surfactants

by

Abdulrahman Jbaily

A dissertation submitted in partial satisfaction of the

requirements for the degree of

Doctor of Philosophy

in

Engineering - Mechanical Engineering

in the

Graduate Division

of the

University of California, Berkeley

Committee in charge:

Professor Andrew J. Szeri, Chair
Professor David Steigmann
Professor James Sethian

Fall 2017

Respiratory Mechanics and Gas Exchange: The Effect of Surfactants

Abstract

Respiratory Mechanics and Gas Exchange: The Effect of Surfactants

by

Abdulrahman Jbaily

Doctor of Philosophy in Engineering - Mechanical Engineering

University of California, Berkeley

Professor Andrew J. Szeri, Chair

The purpose of the lung is to exchange gases, primarily oxygen and carbon dioxide, between the atmosphere and the circulatory system. To enable this exchange, the airways in the lungs terminate in some 300 million alveoli that provide adequate surface area for transport. A common lung defect is the dysfunction of a complex mixture called pulmonary surfactant that is found in a thin layer of fluid coating the alveoli. This is a leading cause of respiratory distress syndrome (RDS), a well-known condition that affects premature infants and adults, and results in mortality rates ranging from 10% to 60% depending on patient age. The main goal of this work is to further the understanding of pulmonary surfactants to improve treatments and consequently decrease the high morbidity that accompanies RDS. To do so, we develop a mathematical model to study the action of pulmonary surfactant and its determinative contributions to breathing. The model is used to explore the influence of surfactants on alveolar mechanics, gas exchange and microscale work of breathing. Using the model, we can also examine the role that individual surfactant components such as phospholipids, proteins and cholesterol play during breathing. This provides insight into the design of exogenous pulmonary surfactants for clinical applications to treat RDS.

To my supportive parents Hwayda and Nazih, my beautiful, kind and caring wife Leila and my awesome siblings Hadi, Rawan and Mohamed.

Contents

List of Figures

List of Tables

Acknowledgments

I would like to first thank Professor Andrew Szeri for his constant patience and guidance. He was an excellent mentor that I would love to emulate one day. I would also like to thank Professors David Steigmann and James Sethian for reviewing my thesis and for their useful feedback. A big Thank You goes to my wife Leila Kamareddine for always being there for me and for motivating me during the tough times. I want to also thank all my friends here at Berkeley for their great friendship and support over the past five years and a half. Special thanks go to my parents Hwayda and Nazih for their constant belief in me. Nothing would be possible without their unconditional love.

Nomenclature

$\overline{\gamma_N}$	Mass fraction of nitrogen at the alveolus opening $[I]$
$[H^+]$	Concentration of hydrogen ions in blood $[ML^{-3}]$
$\alpha(t)$	Equilibration length ratio of oxygen in the capillaries $[I]$
$\beta(t)$	Equilibration length ratio of carbon dioxide in the capillaries $[I]$
ϵ	Parameter in the definition of carbon dioxide full equilibration $[I]$
$\Gamma(t)$	Surfactant surface excess concentration $[ML^{-2}]$
$\gamma_C(t)$	Mass fraction of carbon dioxide in the alveolus $[I]$
$\gamma_N(t)$	Mass fraction of nitrogen in the alveolus $[I]$
$\gamma_O(t)$	Mass fraction of oxygen in the alveolus $[I]$
Γ_{max}	Maximum surfactant surface excess concentration in a dynamic system $[ML^{-2}]$
$\hat{V_0}$	Initial volume of the hypophase $[L^3]$
κ	Percentage of the alveolar wall area covered with capillaries$[I]$
$\mathcal{H}_e(t)$	Hemoglobin model evaluated at the exit of the capillaries $[ML^{-3}]$
$\mathcal{H}_i(t)$	Hemoglobin model evaluated at the inlet of the capillaries $[ML^{-3}]$
μ_h	Dynamic viscosity of the hypophase $[ML^{-1}T{-}1]$
Ω	Effective resistance of the airway tract leading to the alveolus $[MT^{-1}L^{-4}]$
$\overline{\gamma_C}$	Mass fraction of carbon dioxide at the alveolus opening $[I]$
$\overline{\gamma_O}$	Mass fraction of oxygen at the alveolus opening $[I]$
$\overline{\Gamma}$	Maximum equilibrium surfactant surface excess concentration in static conditions $[ML^{-2}]$

$\overline{\sigma}$ Surface tension evaluated at $\overline{\Gamma}$ $[MT^{-2}]$

$\overline{P}_A$ Absolute pressure of the gas mixture in the alveolus (alveolar pressure) $[ML^{-1}T^{-2}]$

$\overline{P}_h(t)$ Absolute pressure in the hypophase $[ML^{-1}T^{-2}]$

$\overline{P}_{pl}(t)$ Absolute pressure in the pleural cavity $[ML^{-1}T^{-2}]$

$\Psi_C(t)$ Interfacial resistance of surfactants to carbon dioxide $[TL^{-1}]$

$\Psi_O(t)$ Interfacial resistance of surfactants to oxygen $[TL^{-1}]$

ρ_0 Base state of the gas mixture density in the alveolus $[ML^{-3}]$

$\rho_G(t)$ Density of the gas mixture in the alveolus $[ML^{-3}]$

$\Sigma(t)$ Hoop stress in the alveolar wall $[ML^{-1}T^{-2}]$

$\sigma(t)$ Surface tension on the interface of the hypophase $[MT^{-2}]$

σ_{min} Surface tension evaluated at Γ_{max} $[MT^{-2}]$

τ Transit time of blood in the exchange zone $[T]$

$\tilde{C}_e(t)$ Concentration of bicarbonate at the exit of the capillaries $[ML^{-3}]$

$\tilde{C}_i$ Concentration of bicarbonate at the inlet of the capillaries $[ML^{-3}]$

ξ_C Solubility of carbon dioxide in the respiratory membrane $[T^2L^{-2}]$

ξ_O Solubility of oxygen in the respiratory membrane $[T^2L^{-2}]$

ζ Fraction of the alveolar wall between the bottom of the hypophase and the perfused capillaries $[I]$

$A(t)$ Surface area of the alveolar wall $[L^2]$

A^c Capillary area involved in gas diffusion L^2

$C_s(r,t)$ Bulk surfactant concentration $[ML^{-3}]$

C_{HB} Concentration of hemoglobin in the capillary blood volume $[ML^{-3}]$

D_s Diffusion coefficient of surfactants in the hypophase $[L^2T^{-1}]$

D_{hC} Diffusion coefficient of carbon dioxide in the hypophase $[L^2T^{-1}]$

D_{hO} Diffusion coefficient of oxygen in the hypophase $[L^2T^{-1}]$

D_{wC} Diffusion coefficient of carbon dioxide in the alveolar wall $[L^2T^{-1}]$

D_{wO} Diffusion coefficient of oxygen in the alveolar wall $[L^2T^{-1}]$

$e(t)$ Thickness of the alveolar wall $[L]$

e_0 $e(t)$ evaluated at $t = t_0$ $[L]$

$H(t)$ Heaviside step function $[I]$

$h(t)$ Thickness of the hypophase $[L]$

h_0 $h(t)$ evaluated at $t = t_0$ $[L]$

K_1 Rate of the chemical reaction that transforms carbon dioxide to bicarbonate $[T^{-1}]$

k_a Adsorption coefficient of surfactants $[L^3M^{-1}T^{-1}]$

k_d Desorption coefficient of surfactants $[T^{-1}]$

K_{-1} Rate of the chemical reaction that transforms bicarbonate to carbon dioxide $[M^{-1}T^{-1}L^3]$

L_c Length of a capillary $[L]$

m Factor in the hemoglobin model $\mathcal{H}(t)$ $[I]$

M_C Molar mass of carbon dioxide $[Mmol^{-1}]$

$M_G(t)$ Molar mass of the gas mixture $[Mmol^{-1}]$

M_O Molar mass of oxygen $[Mmol^{-1}]$

n Number of capillaries in the exchange zone $[I]$

$P_A(t)$ Gauge pressure of the gas mixture in the alveolus (alveolar gauge pressure) $[ML^{-1}T^{-2}]$

$P_C(t)$ Carbon dioxide partial pressure in the alveolus $[ML^{-1}T^{-2}]$

$P_h(t)$ Gauge pressure in the hypophase $[ML^{-1}T^{-2}]$

$P_O(t)$ Oxygen partial pressure in the alveolus $[ML^{-1}T^{-2}]$

P_V Vapor pressure in human lungs $[ML^{-1}T^{-2}]$

$P_{\frac{1}{2}bO}$ Oxygen partial pressure that corresponds to half full hemoglobin saturation $[ML^{-1}T^{-2}]$

P_{atm} Atmospheric pressure $[ML^{-1}T^{-2}]$

$P_{bCe}(t)$ Carbon dioxide partial pressure at the exit of the capillaries $[ML^{-1}T^{-2}]$

P_{bCi} Carbon dioxide partial pressure at the inlet of the capillaries $[ML^{-1}T^{-2}]$

$P_{bC}(s,t)$ Carbon dioxide partial pressure in the capillaries $[ML^{-1}T^{-2}]$

$P^*_{bC}(t)$ Homogenized carbon dioxide partial pressure in the capillaries $[ML^{-1}T^{-2}]$

$P_{bOe}(t)$ Oxygen partial pressure at the exit of the capillaries $[ML^{-1}T^{-2}]$

P_{bOi} Oxygen partial pressure at the inlet of the capillaries $[ML^{-1}T^{-2}]$

$P_{bO}(s,t)$ Oxygen partial pressure in the capillaries $[ML^{-1}T^{-2}]$

$P^*_{bO}(t)$ Homogenized oxygen partial pressure in the capillaries $[ML^{-1}T^{-2}]$

$P_{pl}(t)$ Gauge pressure in the pleural cavity $[ML^{-1}T^{-2}]$

$q(t)$ Volumetric flux of the gas mixture through the alveolar opening $[L^3T^{-1}]$

$Q''_C(s,t)$ Specific mass flux of carbon dioxide between alveolus and blood $[ML^{-2}T^{-1}]$

$Q_C(t)$ Mass flux of carbon dioxide between alveolus and blood $[MT^{-1}]$

$Q''_O(s,t)$ Specific mass flux of oxygen between alveolus and blood $[ML^{-2}T^{-1}]$

$Q_O(t)$ Mass flux of oxygen between alveolus and blood $[MT^{-1}]$

$q_{inh}(t)$ Volumetric flux of the gas mixture inhaled through the alveolar opening $[L^3T^{-1}]$

$R(t)$ Radius of the alveolus $[L]$

R_0 $R(t)$ evaluated at $t = t_0$ $[L]$

s Arclength along capillary in the direction of blood flow

$V(t)$ Volume of the gas mixture in the alveolus $[L^3]$

$v_r(r,t)$ Radial component of the fluid velocity in the hypophase $[LT^{-1}]$

V_{bc} Capillary blood volume in the exchange zone $[L^3]$

Y Parameter in the constitutive model of $\sigma(t)$ $[MT^{-2}]$

Chapter 1

Introduction

The human body is composed of eleven major organ systems. Each organ system comprises a group of organs that work together for a certain bodily function [1]. While the digestive system is responsible for breaking food into the building blocks for the body, the endocrine system secretes hormones to regulate the growth and metabolism of the body. To a great extent, health depends on the well being of each bodily system, but also relies on the efficient and harmonious interaction between systems; for example, both muscular and skeletal systems are needed for body movement. For such reasons, the human body has long been compared to a complex machine that needs to be fueled in order to ensure efficient functioning of its different parts, the body systems. Food, water, and oxygen are the main constituents of the body's fuel and need to be supplied on a regular basis. Studies have shown that an average person can live for a few weeks without food, few days without water but only around three minutes without oxygen [2]. The absence of oxygen causes the death of brain cells. The body ensures that oxygen reaches all living cells by the combined work of the respiratory and cardiovascular systems. Like every other system, the respiratory system is complex and prone to diseases and malfunctions. However, because the respiratory system is responsible for the supply of oxygen to the body through breathing, any respiratory defect or failure can be life-threatening.

A common lung defect is the dysfunction of a complex mixture mainly composed of phospholipids and proteins, called pulmonary surfactant. Surfactant dysfunction causes respiratory distress syndrome (RDS), which is a well-known condition that affects premature infants and also adults [3]. The mortality rates from acute respiratory distress syndrome (ARDS) range from 24% to 60% depending on patient age, and are estimated to result in some 3.6 million hospital days per year in the United States [4]. Neonatal Respiratory Distress Syndrome (NRDS) occurs in 60-80% of infants with less than 28 weeks of gestational age, and 15-30% of those born in weeks 32-36 [5]. Mortality of infants with NRDS is about 10%, but can reach 25% as a consequence of extended time on a mechanical ventilator [5].

The main goal of this dissertation is to further the understanding of pulmonary surfac-

tants; this can help better treatments to improve the unacceptable morbidity and mortality that accompanies RDS. To do so, we develop a mechanical model that allows the investigation of how multiple properties of pulmonary surfactants affect breathing. Gas exchange between the respiratory and cardiovascular systems, and the work of breathing are of particular importance in this dissertation.

In this chapter, we start with a very brief overview of the different functions and parts of the respiratory system to familiarize the reader with the breathing process that will be studied in this dissertation; special attention is given to pulmonary surfactants. A comprehensive literature review of the relevant works on pulmonary surfactants is then presented, followed by the detailed goal of this thesis.

1.1 The Respiratory System

The primary function of the respiratory system is to deliver oxygen to the body tissues and to remove carbon dioxide from the body. This consists of three processes: pulmonary ventilation, external respiration, and internal respiration. Pulmonary ventilation, also known as breathing, is the movement of air into (inhalation) and out of (exhalation) the human body. External respiration is the process by which oxygen and carbon dioxide are exchanged between the lungs and the surrounding bloodstream, and internal respiration is the process by which the bloodstream delivers oxygen to the body cells and removes waste carbon dioxide [6]. External and internal respiration are performed by both the respiratory and cardiovascular systems. Other functions of the respiratory system include filtering and humidifying the air that is entering the human body, and helping to maintain homeostasis. The respiratory system is also fundamental to speech, where moving air vibrates the vocal cords, and in olfaction, which begins with air coming into contact with olfactory fibers lining the nasal cavities [7]. Pulmonary ventilation and external respiration are the main focus of this study and both are explored in greater detail throughout this dissertation.

The respiratory system is composed of two divisions, the upper and lower respiratory tracts. The upper tract consists of the respiratory organs that lie outside of the chest cavity such as the nose, paranasal cavity, part of the oral cavity (or mouth), and the pharynx [8]. The main components of the lower respiratory tract are the trachea, lungs and respiratory muscles. The transition between the two divisions happens at the top of the larynx, where the respiratory and digestive systems cross paths [8]. The nose and oral cavity are the main and secondary external openings of the respiratory system respectively. The nose is made of bone, cartilage, muscle and skin, and supports and protects the paranasal cavity, a hollow space within it that is lined with hairs and a mucus membrane. This cavity warms and moisturizes the air entering the body, and helps in trapping contaminants such as dust before they reach the inside [8]. The oral cavity is essential for the digestive system but can also supplement the nose and nasal cavity by drawing air inside the human body. The pharynx

is a muscular tube that allows air to move from the nose and mouth to the larynx, which is a short section of the airway leading to the trachea. The larynx is also known as the voice box because of its role in human speech [8].

The first organ of the lower respiratory tract is the trachea, which is a tube approximately 12 cm in length and 1.8 cm in diameter for an adult human [9]. It is made of hyaline cartilage rings lined with pseudo-stratified ciliated columnar epithelium. The cartilaginous rings support the trachea and prevent it from collapsing or expanding, which provides a clear airway for air to enter and exit the lung. The inner epithelium of the trachea prevents contaminants from entering the lungs by trapping them in mucus. The cilia lining then moves the mucus towards the pharynx to clear it out [10]. The trachea extends from the larynx until it branches into the two primary bronchi that extend into the lungs. These branches split into secondary and tertiary bronchi and into smaller bronchioles that spread into the lungs. The bronchioles finally split into branches that are less than one millimeter in diameter and are called terminal bronchioles [7]. The smooth muscle tissues on the walls of the bronchi and bronchioles help regulate the airflow into the lungs. For example, the smooth muscles relax during exercise in order to dilate the bronchi and bronchioles and allow greater ventilation [7].

The lungs are the main components of the respiratory system. They are large and spongy organs that fill up the thoracic (or chest) cavity and make up most of the lower respiratory tract. This cavity, in which the lungs are located, is enclosed by the rib cage on all sides except the bottom, where the diaphragm is found. The diaphragm is dome-shaped and consists of a peripheral muscle and a central tendon [11]. It is considered as the main muscle for respiration. Additional respiratory muscles known as the external and internal intercostal muscles are located between the ribs. The external intercostal muscles are used during inhalation, where their contraction elevates and spreads the ribs. On the other hand, the internal ones are used during exhalation, where their contraction lowers the ribs and pushes them closer to each other [10] . In addition to their role in breathing, the intercostal muscles help protect the lungs [8].

Humans have two lungs with different sizes that are mainly responsible for gas exchange. The right lung is the larger one and is composed of three lobes, while the left lung has only two lobes in order to accommodate the heart [8]. The anatomy of the lung is complex and beyond the scope of this chapter; for an excellent review of structural design and physiology of the mammalian and human lung, and the structural determinants of gas exchange, the reader is refered to [9]. Here, we will touch on the main components of the human lungs that are needed to understand the rest of this dissertation, namely, the pleura and the alveoli. The lungs are surrounded by double layered serous membranes called the pleura. The visceral pleura covers the outer surface of the human lung, while the parietal pleura is attached to the thoracic wall. The cavity between the visceral and parietal pleura is called the pleural cavity and is lubricated by a serous fluid [8]. The gauge pressure in this cavity is always negative to prevent the lungs from collapsing and the chest from expanding. Alveoli are microscopic

balloon-like sacs that are found in the form of small clusters at the end of terminal bronchioles in human lungs with a mean diameter of 200 μm, and their number ranges between 274 and 790 million in adult human lungs [12]. The respiratory and cardiovascular systems exchange gases directly through the respiratory membrane, where the thin walls of the alveoli and surrounding capillaries touch. The alveolar wall is made of three different types of cells: type I and type II alveolar epithelial cells, and pulmonary macrophages [13]. Macrophage is a mobile scavenger that serves to keep the lungs free of dust, bacteria, and blood cells from injuries. Type I epithelial cells, also known as membranous pneumocytes, form the structure of the alveolar wall, while type II epithelial cells, or granular pneumocytes, are responsible for the synthesis and secretion of a surface active lipo-protein complex known as pulmonary surfactant [14], which is explored next and extensively studied in later parts of this dissertation.

1.2 Pulmonary Surfactant

The inner face of an alveolus is coated by a layer of fluid, referred to as the hypophase, that is in direct contact with the air filling the lungs. When two different fluids such as liquid and gas are in contact with each other, a thin region known as interface separates them. Whereas molecules suspended in the liquid bulk interact with the liquid molecules surrounding them, those molecules on the interface interact differently with the gas molecules above them. This imbalance results in an additional surface energy per unit area of interface, which is referred to as surface tension [15]. The additional surface energy arising on the alveolar air-liquid interface acts to collapse the alveolus on itself, which decreases lung compliance. This implies that additional breathing work is necessary in order to counteract the recoil forces arising due to surface tension. Furthermore, high surface tension can lead to alveolar collapse, which decreases the total lung area available for gas exchange. The avoidance of such undesired effects is attributed to pulmonary surfactants [16, 17].

In general, surfactants or surface-active agents are molecules that are attracted to interfaces separating aqueous and non-aqueous phases. They possess a bipolar structure composed of a hydrophilic head and a hydrophobic tail. Two main effects are associated with the presence of surfactants at an air-fluid interface: the reduction of surface tension and the formation of a barrier to mass transport [18]. Specifically, pulmonary surfactant is a complex mixture of phospholipids (70-80%), proteins (10%) and neutral lipids (10%, mainly cholesterol) [14]. Four types of proteins exist, two of which are hydrophilic, apoproteins SP-A and SP-D, and the other two are hydrophobic, apoproteins SP-B and SP-C. The main component of the phospholipid portion is Dipalmitoyl Phosphotidylcholine (DPPC), which is able to achieve near-zero surface tension during compression but respreads poorly when the film expands during inhalation [19]. Hence, the phospholipid portion alone cannot serve as a practical lung surfactant [20]. Multiple studies have shown the importance of the surfactant apoproteins in improving the functionality of pulmonary surfactants [20, 21]. In fact,

this will be explored in section 5.5. Pulmonary surfactants adsorb to the air-liquid interface inside the alveolus causing the surface tension to decrease significantly. For example, the surface tension of water at body temperature (37^o) is around 70 dyn/cm and falls to an equilibrium value of about 25 dyn/cm inside the lungs because of the presence of surfactants [22]. Furthermore, surface tension can be reduced to near 0 dyn/cm values during exhalation when the pulmonary surfactant film compresses [23].

A review of the research works on pulmonary surfactants that are relevant to this dissertation is presented next.

1.3 Literature Review

We first refer to [24] for a short history on the discovery of pulmonary surfactants. In 1929, Von Neergard was the first to postulate the existence of surfactants in the human lungs. He performed experimental studies where he found a big difference in the recoil forces of a fluid-filled lung and an air-filled lung with a fluid lining [25]. He realized that this difference is a result of surface tension. It was not until nearly 25 years later that Radford performed more experiments on liquid and air filled lungs, where he was using detergents to manipulate the existing surface tension [26, 27]. Subsequently, Mead stressed the dependence of the lung compliance during breathing on the surface forces in the lungs [28, 29]. About the same time, research studies were performed by Pattle where he used lung tissue to stabilize microscopic suspensions in water [30]. Later, Clements directly demonstrated the surface tension lowering properties of lung extracts by performing experiments using the Langmuir-Wilhelmy surface balance [31–33]. Following that discovery, Brown identified DPPC as the main surfactant component in lungs [34]. At that time, most of the physiological research on lung surfactant and surface forces in the lungs was motivated by the belief that surfactants lower the work of breathing and increase pulmonary compliance. Extensive research in this area was later performed when a correlation between surfactants and diseases in lungs of newborns was pointed out by Avery and Mead [35]. Examples of research works that aimed at understanding the properties of surfactants further in order to improve clinical applications such as surfactant replacement therapies can be found in [36–39]. Controversy still remains about the best type of surfactant to be used, and when and what is the best mode of delivery [40].

Despite the early realization that premature infants in respiratory distress were lacking lung surfactants, and despite the successful development of natural and even some synthetic lung surfactant replacements [41], there remains a significant shortfall in understanding this complex system. Almost sixty years of surfactant research have passed, and the learning curve is still steep. It is important to note that the research efforts to date that we review can be categorized as follows. There is an enormous amount of research into the detailed composition of pulmonary surfactants. There has been some research into fluid mechanics

aspects of the lung, primarily focused on air flow in branched generations of tubes, surface tension driven flows of the hypophase and mucous layers, and reinflation of collapsed airways. There has been very limited research into interfacial resistance to gas transfer as it is related to changing surfactant concentration over the breathing cycle. There has been considerable research on the established concept of Work of Breathing (WoB), applied to the whole lung.

1.3.1 Physiology of Pulmonary Surfactant

Numerous research works are aimed at understanding the physical structure of pulmonary surfactants at various stages of film compression, such as one might find over the breathing cycle, in addition to research into surfactant origin and recycling within the body [42–45]. These studies elucidated many details about pulmonary surfactants such as their precise composition, source of synthesis, secretion, metabolism and degradation. However, multiple characteristics of pulmonary surfactants are yet to be understood [46], such as the details behind the rapid adsorption of selected surfactant components to an air-water interface [47]. Several reviews [22, 48, 49] examined the role of individual surfactant proteins in aiding adsorption and repopulation of the surface upon reinflation, and their biochemistry and biophysics. Distinguishing the different steps in surfactant adsorption was also investigated [50]. Other studies on surfactants have covered their role in health and disease [14, 51], in innate lung defense [52–55], and interestingly their role in the evolution of breathing [56]. Very recently, Baoukina and Tieleman [57] reviewed molecular dynamics simulations of lung surfactant, including relationships between a monolayer and underlying bilayer and coexistence of phases in condensed films.

1.3.2 Fluid Mechanics Aspects

Grotberg [58–60] provided useful reviews of biofluid dynamics in the lung. The dynamic surface tension on the expanding and contracting hypophase has received considerable attention, primarily due to its interesting hysteresis and the possibility of condensed phases near minimum volume. Putz et al. [61, 62] for example explored measurements of dynamic surface tension with different experimental systems; see also [63]. Kamm and coworkers [64] conducted dynamic surface tension measurements with changing area in a pulsating bubble surfactometer (PBS), and developed a model of squeeze-out of some components of the surfactant film; see also [65, 66]. A more recent mathematical model of adsorption, desorption, compression and multi-layer formation was developed by Krueger and Gaver [67].

Multiple studies have considered the flow of surfactant monolayers in various cases. Wei et al. [68, 69] considered hypophase flows driven by nonuniform surfactant coverage. Borgas et al. studied the two-dimensional flow of a surface-active monolayer on a thin viscous film in order to understand the spreading mechanism of surfactants on fluid layers [70]. A model was also developed to explore the effect of surface tension gradients on the generation of

clearance flows from the lungs towards the mouth. The simple case of a membrane with linear variation in strain along its length to model breathing was considered [71]. More recently, Levy et al. added the effect of gravity on surfactant spreading, which was absent in most previous studies. They investigated wave solutions of a lubrication model for surfactant-driven flow of a thin liquid film down an inclined plane [72]. Other studies investigated the effect of the hypophase thickness on surfactant transport and surfactant collapse [73], and the effect of rheological properties of mucus on surfactant spreading behavior [74].

Another area that was carefully explored is the propagation of surfactants towards the lungs after their injection in clinical applications. Suresh et al. studied theoretically the effect of plug propagation speed and gravity on the motion of a liquid plug in a two dimensional channel at an angle with respect to gravity. They obtained expressions for the thickness of the trailing films left behind the plug [75]. Zheng et al. studied experimentally the effect of gravity on liquid plug transport through an airway bifurcation model [76]. Espinosa et al. identified critical parameters of surfactant instillation and their influence on the initial deposition of a surfactant bolus. They also determined conditions under which a meniscus forms in the trachea during bolus injection [77]. The role that pulmonary surfactants play in airway closure was also studied. Among these studies, there is a numerical one done by Otis et al. who developed a model for airway closure by liquid bridging during expiration [78]. In addition, Halpern et al. developed a model to predict the closure of small airways in the region of terminal bronchioles [79].

1.3.3 Gas Exchange

Gas transport across the hypophase has also received some attention, although experimental limitations have made this challenging. Zuo et al. [80] developed the axisymmetric drop shape analysis-captive bubble sufactometer (ADSA-CBS) technique to study a captive bubble surrounded by liquid, with a lung surfactant film in a quasi-static experiment. They examined the mean rate of gas transfer and also surface tension as a function of surfactant characteristics. See also Zuo et al. [81], where they found that the mass transfer coefficient of oxygen decreases by about 30-50% in bovine surfactant suspensions with respect to water. They concluded that at low surface tension value ($\approx$ 2 mJ/m^2), lung surfactant films provide resistance to oxygen transfer. They also found that at a surface tension higher than 6 mJ/m^2, resistance to oxygen transfer was modest. Moller et al. [82] examined the barrier to oxygen transport across condensed phospholipid films, like DPPC, which has very low permeability. Their findings led them to compare the pulmonary surfactant to a valve that allows gas exchange in its expanded state, and restricts it when it is compressed and closely packed. In addition, Aberg et al. [83] considered how multilayer structural details could imply expedited transit of O_2 molecules.

1.3.4 Work of Breathing

Nearly 60 years ago, Campbell [84] developed the concept of the work of breathing (WoB) applied to the whole lung, which is a crucial organizing idea in lung mechanics, and is often used to explain the purpose of lung surfactant, or to motivate surfactant replacement therapy or mechanical ventilation. Among many others, McFadyen et al. [85] considered the components of the WoB for the whole lung, which is increased by a decrease in compliance or an increase in flow resistance. Chowdhury et al. [86] also examined components of the WoB, separating that associated with compliance and that associated with flow resistance, and explored how partial assist ventilation can be used to affect the WoB. Finally, Tulaimat et al. [87] discussed the difficulty in measuring WoB at the patient's bedside, and assessed the ways that elevated WoB can be estimated from other signs.

It is worth emphasizing that all these studies consider the WoB for the whole lung. Anderson et al. argued that exchange of sparingly soluble gases including oxygen and carbon dioxide occurs in alveoli, while other gases such as certain anesthetic components exchange in airways [88]. Because we are mainly interested in the exchange of oxygen and carbon dioxide, our special focus in this dissertation is on the alveolus as will be seen in the next section. Hence, when addressing work of breathing, we refer to it as the microscale work of breathing, or the breathing work at the level of the alveolus. The goal of the dissertation is presented next.

1.4 Dissertation Goal

The research literature has contributed enormously to the improvement of clinical applications by offering much insight on the importance of pulmonary surfactant to breathing. However, to the author's best knowledge, one key aspect is still missing from the literature: a basic connection between the microscale work of breathing and the rate of gas transfer at the alveolar level, where both are enormously influenced by the surfactant dynamics, has never been established.

Experimentally, researchers have been prevented from developing such connection due to limitations in the range of experimental approaches available. In vivo for example, it is not possible to isolate a single alveolus and consider gas exchange to its capillary bed as mediated by the presence of this or that lung surfactant; the system is simply too complicated and interconnected to isolate and control. Furthermore, experimental systems such as the Langmuir trough and Wilhelmy plate [80], suffer from several shortcomings that prevent their use in understanding pulmonary surfactant as it exists in the lung. Among these shortcomings are leaks of surfactant from the air/water interface to the supporting solid trough material, significant limits in the rate at which films can be expanded and contracted without causing

waves and, of course, the lack of curvature at the surfactant interface.

In addition, previously developed mathematical or numerical models have lacked the ability to investigate the response of an alveolus to a changing pleural pressure that drives breathing, when coated by a specific surfactant. Such a model is necessary to asses the effect of surfactants on gas transfer and microscale breathing work, and will be the subject of this dissertation. We develop a mathematical model of the alveolus that is composed of multiple compartments, mainly:

- Gas mixture of oxygen, carbon dioxide and nitrogen in the alveolus
- Surfactant system in a thin fluid layer coating the inner surface of the alveolus (hypophase)
- Alveolar wall where capillaries are perfused
- Capillary bed that exchanges oxygen and carbon dioxide with the alveolar gas mixture
- Pleural cavity where a change in pressure drives breathing

As will be seen throughout this document, this model provides the ability to study multiple aspects of breathing. In relation to surfactants, it allows one to investigate the effect of surfactant characteristics, such as adsorption and diffusion properties, on alveolar mechanics and gas exchange. The effect of interfacial resistance to gas transfer, which changes over the cycle of breathing due to surfactant concentration changes, can also be studied. More importantly, this model can also be used to examine the role that individual surfactant components such as phospholipids, and proteins play during breathing. This sheds light on the importance of every component when preparing exogenous surfactants for clinical applications to treat ARDS. Different commercially available surfactants can also be compared using the model. In addition, because alveolar mechanics are described in this model, the microscale work of breathing can be computed when comparing different surfactants. A brief outline of the dissertation follows.

Before describing the alveolar model, we first focus on the surfactant transport problem in a thin layer of fluid. This is done in chapter 2, where surfactant properties and dynamics are explained for multiple cases that span but are not limited to surfactant diffusion in a constrained static domain and surfactant transport in convective flows. The surfactant model adopted from [66] and that will be used when modeling pulmonary surfactant transport in this dissertation is then explained. In chapter 3, we introduce the alveolar model and cover the modeling of the alveolar gas mixture, the surfactant transport problem, and the alveolar wall. Important relations between the different pressures existing in the system are also presented. In chapter 4, we present the methods used to model oxygen and carbon dioxide exchange between the alveolus and the capillary bed. Oxygen and carbon dioxide transport in the capillaries is also covered. The results of the model are then presented in chapter 5.

A base case is first presented that explains how the different variables of the model behave, followed by studying different breathing aspects such as the effect of holding breath. The remainder of chapter 5 is devoted to studying the effect of surfactants on breathing. Finally, concluding remarks and future work are presented in chapter 6.

Chapter 2

Dynamics of the Hypophase Coating a Flat Sheet

In this chapter, we present short case studies to clarify the dynamics of surfactants in the hypophase coating the inner surface of alveoli. Understanding surfactant behavior is important when developing the alveolar model in chapter 3. Cases presented here include and are not limited to surfactant diffusion in a constrained static domain, and surfactant adsorption and desorption in a deforming fluid domain, etc.

Studies have shown that the thickness of the hypophase is much smaller than the alveolar radius of curvature. The thickness of this layer varies among alveoli, but is in the range of 0.1 to 0.5μm for many portions of the alveolar network [89]. The mean diameter of the alveolus on the other hand is 200μm [12]. This affords the chance to model the system as a flat sheet with a thin layer of fluid resting on it as shown in figure 2.1 when analyzing the physics of the layer. Furthermore, the lubrication approximation is applied to simplify the Navier Stokes equations of an incompressible Newtonian fluid. In the alveolar model however presented in chapter 3, we revert back to a spherical configuration.

First, general expressions for the velocity and thickness profiles of a thin fluid layer resting on a deforming elastic sheet are derived. These expressions are then used in different surfactant transport boundary value problems (BVP). We exploit these BVPs to introduce relevant definitions and mechanisms that are essential to analyze the effect of surfactants on breathing. We also present a Langrangian formulation of the surfactant transport problem that leads to a more accurate computational method in the case of advection-dominated flow. At the end of the chapter, we introduce the pulmonary surfactant model that will be used in the remainder of the dissertation. It is worth mentioning that in this chapter, any deformation of the fluid layer is caused by forced or prescribed motion. In the case of breathing however, free motion of the lung boundary occurs, and is dependent on the existing pressures in the lungs and the surface tension forces that are controlled by surfactant dynamics.

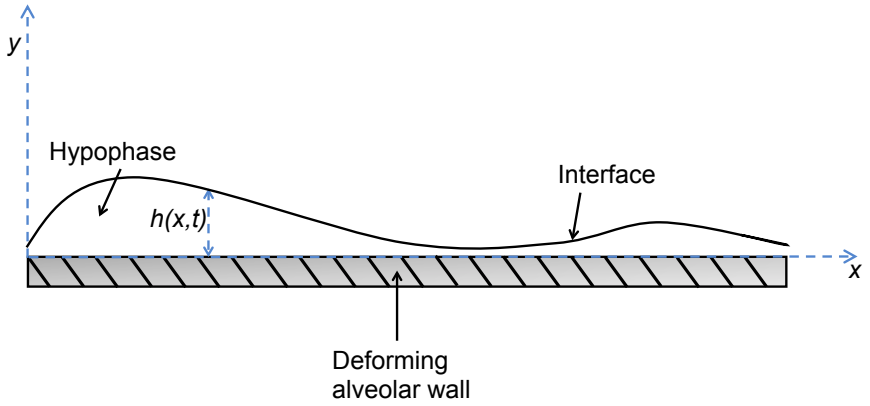

Figure 2.1: Thin Layer Flow Schematic

2.1 Boundary Value Problem

In this section, the general boundary value problem for the model shown in figure 2.1 is formulated, and the expressions for the velocity and thickness profiles are derived.

2.1.1 Governing Equations and Boundary Conditions

The lubrication equations for a two dimensional flow [90], with gravity taken to be $\boldsymbol{g} = g_y \boldsymbol{j}$, are given by:

$$\frac{\partial u}{\partial x} + \frac{\partial v}{\partial y} = 0, \tag{2.1}$$

$$\begin{aligned} -\frac{1}{\rho}\frac{\partial p}{\partial x} + \nu \frac{\partial^2 u}{\partial y^2} &= 0, & (2.2a)\\ -\frac{1}{\rho}\frac{\partial p}{\partial y} + g_y &= 0, & (2.2b) \end{aligned}$$

where u and v are the velocity components of the fluid in the x and y directions respectively, ν is the kinematic velocity of the fluid, ρ is the fluid density, and p is the pressure in the fluid.

At the hypophase bottom ($y = 0$), the no slip and no penetration conditions are imposed. At the hypophase interface ($y = h(x,t)$), the surface is assumed to be material, and surface tension gradients exist as might be the case when surfactants populate the surface non-uniformly. These conditions can be stated mathematically as:
At $y = 0$:

$$\begin{aligned} u(x,0,t) &= U(x,t), & (2.3a)\\ v(x,0,t) &= 0, & (2.3b) \end{aligned}$$

where $U(x,t)$ is the velocity field of the deforming alveolar wall. At $y = h(x,t)$:

$$v(x,h(x,t),t) = \frac{\partial h(x,t)}{\partial t} + u(x,h(x,t),t)\frac{\partial h(x,t)}{\partial x}, \tag{2.4a}$$

$$\mu \frac{\partial u(x,y,t)}{\partial y}\Big|_{y=h(x,t)} = \frac{d\sigma(x,t)}{dx}, \tag{2.4b}$$

$$p(x,h(x,t),t) - P_{atm} = -\sigma(x,t)\frac{\partial^2 h(x,t)}{\partial x^2}. \tag{2.4c}$$

Equation (2.4a) equates the normal velocity of the fluid particles to that of the interface. Equation (2.4b) is the balance of tangential stresses at the interface, and equation (2.4c) is the balance of normal stresses, where a small slope approximation was taken.

2.1.2 Velocity and Thickness Profiles

Solving the governing equations (2.2a) and (2.2b), and applying boundary conditions (2.3a), (2.4b), and (2.4c), the pressure and velocity profiles are respectively expressed as:

$$p(x,y,t) - P_{atm} = \rho g_y (y-h) - \sigma \frac{\partial^2 h}{\partial x^2}, \tag{2.5}$$

$$u(x,y,t) = -(\frac{1}{\mu}\frac{\partial p}{\partial x})(yh(x,t) - \frac{y^2}{2}) + \frac{1}{\mu}\frac{d\sigma(x,t)}{dx}y + U(x,t). \tag{2.6}$$

The hypophase thickness profile can be derived by integrating the continuity equation (2.1) and applying boundary conditions (2.3b), (2.4a):

$$\int_0^{h(x,t)} (\frac{\partial u}{\partial x} + \frac{\partial v}{\partial y})dy = 0,$$

$$\int_0^{h(x,t)} \frac{\partial u}{\partial x}dy + v(h(x,t),t) - \cancelto{0}{v(0,t)}^{(No\ penetration)} = 0,$$

$$\frac{\partial h}{\partial t} + u\frac{\partial h}{\partial x} + \int_0^{h(x,t)} \frac{\partial u}{\partial x}dy = 0.$$

Now, using Leibniz's rule[1], the integral form of the mass conservation equation is obtained:

$$\frac{\partial h}{\partial t} + \frac{\partial}{\partial x}\int_0^{h(x,t)} u(x,y,t)dy = 0. \tag{2.7}$$

Finally, the equation for the thickness profile is obtained by substituting (2.6) into equation (2.7):

$$\frac{\partial h}{\partial t} + \frac{1}{\mu}\frac{\partial}{\partial x}\Big[\frac{h^3}{3}\Big(\sigma\frac{\partial^3 h}{\partial x^3} + \frac{d\sigma}{dx}\frac{\partial^2 h}{\partial x^2} + \rho g_y \frac{\partial h}{\partial x}\Big) + \frac{h^2}{2}\frac{d\sigma}{dx} + \mu U h\Big] = 0. \tag{2.8}$$

[1] **Leibniz's Formula:** $\frac{\partial}{\partial x}\int_{a(x)}^{b(x)} f(x,t)dt = f(x,b(x))\cdot\frac{\partial}{\partial x}b(x) - f(x,a(x))\cdot\frac{\partial}{\partial x}a(x) + \int_{a(x)}^{b(x)}\frac{\partial}{\partial x}f(x,t)dt$

2.1.3 Test Cases

Equation (2.8) is tested for a hump of fluid resting on a static flat sheet. Three cases are considered:

1. Hump deforming under the action of gravity alone.
2. Hump deforming under the action of both gravity and a uniform surface tension field.
3. Hump deforming under the action of both gravity and a non-uniform surface tension field.

The results of the test cases are shown in figures 2.2 to 2.4. Time runs in order of increasing curve density from pale gray to black; the initial hump profile is the palest gray in the figures. For the gravity only case shown in figure 2.2, sharp corners are observed as the film thickness peak shrinks. When uniform surface tension is added, smoother corners form as seen in figure 2.3. Also, the peak height decreases at a faster rate as expected. For the case shown in figure 2.4, we model surface tension to be uniform everywhere but dropping near the middle due to local heating for example or a high local surfactant concentration. The surface tension profile is shown in figure 2.4. This results in a drop in the film thickness where the surface tension is low. Strong surface tension forces from both sides pull the fluid outward, and consequently, two humps form and move away from each other as shown.

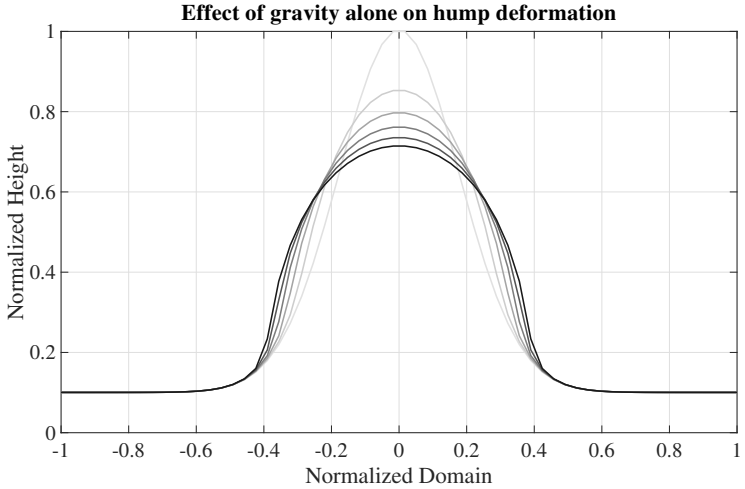

Figure 2.2: Effect of gravity alone. Sharp corners form at the edge of the hump as it deforms.

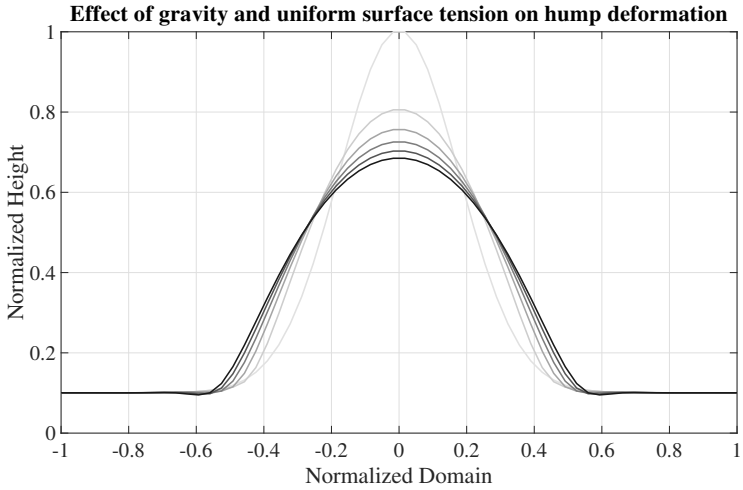

Figure 2.3: Effect of gravity and uniform surface tension. Smoother corners form, and deformation rate increases.

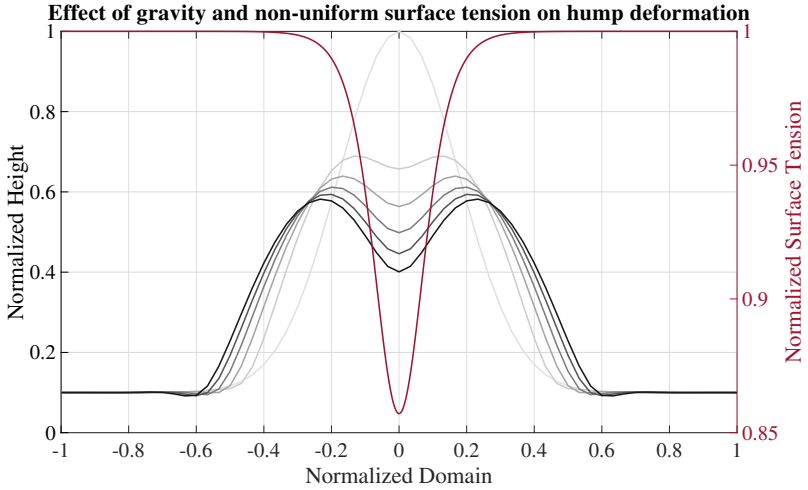

Figure 2.4: Effect of gravity and non-uniform surface tension. Marangoni flow is observed; fluid is pulled away from the center.

We now turn our attention to studying surfactant transport in a static hypophase (section 2.2) and a deforming one (section 2.3). All parameter values for the different studied cases that are not given in text can be found in appendix C.

2.2 Surfactant Transport - Static Hypophase

The transport of surfactant molecules residing in the bulk of the hypophase is governed by the diffusion convection equation below:

$$\frac{\partial C_s}{\partial t} + \nabla \cdot (C_s \boldsymbol{u}) = \nabla \cdot (D_s \nabla C_s) + R \tag{2.9}$$

where C_s is the bulk concentration of surfactants, $\boldsymbol{u}$ is the velocity field, D_s is the surfactant diffusion coefficient in the hypophase, and R is the rate of production or destruction of surfactant species through chemical reactions (source or sink term) in the bulk. For the case of incompressible flow ($\nabla \cdot \boldsymbol{u} = 0$), uniform diffusion coefficient D_s, and absence of sources or sinks ($R = 0$), equation (2.9) simplifies to:

$$\frac{\partial C_s}{\partial t} + \boldsymbol{u} \cdot (\nabla C_s) = D_s \nabla^2 C_s \tag{2.10}$$

In this section, the hypophase has a uniform initial thickness h_0 and the flat sheet over which it resides is static. Hence, it can be concluded from the results of subsection 2.1.2 that there is no fluid flow ($u = v = 0$) and the hypophase thickness does not vary with time ($h(t) = h_0$). It is further assumed for this two dimensional problem that surfactant concentration gradients exist in the y direction only. In this case, equation (2.10) can be simplified to:

$$\frac{\partial C_s(y,t)}{\partial t} = D_s \frac{\partial^2 C_s(y,t)}{\partial y^2}. \tag{2.11}$$

The diffusion of surfactants in this system will be studied for three different boundary conditions at $y = h_0$. The considered boundary conditions are:

1. A prescribed concentration at $y = h_0$ that is periodic in time.
2. A rigid surface at $y = h_0$.
3. Surfactants on the interface with a concentration $\Gamma(t)$ that leads to surfactant exchange with the hypophase bulk.

At the bottom of the hypophase, movement of surfactants into and out of the sheet is not possible. Hence, a no flux condition at $y = 0$ is imposed for all three cases:

$$\frac{\partial C_s(y,t)}{\partial y}\Big|_{y=0} = 0 \tag{2.12}$$

2.2.1 Periodic Concentration at Interface

In this case, a uniform surfactant concentration profile exists in the bulk. At $y = h_0$, we prescribe a surfactant concentration that varies periodically in time This test case serves to

explain the importance of the relative magnitudes of the diffusion time scale and that of the varying boundary concentration. The variables in equation (2.11) can be non-dimensionalized as follows: $t^* = \omega t$, $y^* = y/h_0$ and $C_s^* = \frac{C_s}{C_{ref}}$, where C_{ref} is a reference concentration of surfactants. The dimensionless form of the equation becomes:

$$\frac{\partial C_s^*}{\partial t^*} = \lambda \frac{\partial^2 C_s^*}{\partial y*^2} \tag{2.13}$$

where $\lambda = (1/\omega)/(h_0^2/D)$. λ represents the ratio of the time scale of the concentration change $(1/\omega)$ occurring at $y = h_0$ over that of diffusion (h_0^2/D_s). For small λ, diffusion is slower than the changes prescribed at the boundary; information does not propagate far into the bulk. This is shown in figure 2.5, where time runs in order of increasing curve density from pale gray to black. However for the case of large λ, diffusion happens at a faster rate, and surfactant molecules diffuse throughout the whole bulk as shown in figure 2.6.

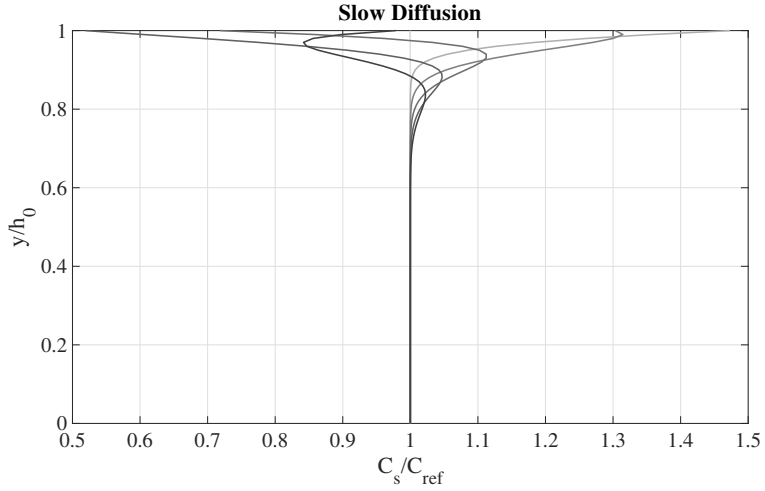

Figure 2.5: For $\lambda = 10^{-3}$, surfactants do not diffuse deep in the bulk.

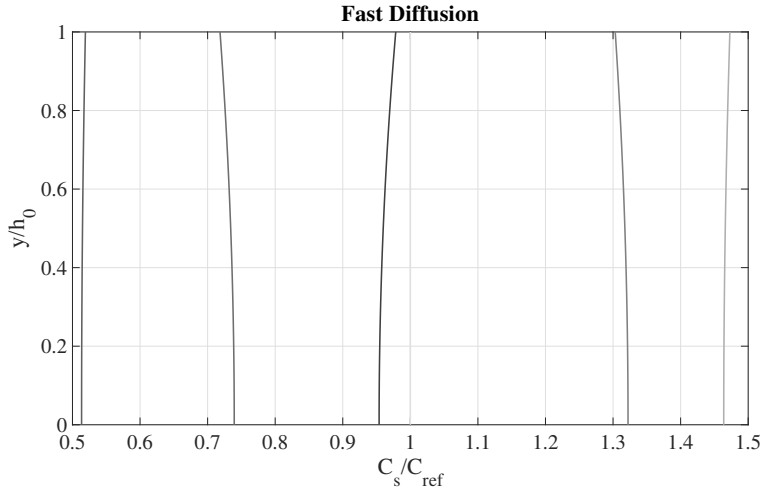

Figure 2.6: For $\lambda = 10$, surfactants diffuse through the full domain.

2.2.2 Rigid Surface at Interface

Here, a rigid boundary is placed at $y = h_0$, and a no flux boundary condition results at that location:

$$\frac{\partial C_s(y,t)}{\partial y}\Big|_{y=h_0} = 0. \tag{2.14}$$

A non uniform concentration profile of surfactants exists initially as shown in figure 2.7; the initial profile is the palest gray in the figure. As time elapses, surfactants diffuse in the direction of the decreasing concentration gradient until the surfactant concentration becomes uniform as shown in figure 2.7. Time runs in order of increasing curve density from pale gray to black.

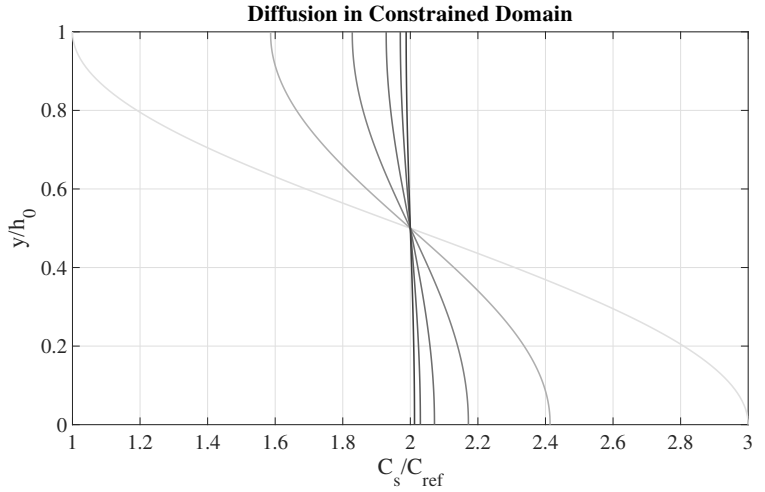

Figure 2.7: Evolution of the non-uniform concentration profile between two rigid surfaces.

The total number of surfactants is conserved as shown in figure 2.7 because molecules are trapped between the two rigid walls. N_0 is the initial number of surfactants in the system.

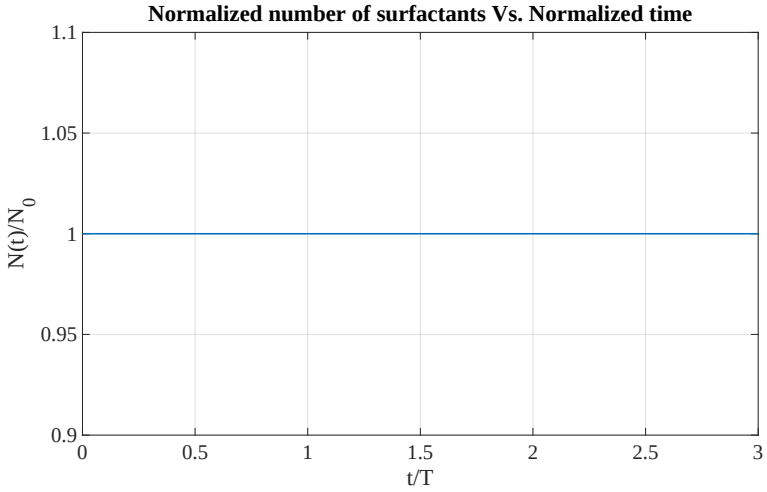

Figure 2.8: Normalized total number of surfactants vs. normalized time. Total number of surfactant molecules is conserved.

2.2.3 Interfacial Surfactant Field at Interface

Now, we consider the presence of surfactant molecules at the interface; an interfacial surfactant concentration profile $\Gamma(x,t)$ exists at the air-water interface. The boundary condition for the bulk surfactant concentration field at $y = h_0$ is determined through the exchange of surfactants between the bulk and the interface. The surfactant field on the interface $\Gamma(x,t)$ is governed by the species conservation equation [15]:

$$\frac{\partial \Gamma}{\partial t} + \nabla_s \cdot (\Gamma \boldsymbol{u_s}) + \Gamma(\nabla_s . \boldsymbol{n})(\boldsymbol{u}.\boldsymbol{n}) = \overline{D}_s \nabla_s^2 \Gamma + (D_s \nabla C_s) \cdot \boldsymbol{n}, \tag{2.15}$$

where ∇_s is the gradient operator in the plane of the interface, $\boldsymbol{u_s}$ is the fluid velocity on the interface, $\boldsymbol{n}$ is the unit normal into the fluid, and $\overline{D}_s$ is the surface diffusion coefficient of the surfactant. In words, equation (2.15) accounts for the changes in local $\Gamma(x,t)$ by surfactant convection on surface, compression and expansion of surface, diffusion in surface and diffusive exchange with the bulk. For the case considered in this section (static sheet and no concentration gradients in x), the boundary condition at $y = h_0$ simplifies to:

$$- D_s \frac{\partial C_s}{\partial y}\bigg|_{y=h_0} = \frac{\partial \Gamma}{\partial t} \tag{2.16}$$

The exchange of soluble surfactants is described by Langmuir kinetics [91]. This is done by equating the exchange term $-D_s \frac{\partial C_s}{\partial y}\Big|_{y=h_0}$ or equivalently in this case $\frac{\partial \Gamma}{\partial t}$ to the kinetic

expression below:

$$-D_s \frac{\partial C_s}{\partial y}\Big|_{y=h_0} = k_a C_s(h_0,t)(\overline{\Gamma} - \Gamma(t)) - k_d \Gamma, \tag{2.17}$$

where k_a and k_d are the adsorption and desorption coefficients of the pulmonary surfactants respectively, and $\overline{\Gamma}$ is explained later. The importance of such surfactant properties will be elucidated in the remainder of this chapter.

Before studying the boundary value problem, the equilibrium interfacial surfactant concentration Γ_{eq} is introduced. At this interfacial surfactant concentration value, the surfactant system is in chemical equilibrium and no net exchange of surfactants occurs between the bulk and the interface. Hence, no flux occurs at $y = h_0$:

$$-D_s \frac{\partial C_s}{\partial y}\Big|_{y=h_0} = 0,$$
$$\text{so,} \quad k_a C_s(h,t)\ (\overline{\Gamma} - \Gamma_{eq}(t)) - k_d\ \Gamma_{eq}(t) = 0.$$

In other words, $\Gamma_{eq}(t)$ can be expressed as:

$$\Gamma_{eq}(t) = \frac{k_a\ C_s(h(t),t)}{k_a\ C_s(h(t),t) + k_d}\overline{\Gamma}. \tag{2.18}$$

Soluble surfactant dynamics occur in such a way as to minimize the free energy of the system, which is done by restoring its chemical equilibrium; for example if the interfacial surfactant concentration is greater than $\Gamma_{eq}(t)$, interfacial surfactants will desorb from the interface into the bulk to decrease $\Gamma(t)$ towards $\Gamma_{eq}(t)$. Interestingly, as the concentration in the subphase $C_s(h_0,t)$ changes (due to surfactant diffusion for example), $\Gamma_{eq}(t)$ also varies. It is also important to note that in a static system, the maximum value that $\Gamma_{eq}(t)$ can reach due to an increase in the subphase concentration $C_s(h_0,t)$ is $\overline{\Gamma}$ as seen from equation (2.18) or figure 2.9. Hence, $\overline{\Gamma}$ is defined as the maximum equilibrium interfacial concentration for a static surfactant system. Clearly, $\overline{\Gamma}$ will also the maximum value of $\Gamma(t)$ in a static system. So $\overline{\Gamma}$ defines the number of adsorption sites that the interface consists of. In a dynamic system however, such as when surface convection is present as will be seen later, $\Gamma(t)$ can exceed $\overline{\Gamma}$ due to areal compression.

Returning to the boundary value problem, we start with the same initial bulk concentration profile given in figure 2.7, and test how $C_s(y,t)$, $\Gamma(t)$, and $\Gamma_{eq}(t)$ change for a chosen set of k_a and k_d. Initially at $t = t_0$, the slope of the bulk concentration profile at $y = h_0$ is equal to zero so $\Gamma(t_0) = \Gamma_{eq}(t_0)$. It is first important to realize that surfactants diffuse in the bulk due to the existing concentration gradient as seen in figure 2.10. Time runs in order of increasing curve density from pale gray to black.

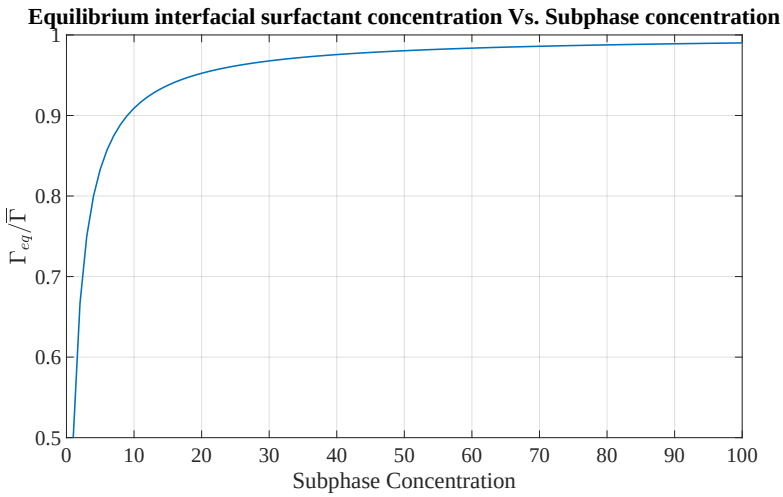

Figure 2.9: Defnition of $\overline{\Gamma}$.

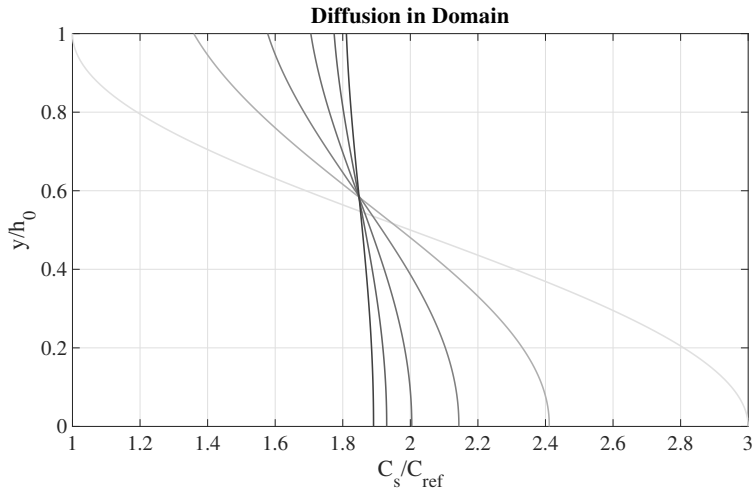

Figure 2.10: Evolution of the non-uniform bulk concentration profile

As the subphase concentration $C_s(h_0, t)$ increases, the equilibrium interfacial concentration $\Gamma_{eq}(t)$ also increases. This drives surfactants to adsorb to the interface, which increases $\Gamma(t)$ until the system reaches equilibrium as seen in figure 2.11.

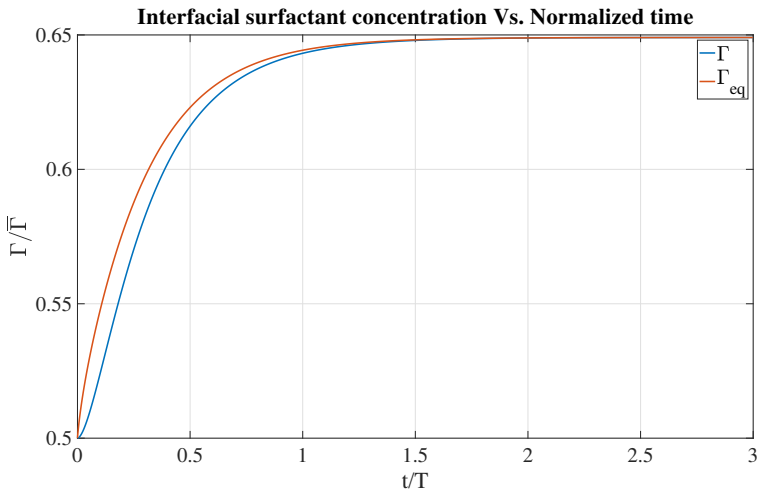

Figure 2.11: $\Gamma_{eq}(t)$ increases due to an increase in the surfactant subphase concentration. This drives surfactants to adsorb, increasing $\Gamma(t)$.

It is important to note that when compared to the case of a contaminated fluid layer between two rigid walls shown in figure 2.7, the final uniform surfactant bulk concentration here is lower. This is due to the fact that some surfactant molecules left the bulk and adsorbed to the interface. The total number of surfactants in the system however remains constant throughout the transient period. This is shown in figure 2.12.

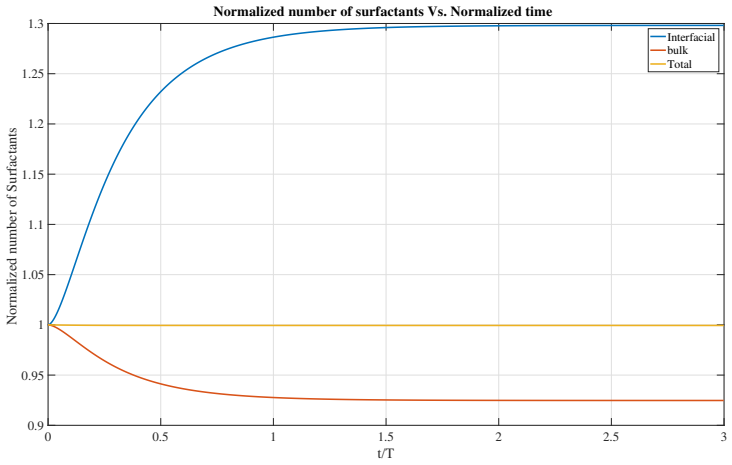

Figure 2.12: Number of surfactants decreases in the bulk, and increases on the interface. Total number remains constant.

The same analysis can be applied to the system if the initial bulk concentration profile is similar to the one seen in figure 2.13. In this case, the subphase concentration decreases due to bulk diffusion, which leads to a drop in $\Gamma_{eq}(t)$ and eventually the desorption of surfactant molecules from the interface.

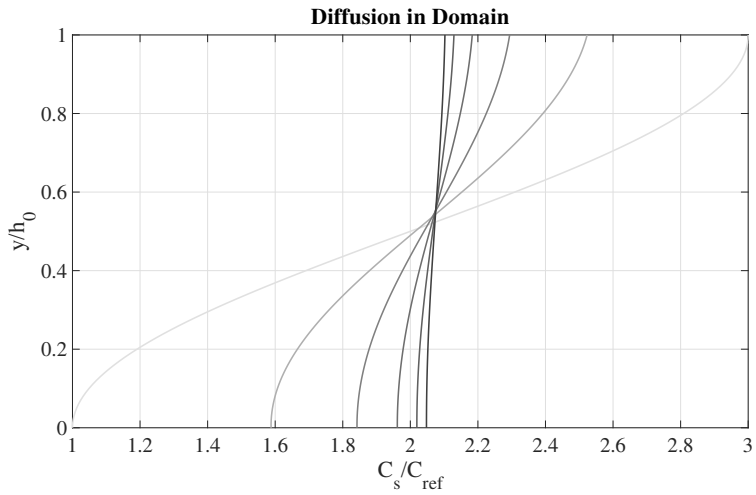

Figure 2.13: Evolution of the non-uniform bulk concentration profile.

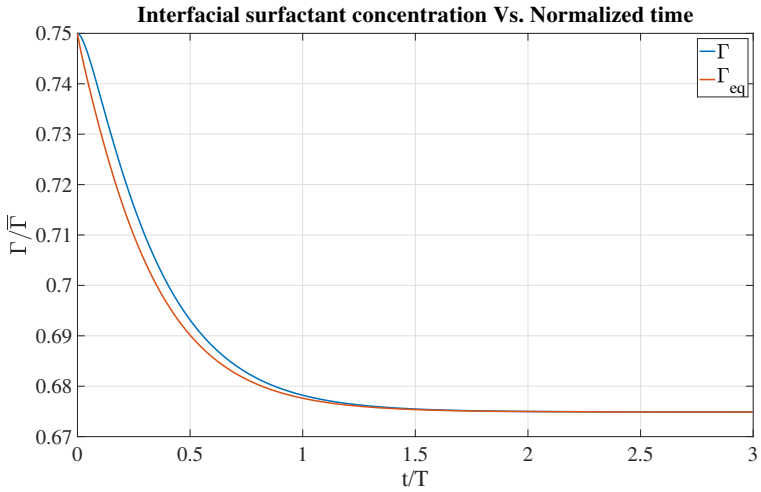

Figure 2.14: $\Gamma_{eq}(t)$ decreases due to a decrease in the surfactant subphase concentration. This drives surfactants to desorb, decreasing $\Gamma(t)$.

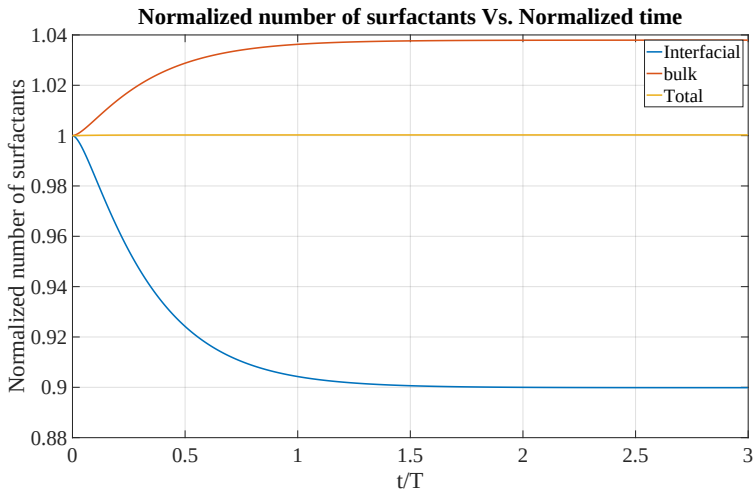

Figure 2.15: Number of surfactants increases in the bulk, and decreases on the interface. Total number remains constant.

2.3 Surfactant Transport - Homogeneous Deformation of Sheet

In this section, surfactant transport is studied when convection is added to the system through changes in the area of the sheet underneath the hypophase. Only homogeneous deformation of the sheet under the hypophase is considered, which means that the sheet is moving at a speed of general form $U(x,t) = a(t)x + b(t)$. It can be proven that for the case of a homogeneous deformation, an intially uniform thickness profile $h(t_0) = h_0$ remains uniform. Subsequently, if surfactants are uniformly distributed in the x direction initially, they remain that way under homogeneous deformation of the sheet. This is shown next: According to the equations derived in subsection 2.1.2, the velocity and thickness profiles take the form:

$$u(x,y,t) = u(x,t) = U(x,t), \tag{2.19}$$

$$\frac{\partial h}{\partial t} + \frac{\partial}{\partial x}(hU) = 0. \tag{2.20}$$

We assume the existence of a separable solution $h(x,t) = F(t)\ G(x)$ for equation (2.20). Substituting, we get:

$$\frac{\partial F}{\partial t}G + F\frac{\partial}{\partial x}(GU) = 0.$$

Therefore,

$$\frac{\frac{\partial F}{\partial t}}{F} = -\frac{\frac{\partial}{\partial x}(GU)}{G} = \lambda = cst. \tag{2.21}$$

Considering the first part of the equation:

$$F' = \lambda F,$$

$$F = Ae^{\lambda t}. \tag{2.22}$$

The second part of equation (2.21) gives:

$$U\frac{\partial G}{\partial x} + G\frac{\partial U}{\partial x} = -\lambda G,$$

$$(ax+b)\frac{\partial G}{\partial x} + (a+\lambda)G = 0.$$

Therefore,

$$G = B(ax+b)^{-\frac{a+\lambda}{a}}. \tag{2.23}$$

Using equations (2.22) and (2.23), $h(x,t) = F(t)G(x)$ yields:

$$h = ABe^{\lambda t}(ax+b)^{-\frac{a+\lambda}{a}}.$$

Using the initial condition: $t = 0$, $h = h_0$, the constants are found to be:

$$\lambda = -a \text{ and } AB = h_0.$$

Hence, the hypophase thickness will remain uniform and vary with time according to:

$$h(t) = h_0 e^{-at}. \tag{2.24}$$

Hence, the homogeneous deformation does not introduce any gradients in the x direction. So if surfactant concentrations in the bulk and interface are initially uniform in x, they remain uniform and only diffusion in the transverse (y) direction is studied.
Under such conditions, equations (2.9) and (2.15) simplify to:

$$\frac{\partial C_s}{\partial t} + v\frac{\partial C_s}{\partial y} = D_s\frac{\partial^2 C_s}{\partial y^2}, \tag{2.25}$$

$$\frac{\partial \Gamma}{\partial t} + \Gamma\frac{\partial u_s}{\partial x} = -D_s\frac{\partial C_s}{\partial y}\Big|_{y=h_0}. \tag{2.26}$$

It can be easily shown from equations (2.19) and (2.20) that:

$$\frac{\partial u_s}{\partial x} = -\frac{1}{h(t)}\frac{\partial h}{\partial t}, \tag{2.27}$$

and consequently from continuity,

$$v(y,t) = \frac{\partial h}{\partial t}\frac{y}{h(t)}. \tag{2.28}$$

Furthermore, in the case of constant density, the volume of the hypophase is conserved, so $-\frac{1}{h}\frac{\partial h}{\partial t} = \frac{1}{A(t)}\frac{\partial A(t)}{\partial t}$, where $A(t)$ is the area of the hypophase and equivalently the area of its interface. Hence, equations (2.25) and (2.26) can be written as:

$$\frac{\partial C_s}{\partial t} + \frac{\partial h}{\partial t}\frac{y}{h(t)}\frac{\partial C_s}{\partial y} = D_s\frac{\partial^2 C_s}{\partial y^2}, \tag{2.29}$$

$$\frac{\partial \Gamma}{\partial t} + \Big(\frac{1}{A(t)}\frac{dA}{dt}\Big)\Gamma = -D_s\frac{\partial C_s}{\partial y}\Big|_{y=h_0}. \tag{2.30}$$

Before studying the coupling between the bulk and the interface when flows in the fluid are present, we first focus on the case where the subphase concentration of surfactants ($C_s(h(t),t)$) is constant in time. This affords the chance to focus on the interfacial surfactant dynamics, and to understand the importance of surfactant properties such as k_a and k_d.

2.3.1 Constant Subphase Concentration

As mentioned, the main focus of this case is on the interfacial surfactant dynamics, where the subphase concentration $C_s(h(t),t)$ is taken to be constant with time. This is the case when diffusion occurs at a much faster time scale as compared to adsorption and desorption (adsorption limited), and when the bulk content of surfactant is unlimited. In other words, as soon as the concentration in the subphase varies, fast diffusion in the bulk occurs which keeps the subphase concentration at an almost constant value equal to that in the bulk bottom C_b.

Langmuir kinetics are used again to describe the exchange of soluble surfactants between the interface and the bulk, so equation (2.30) can be written as:

$$\frac{\partial \Gamma}{\partial t} + \Big(\frac{1}{A(t)}\frac{dA}{dt}\Big)\Gamma = k_a C_b(\overline{\Gamma} - \Gamma(t)) - k_d\,\Gamma(t). \tag{2.31}$$

To better understand how soluble surfactants behave, the dynamics of insoluble surfactants will also be studied. Insoluble surfactants reside on the interface and do not interact with the bulk. Describing their dynamics is straightforward and stems from the basic idea that the total number of insoluble surfactant molecules on the interface is constant with time:

$$\Gamma_{ins}(t_0)A(t_0) = \Gamma_{ins}(t)A(t),$$

so,

$$\Gamma_{ins}(t) = \frac{A(t_0)}{A(t)}\Gamma_{ins}(t_0). \tag{2.32}$$

Three different surfactant systems will be considered to elucidate the significance of the surfactant properties k_a and k_d. Each system has a different set of values for the adsorption and desorption constants but the same $\overline{\Gamma}$ value. Keeping $\frac{k_a}{k_d}$ a constant leads to a similar

Γ_{eq} among all three systems as can be deduced from equation (2.18); this makes interpreting k_a and k_d easier. Figures 2.16 to 2.18 below show how these systems behave relative to each other and to the insoluble surfactant case. The interfacial area of the hypophase is varied periodically with an angular frequency $\omega = 1$ (rev/sec) and the change in interfacial surfactant concentration is studied for each surfactant system. The results below show that the boundary value problem is governed by the ratio of the convective timescale to that of adsorption/desorption. Note that in the simulation below, we keep the convective time scale constant, and we only vary the adsorption and desorption timescales, which is equivalent to varying the ratio of the two timescales.

As seen in figure 2.16, the initial surfactant concentration is equal to Γ_{eq}. As the area expands, the surfactant concentration drops by a different amount for each surfactant system; the bigger k_a is, the smaller the drop. This is due to the fact that a higher k_a value leads to faster adsorption of surfactants to the interface to restore chemical equilibrium ($\Gamma = \Gamma_{eq}$). The concentration of the insoluble surfactant ($k_a = 0$ and $k_d = 0$) decreases the most. When the interfacial area is being compressed, the interfacial concentration increases and crosses Γ_{eq} for all three soluble surfactant systems. At that instant, soluble surfactants desorb to restore equilibirum, where the surfactant with the highest desorption constant deviates from Γ_{eq} the least.

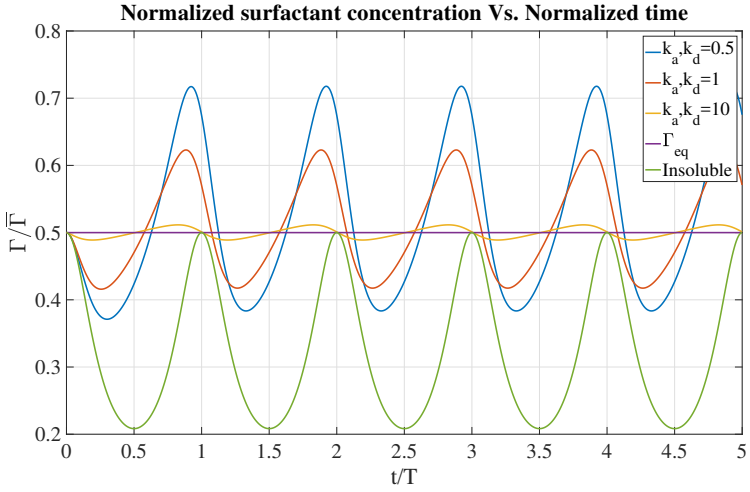

Figure 2.16: $\Gamma(t)$ of surfactants with the highest k_a and k_d deviates the least from $\Gamma_{eq}(t)$.

In figures 2.17 and 2.18, the surfactant concentration is started from above and below Γ_{eq} respectively. Note that in figure 2.17, the concentration of the insoluble surfactant is the biggest at the end of compression. This is a desired effect in the case of breathing because it leads to low surface tension values at the end of exhalation which prevents alveolar collapse. As will be seen later in section 2.4, pulmonary surfactants exhibit this desirable quality and behave as insoluble surfactants in certain regimes.

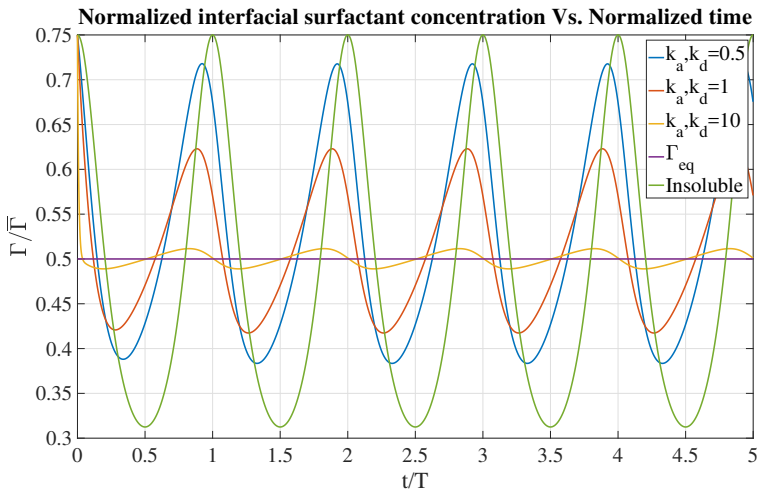

Figure 2.17: Soluble surfactants cause $\Gamma(t)$ to decrease at a faster rate initially to restore $\Gamma_{eq}(t)$, as compared to the insoluble surfactant.

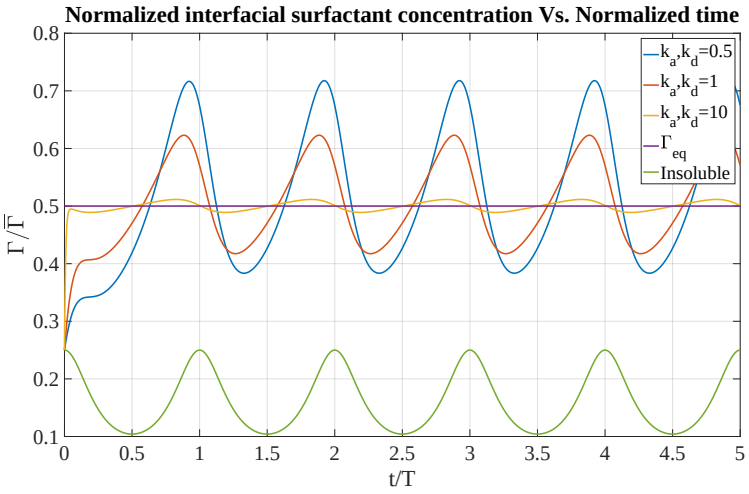

Figure 2.18: Soluble surfactants cause $\Gamma(t)$ to increase at a faster rate initially to restore $\Gamma_{eq}(t)$, as compared to the insoluble surfactant.

2.3.2 Varying Subphase Concentration

Here, diffusion of surfactant molecules in the bulk given by equation (2.29) is considered. First a mapping of the form $\eta = f(y,t)$ or equivalently $y = g(\eta,t)$ will be found such that:

$$\frac{\partial \hat{C}_s(\eta,t)}{\partial t}\Big|_{\eta} = \frac{\partial C_s(y,t)}{\partial t}\Big|_{y} + \frac{\partial h}{\partial t}\frac{y}{h(t)}\frac{\partial C_s(y,t)}{\partial y}, \tag{2.33}$$

where the notation $\Big|_{\dagger}$ means fixing the variable †, and $\hat{C}_s(\eta,t)$ is the surfactant bulk concentration field dependent on the independent variable η. This mapping leads to the elimination of the convective term in equation (2.29) and a far more accurate computational method in the case of advection-dominated flow. Using the chain rule:

$$\begin{aligned}\frac{\partial \hat{C}_s(\eta,t)}{\partial t}\Big|_{\eta} = \frac{\partial C_s(y,t)}{\partial t}\Big|_{\eta} = \frac{\partial C_s(g(\eta),t)}{\partial t}\Big|_{\eta} &= \frac{\partial C_s(g(\eta),t)}{\partial t}\Big|_{g(\eta)} + \frac{\partial C_s(g(\eta),t)}{\partial g(\eta)}\frac{\partial g(\eta)}{\partial t} \\ &= \frac{\partial C_s(y,t)}{\partial t}\Big|_{y} + \frac{\partial C_s(y,t)}{\partial y}\frac{\partial g(\eta)}{\partial t}.\end{aligned}$$

Comparing this equation with (2.33), the following relation is deduced:

$$\frac{\partial g(\eta)}{\partial t} = \frac{\partial h(t)}{\partial t}\frac{y}{h(t)},$$

which leads to $g(\eta) = \eta\frac{h(t)}{h_0}$ or equivalently $\eta = f(y) = yh_0/h(t)$. Substituting this mapping in equation (2.29) results in the elimination of the convective term. The surfactant transport problem can now be written in terms of Lagrangian coordinates:

$$\frac{\partial \hat{C}_s}{\partial t} = D_s\frac{h_0^2}{h(t)}\Big(\frac{\partial}{\partial \eta}\Big(\frac{1}{h(t)}\frac{\partial \hat{C}_s}{\partial \eta}\Big)\Big),$$

$$\frac{\partial \hat{C}_s}{\partial \eta}\Big|_{\eta=0} = 0,$$

$$-\frac{h_0}{h(t)}D_s\frac{\partial \hat{C}_s}{\partial \eta}\Big|_{\eta=h_0} = \frac{\partial \Gamma(t)}{\partial t} + \frac{1}{A(t)}\frac{dA(t)}{dt}\Gamma(t).$$

The Lagmuir isotherm is also applied here so,

$$-\frac{h_0}{h(t)}D_s\frac{\partial \hat{C}_s}{\partial \eta}\Big|_{\eta=h_0} = k_a\hat{C}_s(h_0,t)(\bar{\Gamma}-\Gamma(t)) - k_d\Gamma(t).$$

Next, the relation $A(t)h(t) = A(t_0)h(t_0) \equiv A_0h_0$ is used again, and the problem is non-dimensionalized using the following set of variables:
$\eta^* = \eta/h_0$, $\Gamma^* = \Gamma/\bar{\Gamma}$, $\hat{C_s}^* = \hat{C}_s/(\bar{\Gamma}/h_0)$, $A^* = A/A_0$, and $t^* = \omega t$.

The set of the non-dimensional equations are:

$$\frac{\partial \hat{C_s}^*}{\partial t^*} = \frac{D_s/h_0^2}{\omega}A^*(t^*)\Big(\frac{\partial}{\partial \eta^*}\Big(A^*(t^*)\frac{\partial \hat{C_s}^*}{\partial \eta^*}\Big)\Big),$$

$$\frac{\partial \hat{C_s}^*}{\partial \eta^*}\Big|_{\eta^*=0} = 0,$$

$$-A^*(t^*)\frac{D_s/h_0^2}{\omega}\frac{\partial \hat{C_s}^*}{\partial \eta^*}\Big|_{\eta^*=1} = \frac{\partial \Gamma^*(t^*)}{\partial t^*} + \frac{1}{A^*(t^*)}\frac{dA^*(t^*)}{dt^*}\Gamma^*(t^*),$$

$$-A^*(t^*)\frac{D_s/h_0^2}{\omega}\frac{\partial \hat{C_s}^*}{\partial \eta^*}\Big|_{\eta^*=1} = \frac{k_a\bar{\Gamma}/h_0}{\omega}\hat{C_s}^*(1,t^*)(1-\Gamma^*(t^*)) - \frac{k_d}{\omega}\Gamma^*(t^*).$$

In these equations, $\tau_\omega = 1/\omega$ is the time scale of sheet oscillations, $\tau_{diff} = h_0^2/D_s$ is the time scale of surfactant diffusion in the bulk, $\tau_{ads} = 1/(k_a\bar{\Gamma}/h_0)$ is the time scale of surfactant adsorption at the interface, and $\tau_{des} = 1/k_d$ is the time scale of desorption of surfactants from the interface. The ratios P_1, P_2, and P_3 of these time scales control the problem at hand, where:

$$\begin{aligned} P_1 &= \frac{1/\omega}{1/(k_a\bar{\Gamma}/h_0)} = \frac{\tau_\omega}{\tau_{ads}}, \\ P_2 &= \frac{1/\omega}{(1/k_d)} = \frac{\tau_\omega}{\tau_{des}}, \\ P_3 &= \frac{1/\omega}{h_0^2/D_s} = \frac{\tau_\omega}{\tau_{diff}}. \end{aligned}$$

The surfactant transport problem can now be written in terms of these parameters:

$$\frac{\partial \hat{C_s}^*}{\partial t^*} = P_3A^*(t^*)\Big(\frac{\partial}{\partial \eta^*}\Big(A^*(t^*)\frac{\partial \hat{C_s}^*}{\partial \eta^*}\Big)\Big), \tag{2.34}$$

$$\frac{\partial \hat{C_s}^*}{\partial \eta^*}\Big|_{\eta^*=0} = 0, \tag{2.35}$$

$$-P_3A^*(t^*)\frac{\partial \hat{C_s}^*}{\partial \eta^*}\Big|_{\eta^*=1} = \frac{\partial \Gamma^*(t^*)}{\partial t^*} + \frac{1}{A^*(t^*)}\frac{dA^*(t^*)}{dt^*}\Gamma^*(t), \tag{2.36}$$

$$-P_3A^*(t^*)\frac{\partial \hat{C_s}^*}{\partial \eta^*}\Big|_{\eta^*=1} = P_1\hat{C_s}^*(1,t^*)(1-\Gamma^*(t^*)) - P_2\Gamma^*(t^*). \tag{2.37}$$

The nondimensional equilibrium surfactant concentration is expressed as: $\Gamma^*_{eq}(t^*) = \frac{P_1\hat{C_s}^*(1,t^*)}{P_1\hat{C_s}^*(1,t^*)+P_2}$.

The surfactant transport problem is tested when the area of the flat sheet deforms periodically as shown in figure 2.19 to mimic breathing.

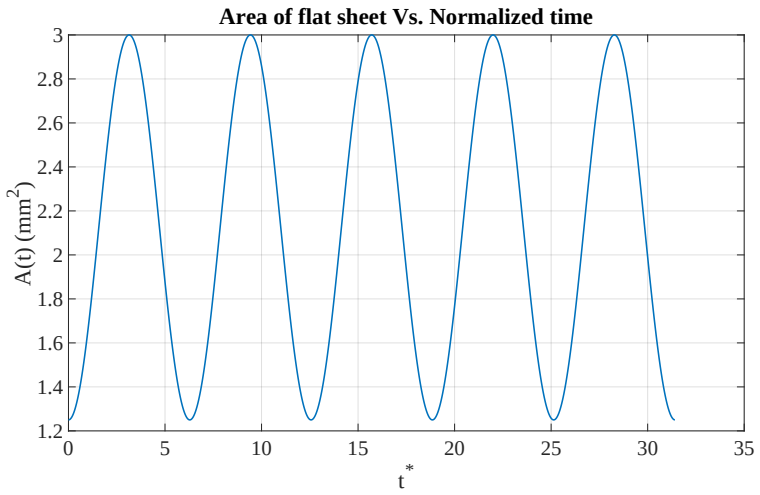

Figure 2.19: Prescribed motion of the flat sheet to mimic breathing.

For this case, P_1, P_2 and P_3 are all chosen to be unity. Initially, a uniform surfactant concentration $\hat{C}^*(\eta^*, 0) = 1$ is chosen, and consequently, the initial interfacial surfactant concentration $\Gamma^*(0) = \Gamma^*_{eq}(0)$. Variation of the interfacial and bulk surfactant concentrations is shown. Hysteresis is observed in the variation of $\Gamma(t)$ with the area because of surfactant adsorption and desorption from the interface.

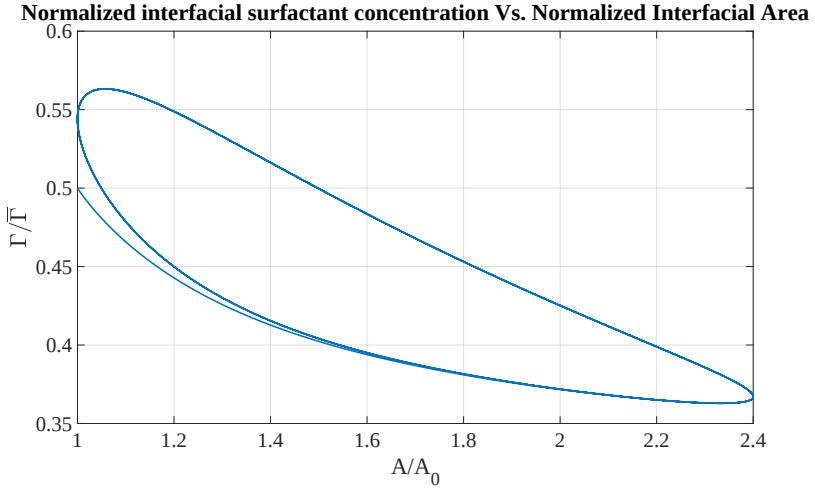

Figure 2.20: Adsorption and desorption of surfactants between the interface and the bulk cause hysteresis in the variation of $\Gamma(t)$ with area.

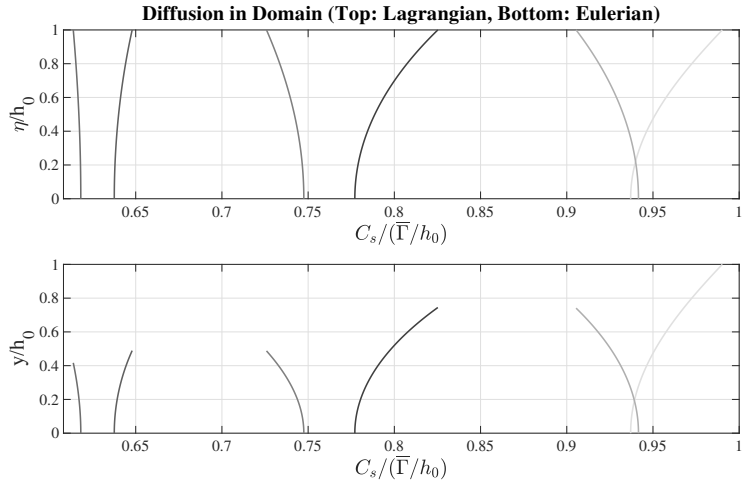

Figure 2.21: Bulk surfactant concentration profile at various phases of sheet deformation. Top figure shows the Lagrangian description of the concentration. Bottom figure shows the spatial description, where the change in hypophase thickness can be seen. Time runs in order of increasing curve density from pale gray to black.

An interesting observation is that if the same quantity of surfactants is redistributed differently in the bulk and interface, the same steady state solution will be reached, granted that the values of P_1, P_2 and P_3 are the same. This is tested by choosing a non-uniform distribution of surfactants initially as the one shown in figure 2.22, where $\hat{C}^*(\eta^*, 0) = \frac{2}{3}\cos(\pi\eta^*) + \frac{7}{6}$, and the initial interfacial surfactant concentration is again $\Gamma^*(0) = \Gamma^*_{eq}(0)$. This combination of bulk and interfacial concentrations yields the same quantity of surfactants as the previous case. The steady state solution is shown in figure 2.23.

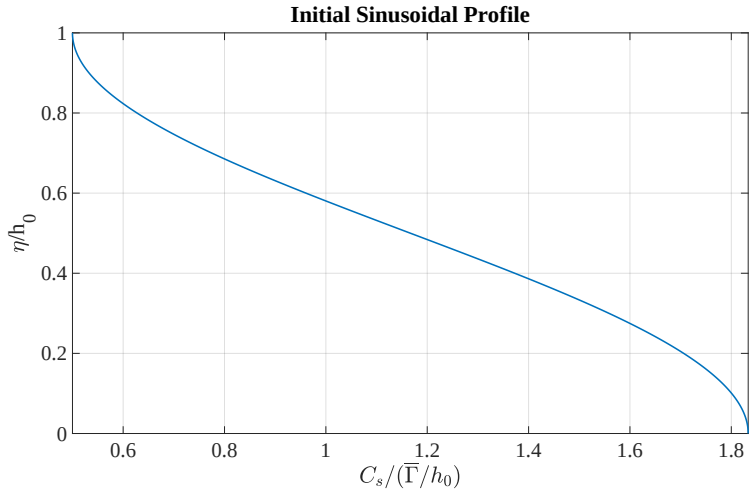

Figure 2.22: Alternative initial bulk concentration profile.

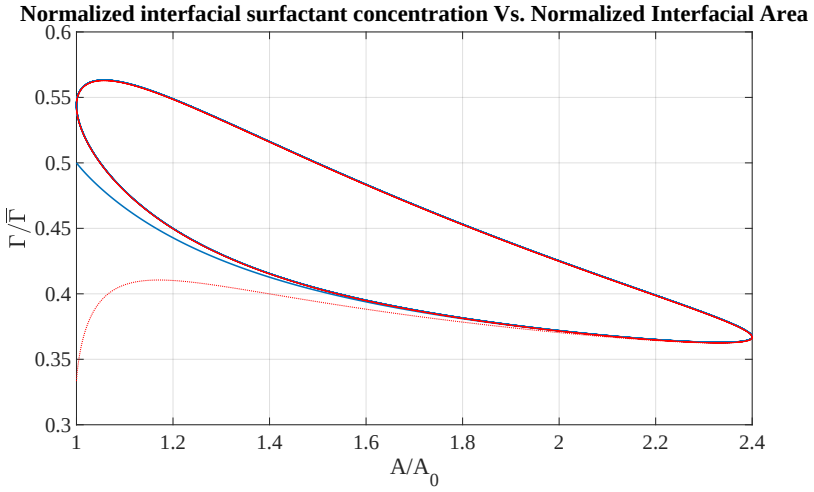

Figure 2.23: The same number of surfactants distributed differently between the bulk and interface lead to the same steady state solution.

We also test the surfactant system for an adsorption limited case with the parameters having the values: $P_1 = 0.2387$, $P_2 = 6.6 * 10^{-5}$ and $P_3 = 127.3$. These numbers are obtained by using values pertaining to the surfactant system in the alveolus[2]; this will be emphasized more in section 5.5. Initially, a uniform surfactant concentration $\hat{C}^*(\eta^*, 0) = 33$ is chosen, and the initial interfacial surfactant concentration $\Gamma^*(0) = \Gamma^*_{eq}(0)$. The variation of the interfacial and bulk surfactant concentrations are shown. It is interesting to point that in figure 2.25, it is clear that the subphase concentration is almost constant with time and equal to that at the bottom of the hypophase. This agrees with the assumption made earlier in subsection 2.3.1.

[2] k_a in this case was chosen to be smaller than the reported values in order to get an adsorption limited case.

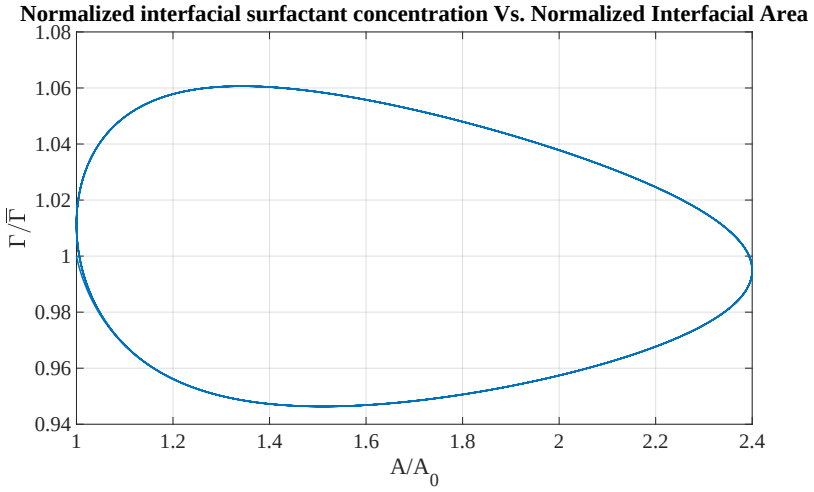

Figure 2.24: Variation of $\Gamma(t)$ with respect to the deforming area.

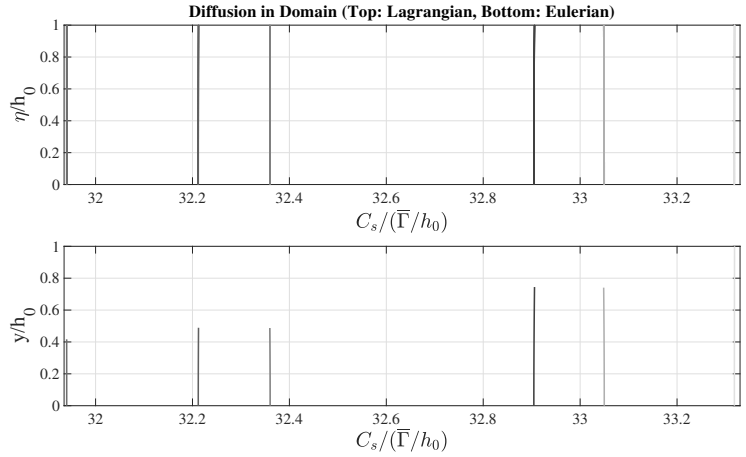

Figure 2.25: Bulk surfactant concentration profile at various phases of sheet deformation. Top figure shows the Lagrangian description of the concentration. Bottom figure shows the spatial description, where the change in hypophase thickness can be seen. Time runs in order of increasing curve density from pale gray to black.

The total number of surfactants normalized by its initial value is also plotted to show conservation of the surfactant species in the case of convection.

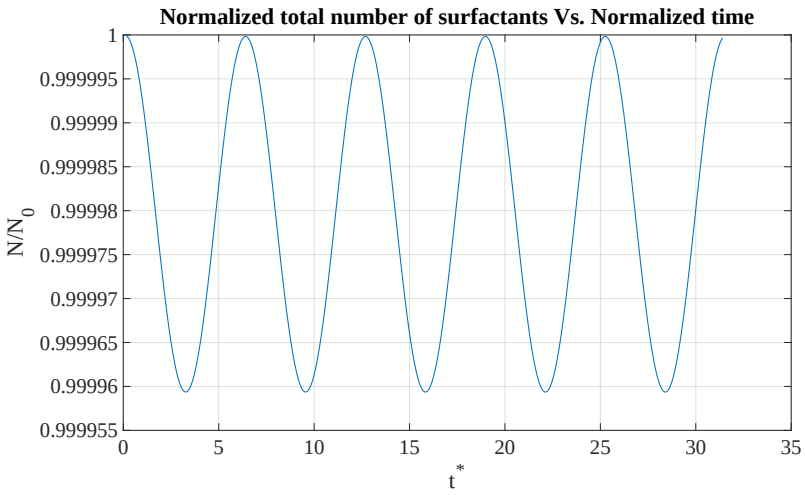

Figure 2.26: Total number of surfactants is conserved when convection is present.

Up to this point, surfactant exchange between the bulk and the interface was governed by Langmuir kinetics at all times. In the next section, more care is given to modeling this exchange. The new method is better at mimicking the behavior of surfactants found in the lungs.

2.4 Pulmonary Surfactant Model

We use a previously validated surfactant model that describes the behavior of pulmonary surfactants as they are cycled dynamically through area changes [64]. The model was developed through performing experiments with a bubble surfactometer on surfactant TA [Tokyo Tanabe, Tokyo (also known as Survanta, Ross Laboratories, Columbus, OH)], a semi-synthetic preparation widely used clinically to treat respiratory distress syndrome (RDS). This model was later used to extract surfactant properties for different surfactant fractions [65]. The adopted model characterizes surfactant exchange between the bulk and the interface in terms of three interfacial concentration regimes.

Regime One: $\Gamma \leq \overline{\Gamma}$:
When the interfacial surfactant concentration is less than $\overline{\Gamma}$ (defined in subsection 2.2.3), adsorption and desorption to and from the interface are governed by the Langmuir isotherm as done previously. In this regime, surface tension $\sigma(t)$ is related to the interfacial concentration $\Gamma(t)$ through a static isotherm relationship which decreases linearly with increasing $\Gamma(t)$. The line passes through the two points corresponding to ($\overline{\Gamma}$, $\overline{\sigma}$) and (0, 70 dyn/cm), where $\overline{\sigma}$ is the minimum equilibrium surface tension in a static system, and 70 dyn/cm is the value of surface tension when no surfactants are present.

Regime Two: $\overline{\Gamma} \leq \Gamma \leq \Gamma_{max}$:

In this regime, experiments show that the surfactant is frozen in the interface and can neither adsorb nor desorb [64]. Hence, the surfactant is modeled as insoluble. The relationship between $\sigma(t)$ and $\Gamma(t)$ in this regime decreases linearly with a slope that is different than the one in regime one. This slope is found through experiments for each type of surfactant.

Regime Three: $\Gamma = \Gamma_{max}$:
Upon large compression of the interface, surfactant molecules may reach a state where they are packed as tightly as possible in the interface, and surface concentration cannot increase further. This observation is attributable to a phase change of the surface film from the liquid-condensed state to a solid state [92]. Any further compression leads to surfactant molecules being lost from the surface to the bulk by squeeze out of the film. This leads to a constant interfacial surfactant concentration. Hence, surface tension is also constant in this regime and is at a minimum value. The value of the minimum surface tension is determined by substituting Γ_{max} in the isotherm used in the second regime. The three regimes adopted for the pulmonary surfactant are shown in figure 2.27. The equations describing

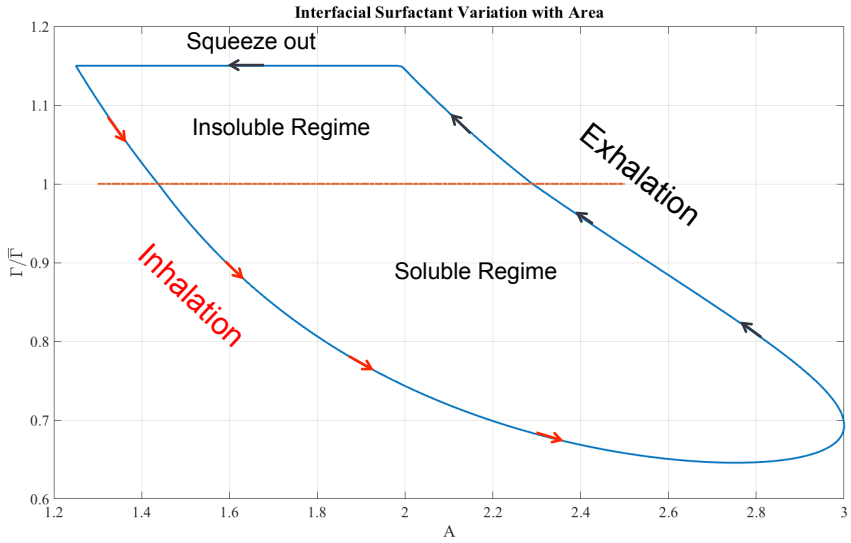

Figure 2.27: Schematic showing the different regimes of $\Gamma(t)$ during dynamic area changes

the transport problem of the pulmonary surfactant are presented next. Equation (2.36) is first manipulated, and written as:

$$-P_3 A^*(t^*)^2 \frac{\partial \hat{C_s}^*}{\partial \eta^*}\Big|_{\eta^*=1} = \frac{dA^*(t^*)\Gamma^*(t^*)}{dt^*}. \tag{2.38}$$

The equations can now be written as:

$$\frac{\partial \hat{C_s}^*}{\partial t^*} = P_3 A^*(t)\Big(\frac{\partial}{\partial \eta^*}\Big(A^*(t^*)\frac{\partial \hat{C_s}^*}{\partial \eta^*}\Big)\Big), \tag{2.39}$$

$$\frac{\partial \hat{C_s}^*}{\partial \eta^*}\Big|_{\eta^*=0} = 0, \tag{2.40}$$

$$-P_3 A^*(t^*)^2 \frac{\partial \hat{C_s}^*}{\partial \eta^*}\Big|_{\eta^*=1} = \frac{dA^*(t^*)\Gamma^*(t^*)}{dt^*}, \tag{2.41}$$

$\underline{\Gamma^* \leq 1}$:

$$\frac{dA^*(t^*)\Gamma^*(t^*)}{dt^*} = A^*\Big(P_1 \hat{C_s}^*(1,t^*)(1-\Gamma^*(t^*)) - P_2\Gamma^*(t^*)\Big). \tag{2.42}$$

$\underline{1 \leq \Gamma^* \leq \Gamma^*_{max}}$:

$$\frac{dA^*(t^*)\Gamma^*(t^*)}{dt^*} = 0. \tag{2.43}$$

$\underline{\Gamma^* = \Gamma^*_{max}}$:

$$\frac{dA^*(t^*)\Gamma^*(t^*)}{dt^*} = \Gamma^*_{max}\frac{dA^*(t^*)}{dt^*}. \tag{2.44}$$

Here, we compare the pulmonary surfactant model to a soluble surfactant governed by the Langmuir isotherm only. To do so, we re-solve the adsorption limited case presented in figure 2.24 for the case of a pulmonary surfactant undergoing three different regimes of exchange. As shown in figure 2.28, the two surfactants start with the same interfacial surfactant concentration which remains identical during the expansion of the hypophase. When compression starts, and $\Gamma^*(t)$ exceeds 1, the soluble surfactant starts desorbing from the interface into the bulk in order to restore equilibrium of the system. The pulmonary surfactant on the other hand acts as an insoluble surfactant in this regime , which causes the interfacial surfactant concentration to increase further until eventually reaching a set Γ^*_{max} where squeeze out of the film into the bulk occurs. Such dynamics are desirable because they cause a big drop in the surface tension values at the end of the compression cycle. In analogy to breathing, the decrease in surface tension is very important at the end of exhalation in order to keep the alveolus stable and to prevent pressure buildup that leads into its collapse to neighboring alveoli.

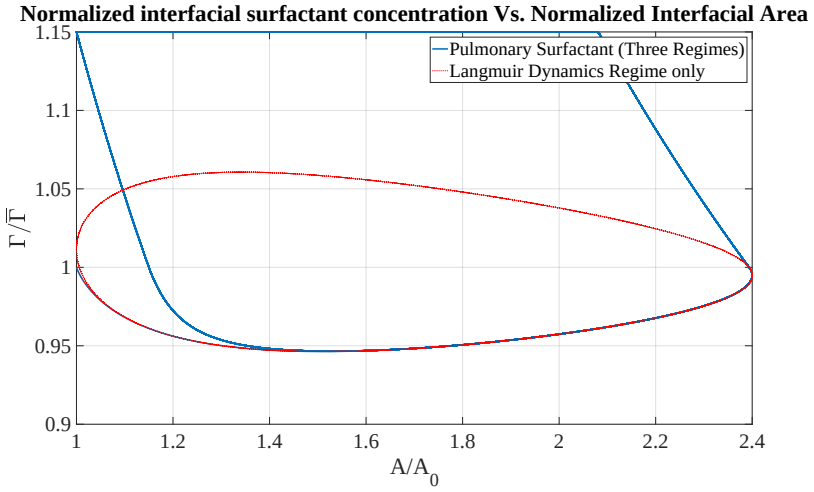

Figure 2.28: Adopted pulmonary surfactant model allows the surfactant film to compress until squeeze out. This mimics surfactant behavior during breathing.

In this chapter, we studied surfactant dynamics in a thin fluid layer coating an elastic sheet. Both static and dynamic configurations of the sheet were considered. Several boundary value problems of surfactant transport were analyzed, which explained the mechanisms of surfactant diffusion, adsorption and desorption. Important terminology that will be used throughout this dissertation was also introduced. A Langrangian formulation of the surfactant transport problem was derived and applied in the case of the deforming flat sheet. This will be essential when studying surfactant transport in the alveolus, where a similar technique will be applied to the deforming spherical hypophase coating the alveolus as explained in section 3.4. Also, the surfactant transport problem was non dimensionalized and shown to be controlled by three ratios of time scales. Finally, the model of the pulmonary surfactant that will be used in this dissertation was introduced and studied.

Chapter 3

Alveolar Model - Ventilation

3.1 Model Design of the Alveolus

As mentioned in section 1.4, the alveolar model that we develop has multiple compartments that consist of a gas mixture in the alveolus, a fluid coating with pulmonary surfactants either adsorbed to its surface or diffusing through its bulk, an alveolar wall perfused with capillaries, and a pleural cavity enclosing the alveolus. A schematic of the alveolus being modeled is shown in figure 3.1.

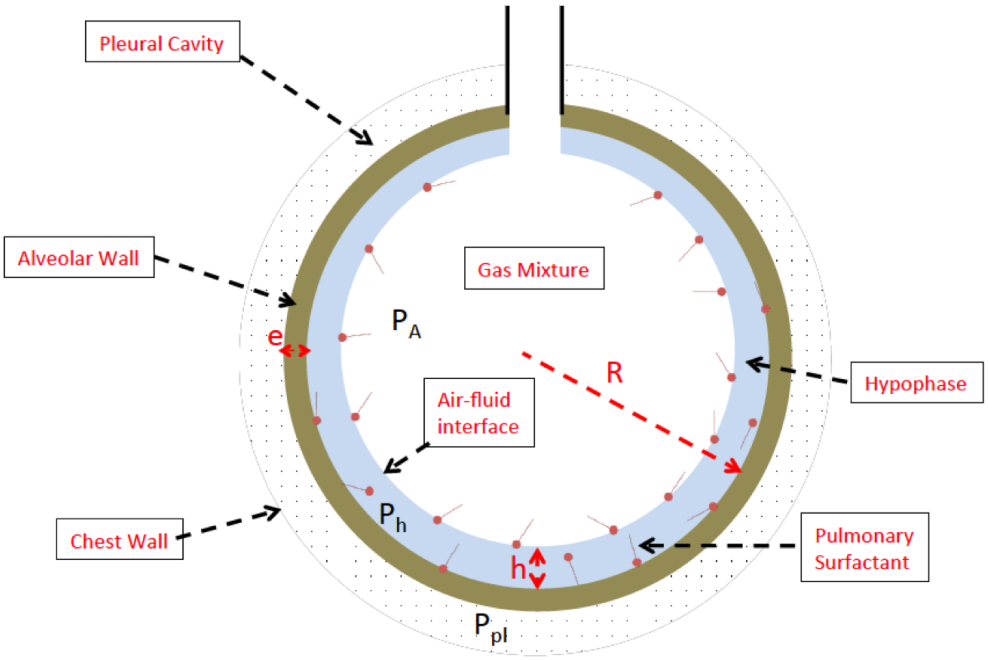

Figure 3.1: Sketch of modeled alveolus.

Several mechanical and transport processes have to be modeled in order to fully describe the system; the main ones are listed:

- Inhalation and exhalation of air into and out of the alveolus. This is accounted for by a tube that allows the exchange of air between the alveolus and the outside. The tube is modeled to have an effective resistance that replaces that of the bronchial tree leading into the alveolus.
- Diffusion of oxygen between the alveolus and the capillaries perfused in the alveolar wall.
- Diffusion of carbon dioxide between the alveolus and the capillaries perfused in the alveolar wall.
- Transport of surfactants molecules in the hypophase. These can diffuse in the bulk, adsorb, desorb and squeeze out from the interface.
- Variation of alveolar wall stresses over a breathing period.
- Transport of oxygen in the perfused capillaries. Oxygen interaction with hemoglobin is also accounted for.
- Transport of carbon dioxide in the perfused capillaries. Carbon dioxide in the form of bicarbonate is also considered.

The listed items are explained thoroughly in this and the following chapters. We first cover details on the gas mixture and alveolar mechanics in chapter 3. Oxygen and carbon dioxide diffusion and transport are then considered in chapter 4. Finally, the results obtained from coupling all the different aspects of the alveolar model are presented in chapter 5.

We start with a short description of the mechanism of breathing that will be modeled throughout. Pulmonary ventilation is composed of two main processes generally known as inhalation and exhalation. These correspond to the movement of air into and out of the human body respectively. Air ventilation in the body is conducted through the movement of the multiple respiratory muscles. Such motions induce pressure gradients in the respiratory system, which eventually result in air flow. Before presenting the detailed steps of inhalation and exhalation, some important definitions are necessary and are given next. The pressure $\overline{P}_A$ corresponds to the pressure [1] inside the alveolus, while the intrapleural pressure $\overline{P}_{pl}$ is the pressure in the pleural cavity. The transmural or transpulmonary pressure is the difference between the alveolar pressure and the pleural pressure $P_{tp} = \overline{P}_A - \overline{P}_{pl}$. The atmospheric pressure P_{atm} is the pressure outside at the mouth level. In the beginning of inhalation, the alveolar pressure $\overline{P}_A$ is equal to the atmospheric pressure P_{atm}, which means that no air flows into or out of the body due to the absence of a pressure gradient. The diaphragm and external intercostal muscles then contract causing the chest cavity to expand. This increase in volume results in a drop in $\overline{P}_{pl}$, which disturbs the equilibrium at the visceral

[1] For the alveolar and pleural pressures, the presence of an over-bar denotes absolute pressure, while its absence denotes gauge pressure.

pleura and consequently causes the alveolus to expand. A drop in the alveolar pressure $\overline{P}_A$ accompanies the volume increment of the alveolus. Because the resulting alveolar pressure $\overline{P}_A$ is sub-atmospheric, a pressure gradient between the outside of the human body and the lungs drives air into the alveolus, which causes the radius of the alveolus to increase further. Air keeps flowing into the alveolus until the alveolar pressure is restored to its initial atmospheric value. This marks the end of the inhalation. Exhalation is a process that drives the lung system back to its initial state. First, the diaphragm expands and the internal intercostal muscles contract causing the volume of the chest cavity to decrease. This leads to an increase in $\overline{P}_{pl}$, which again drives the visceral pleura to move in order to re-establish equilibrium. The movement of the visceral pleura causes the alveolus to contract, which increases the alveolar pressure $\overline{P}_A$ to a value higher than the atmospheric pressure. The resultant pressure gradient drives air out of the lung to the atmosphere, which further decreases the radius of the alveolus. Air keeps flowing out until the alveolar pressure $\overline{P}_A$ is brought back to atmospheric pressure. At this point, the cycle is complete, and inhalation is imminent. We now move to derive the relations corresponding to pulmonary ventilation.

3.2 Gas Mixture

The alveolus contains a gas mixture of oxygen, carbon dioxide, and nitrogen with $\gamma_O(t)$, $\gamma_C(t)$, and $\gamma_N(t)$ being their respective mass fractions. There is a continuous flux of oxygen and carbon dioxide between the alveolus and the passing blood stream in the capillaries that are perfused in the alveolar wall, and it is assumed that the concentration of nitrogen in the alveolus is always in equilibrium with that in blood. Expressions of the time variation of each mass fraction and of the total mass of the gas mixture are derived.

The mass conservation for oxygen in the alveolus is given by:

$$\frac{d(\gamma_O(t)\rho_G(t)V(t))}{dt} = \overline{\gamma_O}\rho_G(t)q(t)H(q(t)) + \gamma_O(t)\rho_G(t)q(t)(1 - H(q(t))) - Q_O(t), \quad (3.1)$$

where $V(t)$ and $\rho_G(t)$ are the volume and density of the gas mixture, $Q_O(t)$ is the mass flux of oxygen between the alveolus and blood, $\overline{\gamma_O}$, is the mass fraction of oxygen at the alveolus opening, and $q(t)$ is the volumetric flux of the gas mixture through the alveolar opening. $H(t)$ is the Heaviside step function. The term on the left hand side (LHS) of the equation is the time rate of change of oxygen mass in the alveolus. The first term on the right hand side (RHS) is the mass flux of oxygen inhaled, the second one is the mass flux of oxygen exhaled, and the third is the mass flux of oxygen diffused between the alveolus and the capillaries. Similarly for carbon dioxide, we get:

$$\frac{d(\gamma_C(t)\rho_G(t)V(t))}{dt} = \overline{\gamma_C}\rho_G(t)q(t)H(q(t)) + \gamma_C(t)\rho_G(t)q(t)(1 - H(q(t))) + Q_C(t), \quad (3.2)$$

where $Q_C(t)$ is the mass flux of carbon dioxide between the alveolus and blood, and $\overline{\gamma_C}$, is the mass fraction of carbon dioxide at the alveolus opening. The equation for nitrogen is

similar but lacks net diffusion of nitrogen between the alveolus and bloodstream:

$$\frac{d(\gamma_N(t)\rho_G(t)V(t))}{dt} = \overline{\gamma_N}\rho_G(t)q(t)H(q(t)) + \gamma_N(t)\rho_G(t)q(t)(1 - H(q(t))), \tag{3.3}$$

where $\overline{\gamma_N}$, is the mass fraction of nitrogen at the alveolus opening. We sum equations (3.1), (3.2) and (3.3) to get the mass conservation for the gas mixture in the alveolus:

$$\begin{aligned}\frac{d([\gamma_O(t) + \gamma_C(t) + \gamma_N(t)]\rho_G(t)V(t))}{dt} &= (\overline{\gamma_O} + \overline{\gamma_C} + \overline{\gamma_N})\rho_G(t)q(t)H(q(t)) \\ &+ (\gamma_O(t) + \gamma_C(t) + \gamma_N(t))\rho_G(t)q(t)(1 - H(q(t))) \\ &- Q_O(t) + Q_C(t).\end{aligned}$$

We use the fact that $\gamma_O(t) + \gamma_C(t) + \gamma_N(t) = 1$, and $\overline{\gamma_O} + \overline{\gamma_C} + \overline{\gamma_N} = 1$, to obtain:

$$\frac{d(\rho_G(t)V(t))}{dt} = \rho_G(t)q(t) - Q_O(t) + Q_C(t). \tag{3.4}$$

Equation (3.4) is substituted into (3.1) to yield:

$$\rho_G(t)V(t)\frac{d\gamma_O(t)}{dt} = (\overline{\gamma_O} - \gamma_O)\rho_G(t)q(t)H(q(t)) + \gamma_O(t)(Q_O(t) - Q_C(t)) - Q_O(t).$$

Hence, the ODE for $\gamma_O(t)$ is given by:

$$\frac{d\gamma_O(t)}{dt} = \frac{1}{V(t)}\left[(\overline{\gamma_O} - \gamma_O(t))q_{inh}(t) + (\gamma_O(t) - 1)\frac{Q_O(t)}{\rho_G(t)} - \gamma_O(t)\frac{Q_C(t)}{\rho_G(t)}\right]. \tag{3.5}$$

Similiarly, equations (3.6) and (3.7) are the ODEs for $\gamma_C(t)$ and $\gamma_N(t)$ respectively:

$$\frac{d\gamma_C(t)}{dt} = \frac{1}{V(t)}\left[(\overline{\gamma_C} - \gamma_C(t))q_{inh}(t) + (1 - \gamma_C(t))\frac{Q_C(t)}{\rho_G(t)} + \gamma_C(t)\frac{Q_O(t)}{\rho_G(t)}\right], \tag{3.6}$$

$$\frac{d\gamma_N(t)}{dt} = \frac{1}{V(t)}\left[(\overline{\gamma_N} - \gamma_N(t))q_{inh}(t) + \gamma_N(t)\frac{(Q_O(t) - Q_C(t))}{\rho_G(t)}\right], \tag{3.7}$$

where $q_{inh}(t)$ is the volumetric flux of the gas mixture inhaled through the alveolar opening and is given by $q(t)H(q(t))$. Further simplifications can be applied to equations (3.4), (3.5), (3.6) and (3.7). In a breathing cycle, the density $\rho_G(t)$ is only slightly perturbed, so $\rho_G(t) = \rho_0 + \Delta\rho_G(t)$ where ρ_0 is a base state of the gas mixture density and $\frac{\Delta\rho_G(t)}{\rho_0} << 1$. This allows us to rewrite $\frac{1}{\rho_G(t)}$ in the following manner:

$$\frac{1}{\rho_G(t)} = \frac{1}{\rho_0 + \Delta\rho_G(t)} = \frac{1}{\rho_0(1 + \frac{\Delta\rho_G(t)}{\rho_0})} = \frac{1}{\rho_0}\left(1 - \frac{\Delta\rho_G(t)}{\rho_0} + (\frac{\Delta\rho_G(t)}{\rho_0})^2 + ...\right)$$

Keeping the $\mathcal{O}(1)$ terms, equations (3.4), (3.5), (3.6) and (3.7) become:

$$\frac{dV(t)}{dt} = q(t) + \frac{1}{\rho_0}(Q_C(t) - Q_O(t)), \tag{3.8}$$

$$\frac{d\gamma_O(t)}{dt} = \frac{1}{V(t)}\left[(\overline{\gamma_O} - \gamma_O(t))q_{inh}(t) + (\gamma_O(t) - 1)\frac{Q_O(t)}{\rho_0} - \gamma_O(t)\frac{Q_C(t)}{\rho_0}\right], \tag{3.9}$$

$$\frac{d\gamma_C(t)}{dt} = \frac{1}{V(t)}\left[(\overline{\gamma_C} - \gamma_C(t))q_{inh}(t) + (1 - \gamma_C(t))\frac{Q_C(t)}{\rho_0} + \gamma_C(t)\frac{Q_O(t)}{\rho_0}\right], \tag{3.10}$$

$$\frac{d\gamma_N(t)}{dt} = \frac{1}{V(t)}\left[(\overline{\gamma_N} - \gamma_N(t))q_{inh}(t) + \gamma_N(t)\frac{(Q_O(t) - Q_C(t))}{\rho_0}\right]. \tag{3.11}$$

The volumetric flux of the gas mixture through the alveolar opening $q(t)$ is expressed as:

$$q(t) = -\frac{\overline{P}_A(t) - P_{atm}}{\Omega} = -\frac{P_A(t)}{\Omega}, \tag{3.12}$$

where $\overline{P}_A(t)$ is the absolute pressure in the alveolus, P_{atm} is the atmospheric pressure, and $P_A(t)$ is the gauge pressure of the gas mixture in the alveolus or the 'alveolar gauge pressure'. Ω is an effective resistance of the respiratory tract leading into the alveolus. An expression that relates Ω to the resistances of the different airway tubes in the bronchial tree is given in appendix A.

3.3 Pressure Relations

Here, a relation between the alveolar pressure and the pleural pressure is established. In order to do so, the strain rate tensor in the hypophase is needed, so the fluid velocity in the hypophase and its gradient have to be found first. The fluid velocity is assumed to have a radial component only $\boldsymbol{v} = v_r(r,t)\boldsymbol{e_r}$, which does not depend on θ and ϕ because of the axi-symmetry of the problem. In spherical coordinates, an orthonormal basis with the three unit vectors $\boldsymbol{e_r}$, $\boldsymbol{e_\theta}$, and $\boldsymbol{e_\phi}$ given below is defined.

$$\begin{aligned}
\boldsymbol{e_r} &= sin\phi\ cos\theta\mathbf{i} + sin\phi\ sin\theta\mathbf{j} + cos\phi\mathbf{k},\\
\boldsymbol{e_\phi} &= cos\phi\ cos\theta\mathbf{i} + cos\phi\ sin\theta\mathbf{j} - sin\phi\mathbf{k},\\
\boldsymbol{e_\theta} &= -sin\theta\mathbf{i} + cos\theta\mathbf{j}.
\end{aligned}$$

In this coordinate system, the position vector $\boldsymbol{x} = r\boldsymbol{e_r}(\theta,\phi)$, and its differential $d\boldsymbol{x} = dr\boldsymbol{e_r} + rd\boldsymbol{e_r}$, where

$$\begin{aligned}
d\boldsymbol{e_r} &= (-sin\phi\ sin(\theta)\mathbf{i} + sin\phi\ cos\theta\mathbf{j})d\theta + (cos\phi\ cos\theta\mathbf{i} + cos\phi\ \sin\theta\mathbf{j} - sin\phi\mathbf{k})d\phi,\\
d\boldsymbol{e_r} &= sin\phi\ \boldsymbol{e_\theta}d\theta + \boldsymbol{e_\phi}d\phi.
\end{aligned}$$

In this coordinate system, the differential of the velocity $d\boldsymbol{v}$ is:

$$d\boldsymbol{v} = \frac{\partial v_r}{\partial r} dr \boldsymbol{e_r} + v_r d\boldsymbol{e_r}. \tag{3.13}$$

which can be written as:

$$d\boldsymbol{v} = \frac{\partial v_r}{\partial r} dr \boldsymbol{e_r} + v_r (sin\phi\ \boldsymbol{e_\theta} d\theta + \boldsymbol{e_\phi} d\phi),$$

$$d\boldsymbol{v} = \frac{\partial v_r}{\partial r} (d\boldsymbol{x}.\boldsymbol{e_r})\boldsymbol{e_r} + v_r \Big(sin\phi\ \boldsymbol{e_\theta} (\frac{d\boldsymbol{x}.\boldsymbol{e_\theta}}{r sin\phi}) + \boldsymbol{e_\phi} (\frac{d\boldsymbol{x}.\boldsymbol{e_\phi}}{r}) \Big),$$

$$d\boldsymbol{v} = \Big[\frac{\partial v_r}{\partial r} \boldsymbol{e_r} \otimes \boldsymbol{e_r} + \frac{v_r}{r} (\boldsymbol{e_\theta} \otimes \boldsymbol{e_\theta} + \boldsymbol{e_\phi} \otimes \boldsymbol{e_\phi}) \Big] d\boldsymbol{x}.$$

Noting that the gradient $\nabla \boldsymbol{g}$ of a vector field $\boldsymbol{g}$ is defined by $d\boldsymbol{g} = \nabla \boldsymbol{g} d\boldsymbol{x}$, we conclude that the spatial velocity gradient is $\nabla \boldsymbol{v} = \frac{\partial v_r}{\partial r} \boldsymbol{e_r} \otimes \boldsymbol{e_r} + \frac{v_r}{r} (\boldsymbol{e_\theta} \otimes \boldsymbol{e_\theta} + \boldsymbol{e_\phi} \otimes \boldsymbol{e_\phi})$. The fluid strain rate tensor $\boldsymbol{D}$ is the symmetric part of the velocity gradient, which in this case ends up being the velocity gradient itself.

$$\boldsymbol{D} = \frac{\partial v_r}{\partial r} \boldsymbol{e_r} \otimes \boldsymbol{e_r} + \frac{v_r}{r} (\boldsymbol{e_\theta} \otimes \boldsymbol{e_\theta} + \boldsymbol{e_\phi} \otimes \boldsymbol{e_\phi}). \tag{3.14}$$

The fluid in the hypophase is assumed to be incompressible so from mass conservation, we have $div(\boldsymbol{v}) = tr(\boldsymbol{D}) = 0$, which yields the following differential equation

$$\frac{\partial v_r(r,t)}{\partial r} + 2\frac{v_r(r,t)}{r} = 0.$$

The solution of this equation is simple and is given by $v_r(r,t) = \frac{K(t)}{r^2}$, where $K(t)$ is found from boundary conditions. The fluid velocity at the alveolus wall is equal to the velocity of the alveolar wall; so at $r = R(t)$, $v_r(R,t) = \dot{R}(t)$, which results in :

$$v_r(r,t) = \frac{R(t)^2}{r^2} \frac{dR(t)}{dt}, \tag{3.15}$$

This velocity expression can be substituted in equation (3.14) above to get:

$$\boldsymbol{D} = -\frac{2R^2(t)\dot{R}(t)}{r^3} \boldsymbol{e_r} \otimes \boldsymbol{e_r} + \frac{R^2(t)\dot{R}(t)}{r^3} (\boldsymbol{e_\theta} \otimes \boldsymbol{e_\theta} + \boldsymbol{e_\phi} \otimes \boldsymbol{e_\phi}). \tag{3.16}$$

Relations between the different existing pressures will now be derived. It is worth noting that the gas mixture in the alveolus and the pleural fluid are both assumed to be inviscid, and inertial forces are neglected. At $r = R(t) - h(t)$, we refer to figure 3.2 and apply an interfacial balance of normal stresses to find a relation between the alveolar pressure $\overline{P}_A(t)$ and the absolute pressure in the hypophase $\overline{P_h}(r,t)$. It can be shown using the radial component of the Navier-Stokes equation that the hypophase pressure $\overline{P_h}(r,t)$ is uniform, so we delete its

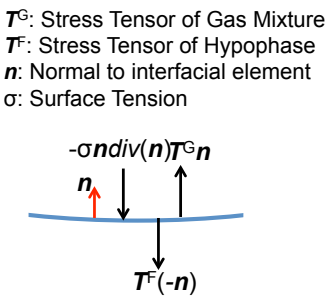

Figure 3.2: Free body diagram of an interfacial element.

space dependence and use $\overline{P_h}(t)$.

$$(-\overline{P_h}(t)\boldsymbol{I} + 2\mu_h \boldsymbol{D}(t))\boldsymbol{e}_r - (-\overline{P}_A(t)\boldsymbol{I})\boldsymbol{e}_r - \frac{2\sigma(t)}{R(t)-h(t)}\boldsymbol{e}_r = 0,$$

which can be written as

$$\overline{P}_A(t) - \overline{P_h}(t) = \frac{2\sigma(t)}{R(t)-h(t)} + \frac{4\mu_h \dot{R}(t)R^2(t)}{(R(t)-h(t))^3}, \tag{3.17}$$

where $\sigma(t)$ is the surface tension at the hypophase interface, $R(t)$ is the radius of the alveolus, $h(t)$ is the thickness of the hypophase, and μ_h is the dynamic viscosity of the hypophase. Using the fact that $h(t)/R(t) << 1$, and keeping terms to the order $\mathcal{O}(h)$, (3.17) is simplified to:

$$\overline{P}_A(t) - \overline{P_h}(t) = \frac{2\sigma(t)}{R(t)-h(t)} + \frac{4\mu_h \dot{R}(t)}{R(t)}\Big(1 + \frac{3h(t)}{R(t)}\Big). \tag{3.18}$$

To find a relation between $\overline{P_h}(t)$ and $\overline{P}_{pl}(t)$, we refer to the free body diagram shown in figure 3.3 and apply a force balance across the alveolar tissue $R(t) \le r \le R(t) + e(t)$ to get:

$$\overline{P}_{pl}(t)\pi(R(t)+e(t))^2 - (P_h(t) + \frac{4\mu_h \dot{R}(t)R^2(t)}{R^3(t)})\pi R^2(t) = -\Sigma(t)\pi((R(t)+e(t))^2 - R^2(t)),$$

where $e(t)$ is the thickness of the alveolar wall, and $\Sigma(t)$ is a uniform hoop stress in the alveolar wall. Using the fact that $e(t)/R(t) << 1$, and keeping terms to the order $\mathcal{O}(e)$ yield:

$$\overline{P_h}(t) - \overline{P}_{pl}(t) = \frac{2e(t)(\Sigma(t) + \overline{P}_{pl}(t))}{R(t)} - \frac{4\mu_h \dot{R}(t)R^2(t)}{R^3(t)}. \tag{3.19}$$

Combining equations (3.18) and (3.19), we get an equation to the leading order $\mathcal{O}(e(t), h(t))$ that relates the alveolar pressure to the pleural pressure:

$$\overline{P}_A(t) - \Big(1 + \frac{2e(t)}{R(t)}\Big)\overline{P}_{pl}(t) = \frac{2\sigma(t)}{R(t)-h(t)} + \frac{2e(t)\Sigma(t)}{R(t)} + 12\mu_h \dot{R}\frac{h(t)}{R^2(t)}. \tag{3.20}$$

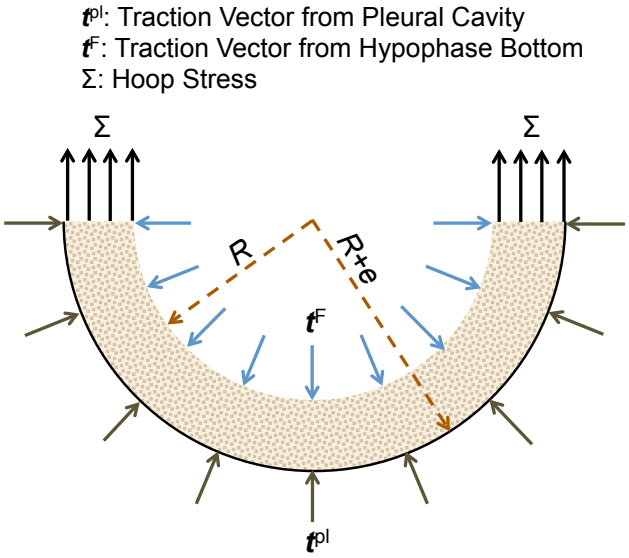

Figure 3.3: Free body diagram of the alveolar wall.

In the literature of respiratory physiology, quantities are measured relative to the transpulmonary pressure which is the difference between the alveolar and pleural pressures $(\overline{P}_A(t) - \overline{P}_{pl}(t))$ or equivalently $(P_A(t) - P_{pl}(t))$. For convenience, and because of the fact that $e(t)/R(t) << 1$ during the breathing cycle, we simplify equation (3.20) further and write it as:

$$P_A(t) - P_{pl}(t) = \frac{2\sigma(t)}{R(t) - h(t)} + \frac{2e(t)\Sigma(t)}{R(t)} + 12\mu_h \dot{R}\frac{h(t)}{R^2(t)}. \tag{3.21}$$

The hypophase and alveolar wall are modeled to be incompressible with uniform thicknesses that vary with time as:

$$h(t) = R(t) - \left(R(t)^3 + (R_0 - h_0)^3 - R_0^3\right)^{1/3}, \tag{3.22}$$

$$e(t) = \left(R(t)^3 + (R_0 + e_0)^3 - R_0^3\right)^{1/3} - R(t), \tag{3.23}$$

where R_0, h_0 and e_0 are $R(t_0)$, $h(t_0)$,and $e(t_0)$ respectively. The variable $\Sigma(t)$ depends on time through the radius $R(t)$, whereas $\sigma(t)$ depends on time through the surfactant surface excess concentration $\Gamma(t)$ on the hypophase interface. In the next two sections, the constitutive equations used for $\sigma(t)$ and $\Sigma(t)$ are presented.

3.4 Surface Tension and Surfactant Transport in the Alveolar Hypophase

With the use of equation (3.15), the surfactant concentration field $C_s(r,t)$ in the hypophase bulk is described by the convection-diffusion equation:

$$\frac{\partial C_s(r,t)}{\partial t} + \frac{R(t)^2}{r^2}\frac{dR(t)}{dt}\frac{\partial C_s(r,t)}{\partial r} = \frac{D_s}{r^2}\frac{\partial}{\partial r}\left(r^2\frac{\partial C_s(r,t)}{\partial r}\right), \tag{3.24}$$

where D_s is the diffusion coefficient of the soluble surfactants in the bulk. Two Neumann boundary conditions are imposed on equation (3.24). Although surfactants are secreted from type II epithelial cells from the alveolar wall, the flux there is set to zero as shown in equation (3.25), which indicates that surfactants cannot enter or exit the alveolar wall. This is a good assumption because half life of surfactants has been shown to be on the order of days (~ 113 hours) [93], whereas we are studying the system at a time scale of a breathing period (~ 5 seconds). In other words, we work with a constant number of surfactant molecules that can either reside on the interface or in the hypophase bulk.

$$\frac{\partial C_s(r,t)}{\partial r}\Big|_{r=R(t)} = 0. \tag{3.25}$$

At $r = R(t) - h(t)$ or the subphase, the boundary condition reflects the non-equilibrium partitioning of soluble surfactants between the interface and bulk. This is written in the form of a transport equation of the surfactant surface excess concentration $\Gamma(t)$:

$$\frac{\partial \Gamma(t)}{\partial t} + \Gamma(t)\left(\frac{2R(t)^2}{r^3}\frac{dR(t)}{dt}\Big|_{r=R(t)-h(t)}\right) = D_s\frac{\partial C_s(r,t)}{\partial r}\Big|_{r=R(t)-h(t)}. \tag{3.26}$$

By realizing that $\frac{d}{dt}(R(t)^3 - (R(t)-h(t))^3) = 0$, equation (3.26) can be rewritten in the form given in (3.27):

$$(R(t)-h(t))^2 D_s\frac{\partial C_s(r,t)}{\partial r}\Big|_{r=R(t)-h(t)} = \frac{d\Big(\Gamma(t)(R(t)-h(t))^2\Big)}{dt} \tag{3.27}$$

As discussed in section 2.4, surfactant dynamics enter three different regimes depending on the interfacial surfactant concentration $\Gamma(t)$.

$\underline{\Gamma \leq \overline{\Gamma}}$:
In this regime, the flux at the interface is equated to a kinetic expression given by the Langmuir isotherm:

$$\frac{d\Big(\Gamma(t)(R(t)-h(t))^2\Big)}{dt} = (R(t)-h(t))^2\Big(k_a C_s(R(t)-h(t),t)(\overline{\Gamma}-\Gamma(t)) - k_d\Gamma(t)\Big), \tag{3.28}$$

where k_a and k_d are the adsorption and desorption coefficients of the pulmonary surfactants respectively.

$\underline{\overline{\Gamma} \leq \Gamma \leq \Gamma_{max}}$:
In this regime, pulmonary surfactants behave as insoluble surfactants:

$$\frac{d\Big(\Gamma(t)(R(t)-h(t))^2\Big)}{dt} = 0. \tag{3.29}$$

$\underline{\Gamma = \Gamma_{max}}$:
When Γ reaches Γ_{max}, squeeze out of the surfactant film occur as the interface is being compressed, and $\Gamma(t) = \Gamma_{max}$.

The surfactant transport problem is recast in terms of a Lagrangian coordinate as was done in subsection 2.3.2. This leads to the elimination of the convective term in equation (3.24) and a far more accurate computational method in the case of advection-dominated flow. Unlike r, the new coordinate η ranges between two fixed values. It is defined as:

$$\eta = \frac{r^3 - b(t)^3}{3\hat{V}_0^{2/3}}, \tag{3.30}$$

where $b(t) = R(t) - h(t)$ and $\hat{V}_0 = R_0^3 - (R_0 - h_0)^3$.

$$\left\{ \begin{array}{cc} At\ r = R(t) - h(t) & \eta = 0 \\ At\ r = R(t) & \eta = \frac{1}{3}\hat{V}_0^{1/3} \end{array} \right\}.$$

The surfactant transport problem can now be written as:

$$\frac{\partial \hat{C}_s(\eta,t)}{\partial t} = \frac{D_s}{\hat{V}_0^{4/3}} \frac{\partial}{\partial \eta} \left(\Big[3\eta \hat{V}_0^{2/3} + b(t)^3 \Big]^{4/3} \frac{\partial \hat{C}_s(\eta,t)}{\partial \eta} \right), \tag{3.31}$$

$$\frac{\partial \hat{C}_s(\eta,t)}{\partial \eta}\Big|_{\eta=\frac{1}{3}\hat{V}_0^{1/3}} = 0, \tag{3.32}$$

$$\frac{D_s b(t)^4}{\hat{V}_0^{2/3}} \frac{\partial \hat{C}_s(\eta,t)}{\partial \eta}\Big|_{\eta=0} = \frac{d\Big(\Gamma(t)b(t)^2\Big)}{dt}. \tag{3.33}$$

$\underline{\Gamma \leq \overline{\Gamma}}$:

$$\frac{d\Big(\Gamma(t)b(t)^2\Big)}{dt} = b(t)^2\Big(k_a \hat{C}_s(0,t)(\overline{\Gamma} - \Gamma(t)) - k_d \Gamma(t)\Big). \tag{3.34}$$

$\underline{\overline{\Gamma} \leq \Gamma \leq \Gamma_{max}}$:

$$\frac{d\Big(\Gamma(t)b(t)^2\Big)}{dt} = 0. \tag{3.35}$$

$\underline{\Gamma = \Gamma_{max}}$:

$$\Gamma(t) = \Gamma_{max}. \tag{3.36}$$

More details on the coordinate transformation are given in Appendix B. The relation between the surface tension (dyn/cm) and the interfacial surfactant concentration is based on the explanation given in section 2.4. The relations are shown below:

$\underline{\Gamma \leq \overline{\Gamma}}$:

$$\sigma(t) = (\overline{\sigma} - 70)\frac{\Gamma(t)}{\overline{\Gamma}} + 70. \tag{3.37}$$

$\underline{\Gamma > \overline{\Gamma}}$:

$$\sigma(t) = -Y\frac{\Gamma(t)}{\overline{\Gamma}} + (Y + \overline{\sigma}). \tag{3.38}$$

As defined earlier $\overline{\sigma}$ is the minimum equilibrium surface tension in a static system existing when $\Gamma(t) = \overline{\Gamma}$ and 70 dyn/cm is the value of surface tension when no surfactants are present. Y is the slope of the isotherm in the second regime and is determined experimentally for a given surfactant.

3.5 Alveolar Wall Stress

Multiple researchers attempted to derive a constitutive model for the alveolar wall. Maksym and Bates developed a distributed nonlinear model of lung tissue elasticity where they presented a theory relating the static stress-strain properties of lung tissue to the existing collagen and elastin [94]. Other work led to the formulation of a constitutive relation for lung tissue elasticity for a simplified alveolar geometry and a pseudo-strain-energy function for the inter-alveolar septa [95]. In [96], the strain energy for the air-filled lung was calculated from a model of the parenchymal microstructure . More recently, Rausch et al. experimentally determined the nonlinear material behavior of the rat lung parenchyma, and presented a new constitutive model that contained the contribution of the ground substance, elastin fibers, collagen fibers and volumetric changes [97]. There have also been multiple studies that investigated the lung elasticity in disease states such as pulmonary fibrosis [98–100]. For the purpose of the model developed here, a relation between the hoop stress in the alveolar wall and the alveolar radius was desired. No such relation could be found in the literature, so we collaborated with the Berkeley BioMechanics laboratory advised by professor Grace

O'Connell to model the alveolar wall stress [101].

A Finite element model of a single alveolus was developed in FEBIO [102]. The alveolar wall was modeled to be composed of collagen fibers embedded in a ground matrix that encompassed elastin, different types of cells, capillaries, etc. Collagen fibers were described with an exponential stress-strain response governed by three material coefficients: ζ_c, ψ, and χ, while the ground matrix was described as a Neo-Hookean material with two material coefficients E and ν_g. Due to the paucity of data on the alignment of collagen fibers in the alveolar wall, we assumed that twelve groups of fibers (15^o between two adjacent groups) of equal strength were laid in the tangential plane of the alveolar wall. The opening of the alveolus was constrained in all directions, and varying pressure was exerted on the inner surface, resulting in cycles of inflation and deflation. The material coefficients were determined by parameter identification of the PV response from our simulation with data in the literature [103]. Because the specific interest in this section is alveolar tissue mechanics, we used PV curves determined quasi-statically from saline-filled lungs, which eliminates the contribution of surface tension during lung recoil [104]. Furthermore, we assumed that the PV curve of the whole lung applies to a single alveolus, due to the fact that major changes in lung volume are attributed to changes in the alveolar configuration [104]. Also, results were validated with PV curves of saline-filled cat lungs due to the absence of saline-filled human lung data. The following parameters for the matrix and fibers were found: $E = 1KPa,\ \nu_g = 0.45,\ \zeta_c = 0.03KPa,\ \psi = 0.1$, and $\chi = 2.5$. The obtained elastic modulus E matches the value reported in literature [105]. Next, stresses on the inner and outer walls were evaluated when a pressure difference was applied across the alveolar wall. Figure 3.4 shows how the average stresses on the inner and outer walls vary with the effective alveolar radius (cubic root of the alveolar volume).

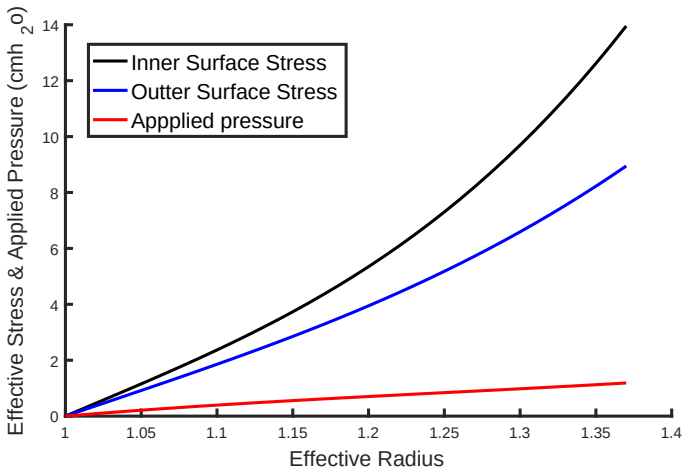

Figure 3.4: Variation of hoop stress with the effective radius of the alveolus.

Equation (3.39) for the hoop stress $\Sigma(t)$ is derived by fitting the inner surface stress curve. In our model, $\Sigma(t)$ is assumed to be uniform across the alveolar wall.

$$\Sigma(t) = 0.0022e^{6.3701(R(t)/Ro)}. \tag{3.39}$$

It is worth mentioning that the results of this preliminary model are limited by the lack of necessary information and data in the literature. A notable improvement to our model would be the replacement of the homogeneous material description with a more specific one that contains information on fiber arrangements, and elastin and collagen densities. Also, the implications of assuming equivalence between the PV curve of a single alveolus and that of a whole lung are not well understood; nor are the limitations of the quasi-static PV curves determined from saline experiments clear. Nonetheless, this model serves as a good first order approximation of the alveolar wall stresses in the model developed with the purpose of studying the effect of surfactants on breathing. In most results shown in chapter 5, an alternative model for the alveolar hoop stress is used, where the alveolar wall is modeled as a spring. More information is given in appendix C.

Chapter 4

Alveolar Model - Gas Exchange

4.1 Diffusion of Gases in the Lungs

Diffusion is the main mode of gas transport in the final generations of the respiratory tract [106]. The diffusion of oxygen and carbon dioxide is driven by the difference in their alveolar and blood concentrations. Oxygen for example diffuses through the alveolus to reach the hypophase interface. It then crosses the surfactant layer to diffuse through the hypophase bulk and alveolar wall, eventually reaching the blood in the capillaries. Carbon dioxide goes through the same steps in reverse order.

Gases in the alveolus are assumed to be well-mixed. For example, an oxygen molecule has a diffusion coefficient of 0.2 cm^2/s in air [107]. The diffusion time scale of the molecule from the center of a spherical alveolus with an average radius of 0.01 cm to its edge is around $\frac{0.01^2}{0.2} \approx 0.5$ ms, which is considerably lower than both the breathing period and the blood transit time in capillaries; a similar argument applies to carbon dioxide. Hence, the partial pressures of oxygen and carbon dioxide there are considered uniform and are given respectively by:

$$P_O(t) = \gamma_O(t)\frac{M_G(t)}{M_O}(P_A(t) + P_{atm} - P_V), \tag{4.1}$$

$$P_C(t) = \gamma_C(t)\frac{M_G(t)}{M_C}(P_A(t) + P_{atm} - P_V), \tag{4.2}$$

where $M_G(t)$, M_O and M_C are the molar masses of the gas mixture, oxygen and carbon dioxide respectively, P_{atm} is the atmospheric pressure and P_V is the vapor pressure in the lungs.

The partial pressures of oxygen $P_{bO}(s,t)$ and of carbon dioxide $P_{bC}(s,t)$ in the capillaries are space dependent because gases are picked up and released by the blood stream passing in the exchange zone; s is the arclength along the capillary in the direction of blood flow. Because the trajectories of oxygen and carbon dioxide are the same in reverse, the

expressions of the flux for both gases are similar. Oxygen will first be used to model its transport between the alveolus and capillary bed and get an expression for $Q_O(s,t)$. The same methodology is applied to carbon dioxide to get $Q_C(s,t)$.

The alveolus is perfused with a capillary bed with n individual capillaries oriented in many directions (reader is referred to figure 18 in [9][1]), so we express the specific flux (flux per unit area) of oxygen from the alveolus to each capillary j (where j goes from 1 to n) as:

$$\begin{aligned} Q''_{O1}(s_1,t) &= \mathcal{D}_O(t)(P_O(t) - P_{bO1}(s_1,t)), \\ Q''_{O2}(s_2,t) &= \mathcal{D}_O(t)(P_O(t) - P_{bO2}(s_2,t)), \\ &\vdots \\ Q''_{On}(s_n,t) &= \mathcal{D}_O(t)(P_O(t) - P_{bOn}(s_n,t)), \end{aligned}$$

where $\mathcal{D}_O(t)$, usually referred to as the diffusing capacity in the literature, is a time function uniform in space and is defined later, and s_j and $P_{bOj}(s_j,t)$ are the arclength and partial pressure of oxygen along each capillary j respectively. The total oxygen flux to the capillary bed at a fixed time is then equal to:

$$\begin{aligned} Q_O(t) = \sum_{j=1}^{n} \iint_{A_j^c(t)} Q''_{Oj}(s_j,t)dA_j^c(t) &= \sum_{j=1}^{n} \iint_{A_j^c(t)} \mathcal{D}_O(t)(P_O(t) - P_{bOj}(s_j,t))dA_j^c(t) \\ &= \mathcal{D}_O(t) \sum_{j=1}^{n} (P_O(t) - P^*_{bOj}(t))A_j^c(t), \end{aligned}$$

where $A_j^c(t)$ is the area of capillary j that is involved in gas diffusion. The mean value theorem of integral calculus was used in the last step to obtain $P^*_{bOj}(t)$, which is the homogenized oxygen partial pressure in capillary j. $P^*_{bOj}(t)$ is therefore defined as the average oxygen partial pressure in the capillary that yields the same overall flux as $P_{bOj}(s_j,t)$. We assume that the homogenized mean pressure in every capillary passing through the exchange zone is almost identical, i.e. $P^*_{bO1}(t) = P^*_{bO2}(t) = ... = P^*_{bOn}(t) = P^*_{bO}(t)$. Then the total oxygen flux $Q_O(t)$ is written as:

$$Q_O(t) = \mathcal{D}_O(t)\Big(P_O(t) - P^*_{bO}(t)\Big) \sum_{j=1}^{n} A_j^c(t).$$

Almost 90% of the alveolar wall is perfused with capillaries [9], so we set $\sum_{j=1}^{n} A_j^c(t) = \kappa A(t)$, where $A(t)$ is the area of the alveolar wall, and κ is a constant set to 0.9.

[1]Figure is not reproduced here because permission to reproduce was not requested.

The diffusing capacity $\mathcal{D}_O(t)$ still has to be replaced by physical parameters pertaining to the alveolar system. Before doing so, it is important to mention that after reaching the plasma, oxygen molecules still have to diffuse through a few media. Namely, oxygen molecules have to travel through the plasma and then across the red blood cell membrane. Finally, oxygen molecules diffuse through the cytoplasm of the red blood cell before binding to hemoglobin. The diffusion of oxygen through the red blood cell wall is usually neglected as it happens as a much shorter time scale as compared to the other diffusive steps [107].

The diffusing capacity is often split into two components in the literature [108, 109], such as:

$$\frac{1}{\mathcal{D}(t)} = \frac{1}{\mathcal{D}_m(t)} + \frac{1}{\theta V_c},$$

where $\mathcal{D}_m$ is the diffusing capacity that corresponds to the diffusion of oxygen from the alveolus all the way to the red blood cell. It is referred to as the alveolar-capillary membrane diffusing capacity or the diffusive conductance [110]. V_c is the capillary blood volume and θ represents the binding rate of hemoglobin with oxygen. The physiological meaning of the second term on the right hand side is unclear because it describes the complex phenomenon of oxygen binding to hemoglobin as a diffusive process, which is not the case. A critique of this formulation of the diffusing capacity is presented in [111]. In this dissertation, we use a different approach that was presented by Martin and Maury to express the diffusing capacity [112, 113]. Only the diffusing capacity that corresponds to oxygen diffusion through the respiratory membrane is considered; the chemical reactions of oxygen and hemoglobin are not simply modeled as an extra resistance. Instead, they are described by Hill's curve that relates the partial pressure of oxygen in the plasma to the oxygen quantity bound to hemoglobin. This is then used in the transport equation of oxygen in the capillary as blood passes through the exchange zone. This is explored further in section 4.2. We now return to replacing $\mathcal{D}_O(t)$ by the relevant parameters corresponding to the respiratory membrane.

As shown in figure 4.1, oxygen diffuses from the alveolus and reaches the capillary bed after crossing the surfactant layer, the hypophase and the alveolar wall. $C_{O1}(t)$, $C_{O2}(t)$ and $C_{O3}(t)$ are the oxygen concentrations in the respiratory membrane at the hypophase interface, at the hypophase-alveolar wall boundary and at the alveolar wall-capillary boundary respectively.
If the hypophase had a clean interface (no surfactants), Henry's law would relate the concentration of a gas in a liquid to the partial pressure of the gas above the liquid. The surfactant monolayer affects the mass transfer characteristics of the interface which leads to a non-equilibrium partitioning of the gas across it. This results in an oxygen flux through the hypophase interface which is proportional to the difference of the surface concentration and the equilibrium concentration:

$$Q_O(t) = \frac{\kappa A(t)}{\Psi_O(t)}(\xi_O P_O(t) - C_{O1}(t)), \tag{4.3}$$

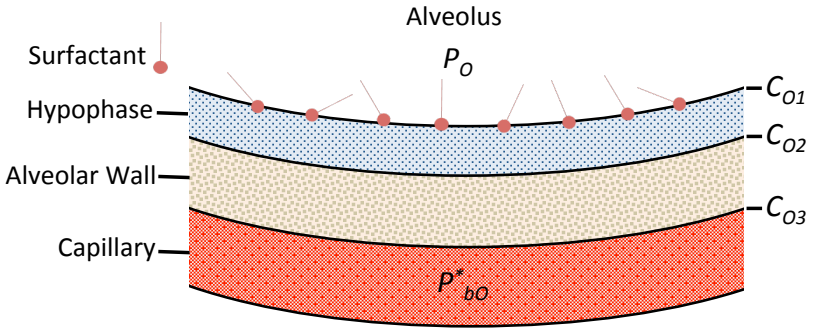

Figure 4.1: Oxygen flux trajectory between alveolus and capillary.

where ξ_O is the solubility constant of oxygen in the respiratory membrane, and $\Psi_O(t)$ is the interfacial resistance to oxygen caused by the presence of surfactant molecules on the interface. The interfacial resistance is thus a function of the surfactant surface excess concentration $\Gamma(t)$ (or equivalently of $\sigma(t)$). A preliminary model for $\Psi_O(t)$ is extracted from the experimental values given in [81]:

$$\Psi_O(t) = 0.5404\sigma(t)^{-0.247}, \tag{4.4}$$

where $\Psi_O(t)$ is in units of sec/cm, and $\sigma(t)$ is in units of mN/m.

All other media are assumed to be in instantaneous equilibrium with each other. It is for this reason $C_{O2}(t)$ and $C_{O3}(t)$ apply on both sides of their respective interfaces. For example, the concentration at the boundary between the hypophase and alveolar wall is continuous and equal to $C_{O2}(t)$. Oxygen diffusion through the hypophase and alveolar wall is given by Fick's law:

$$Q_O(t) = \frac{\kappa A(t) D_{hO}}{h(t)}(C_{O1}(t) - C_{O2}(t)), \tag{4.5}$$

$$Q_O(t) = \frac{\kappa A(t) D_{wO}}{\zeta e(t)}(C_{O2}(t) - C_{O3}(t)), \tag{4.6}$$

where D_{hO} and D_{wO} are the diffusion coefficients of oxygen in the hypohase and alveolar wall respectively, and ζ is a fraction of the alveolar wall that oxygen molecules cross before reaching the perfused capillaries. Because oxygen in the capillary bed is in instantaneous equilibrium with that in the alveolar wall, we have:

$$C_{O3}(t) = \xi_O P^*_{bO}(t). \tag{4.7}$$

We combine equations (4.3) to (4.7) to express the oxygen mass flux as:

$$Q_O(t) = \frac{\kappa A(t)\xi_O}{\Psi_O(t) + h(t)/D_{hO} + \zeta e(t)/D_{wO}}\Big(P_O(t) - P^*_{bO}(t)\Big). \tag{4.8}$$

It is worth noting that there is a discrepancy between the values of physiological and morphometric diffusing capacities, that is still under investigation until today [113]. Interested readers are referred to [114].

A similar methodology is applied to the modeling of carbon dioxide. The mass flux of carbon dioxide is expressed as:

$$Q_C(t) = \frac{\kappa A(t)\xi_C}{\Psi_C(t) + h(t)/D_{hC} + \zeta e(t)/D_{wC}}\Big(P^*_{bC}(t) - P_C(t)\Big), \tag{4.9}$$

where D_{hC} and D_{wC} are the diffusion coefficients of carbon dioxide in the hypophase and alveolar wall respectively, and ζ here is a fraction of the alveolar wall that carbon dioxide molecules cross before reaching the bottom of the hypophase. ξ_C is the solubility constant of carbon dioxide in the respiratory membrane, and $\Psi_C(t)$ is the interfacial resistance to carbon dioxide caused by the presence of surfactant molecules on the interface. A model for $\Psi_C(t)$ is lacking in the literature, so it is assumed that $\Psi_C(t)$ is equivalent to $\Psi_O(t)$. $P^*_{bC}(t)$ is the homogenized partial pressure of carbon dioxide in the blood, which is found by applying the mean value theorem of integrals to $P_{bC}(s,t)$ in a capillary.

4.2 Oxygen Transport

We now turn to the determination of $P^*_{bO}(t)$ to complete the theory for the oxygen gas exchange. Figure 4.2 shows how $P_{bO}(s,t)$ in general varies along the capillary at a fixed time [113, 115]. Blood enters the capillary from the arterial end at a fixed value of $P_{bOi} = 40$ mmHg [115] and exits at a partial pressure $P_{bOe}(t)$ after spending a transit time of τ seconds in the exchange zone. We apply a control volume analysis to the blood present in the capillary bed perfused in the alveolus under study. We assume that a volume of blood V_{bc} enters the whole capillary bed at a constant speed and exits after τ seconds. We further assume that all capillary inlets have the same oxygen partial pressure P_{bOi}, and all exists have the same oxygen partial pressure $P_{bOe}(t)$. If at a specific location in the blood volume, the oxygen partial pressure is $\mathcal{P}(t)$, then the oxygen concentration there is equal to $\xi_O\mathcal{P}(t)$ plus a contribution from the oxygen molecules bound to hemoglobin at that location, which is given by the hemoglobin model $\mathcal{H}(t)$ [112, 116]:

$$\mathcal{H}(t) = 4C_{HB}\frac{\mathcal{P}^m(t)}{\mathcal{P}^m(t) + P^m_{\frac{1}{2}bO}}, \tag{4.10}$$

where C_{HB} is the concentration of hemoglobin in the blood, $P_{\frac{1}{2}bO}$ is the oxygen partial pressure that corresponds to half full hemoglobin saturation, and m is an exponent set to 2.5 in the literature [116], which reflects the cooperative character of the reaction between oxygen and hemoglobin [117]. The portion $\frac{\mathcal{P}^m(t)}{\mathcal{P}^m(t)+P^m_{\frac{1}{2}bO}}$ of equation 4.10 is referred to as the

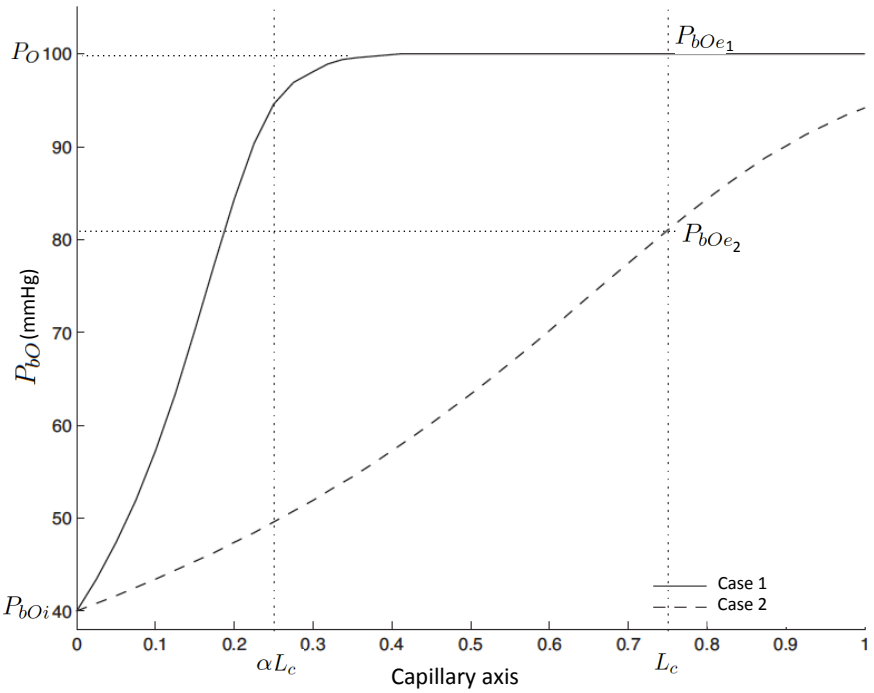

Figure 4.2: Oxygen partial pressure in exchange zone - Reproduced (and modified) from [113].

hemoglobin saturation function and corresponds to Hill's curve [112]. A plot of this function with respect to the oxygen partial pressure in the plasma is shown in figure 4.3. As can be seen, the function is very nonlinear. Furthermore, when blood enters the exchange zone ($\mathcal{P}$=40 mmHg), hemoglobin is almost 75% saturated with oxygen. When the partial pressure of oxygen in the plasma reaches 100 mmHg, almost full hemoglobin saturation occurs; following saturation, oxygen molecules that continue to diffuse into the capillary bed dissolve into plasma. Other means to model hemoglobin saturation such as the Kelman dissociation curve [118] and the MonodWymanChangeux model [119], were used by various researchers [120, 121].

Mass conservation applied to oxygen in the control volume yields:

$$\frac{V_{bc}}{\tau}\left[\Big(\xi_O P_{bOe}(t)+\mathcal{H}_e(t)\Big)-\Big(\xi_O P_{bOi}+\mathcal{H}_i\Big)\right] = \frac{\kappa A(t)\xi_O}{\Psi_O(t)+h(t)/D_{hO}+\zeta e(t)/D_{wO}}\Big(P_O(t)-P^*_{bO}(t)\Big), \tag{4.11}$$

where $\mathcal{H}_i$ and $\mathcal{H}_e(t)$ correspond to $\mathcal{H}(t)$ evaluated at P_{bOi} and $P_{bOe}(t)$ respectively.

Two different scenarios are possible regarding the oxygen partial pressure at the exit $P_{bOe}(t)$ as shown in figure 4.2. In case 1, oxygen in the blood reaches full equilibration with that in the alveolus before exiting, so $P_{bOe}(t) = P_O(t)$. In case 2, equilibration does not occur and blood exits with $P_{bOe}(t) < P_O(t)$. We define the oxygen equilibration ratio $\alpha(t)$ as the length traversed by blood before equilibration would occur divided by the capillary

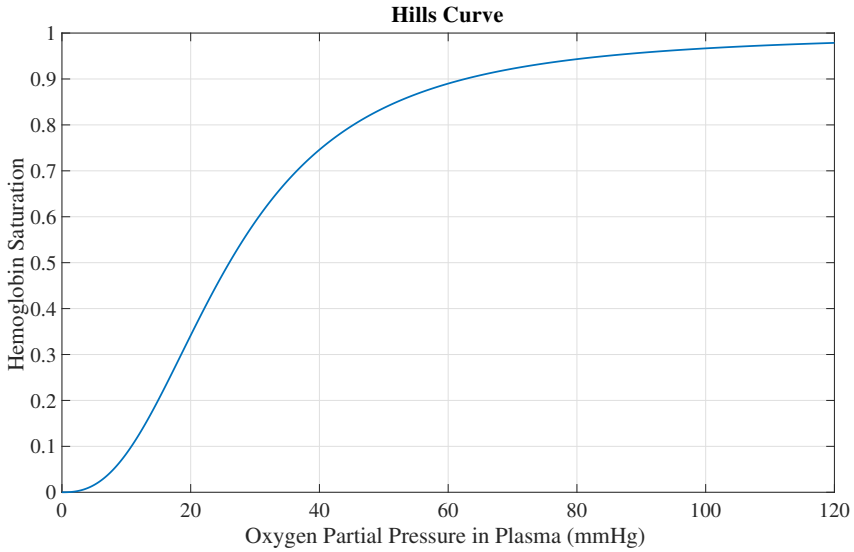

Figure 4.3: Hemoglobin saturation model.

length L_c.

$$\left\{ \begin{array}{cc} 0<\alpha(t)\leq 1 & \text{Case 1} \\ \alpha(t)>1 & \text{Case 2} \end{array} \right\}.$$

The general shape of the oxygen blood partial pressure in a capillary (figure 4.2, see also [115]) allows us to assume that $P_{bO}(s,t)$ changes linearly in the exchange zone. We exploit this information to express the variables $P_{bOe}(t)$ and $P^*_{bO}(t)$ in equation (4.11) as a function of P_{bOi}, $P_O(t)$, and $\alpha(t)$ as will be shown below. We shall use the following notation; the function $f_O(P_{bOi}, P_O(t), \alpha(t))$ describes $P_{bOe}(t)$, and the function $g_O(P_{bOi}, P_O(t), \alpha(t))$ describes $P^*_{bO}(t)$. These have different forms in each one of the cases described above. Equation (4.11) is next specified for each case.

Case 1: $0 < \alpha \leq 1$ (Full equilibration of oxygen)

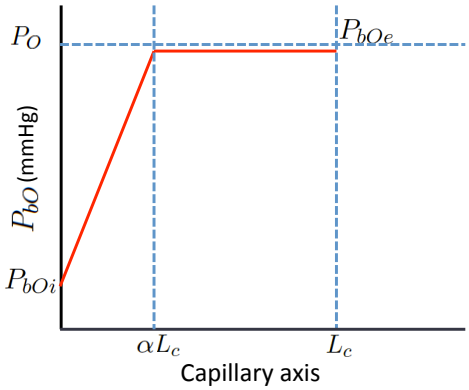

- $P_{bOe}(t) = f_O\Big(P_{bOi}, P_O(t), \alpha(t)\Big) = P_O(t)$
- $P^*_{bO}(t) = g_O\Big(P_{bOi}, P_O(t), \alpha(t)\Big) = P_O(t) + \frac{\alpha}{2}\Big(P_{bOi} - P_O(t)\Big)$ (Found through MVT)

In this case, equation (4.11) can be written as:

$$\frac{V_{bc}}{\tau}\left[\xi_O\Big(P_O(t)-P_{bOi}\Big)+\mathcal{H}_e(t)-\mathcal{H}_i\right]=\frac{\kappa A(t)\xi_O}{\Psi_O(t)+h(t)/D_{hO}+\zeta e(t)/D_{wO}}\alpha(t)\left(\frac{P_O(t)-P_{bOi}}{2}\right). \tag{4.12}$$

Case 2: $\alpha > 1$ (Partial equilibration of oxygen)

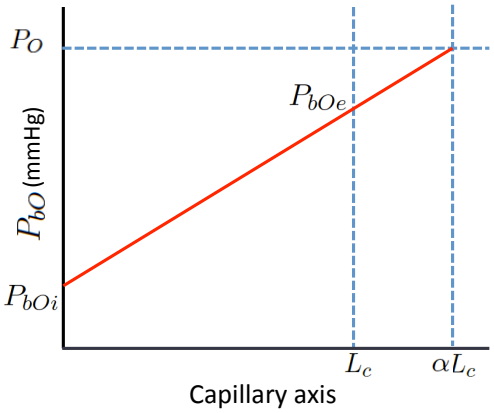

- $P_{bOe}(t) = f_O\Big(P_{bOi}, P_O(t), \alpha(t)\Big) = P_{bOi} + \frac{P_O(t)-P_{bOi}}{\alpha(t)}$
- $P^*_{bO}(t) = g_O\Big(P_{bOi}, P_O(t), \alpha(t)\Big) = P_{bOi} + \frac{P_O(t)-P_{bOi}}{2\alpha(t)}$ (Found through MVT)

In this case, equation (4.11) can be written as:

$$\frac{V_{bc}}{\tau}\left[\frac{\xi_O}{\alpha(t)}\Big(P_O(t)-P_{bOi}\Big)+\mathcal{H}_e(t)-\mathcal{H}_i\right]= \frac{\kappa A(t)\xi_O}{\Psi_O(t)+h(t)/D_{hO}+\zeta e(t)/D_{wO}}\left(\frac{2\alpha(t)-1}{\alpha(t)}\right)\left(\frac{P_O(t)-P_{bOi}}{2}\right). \tag{4.13}$$

An iterative process is followed to know whether equation (4.12) or (4.13) should be solved at a specific time t_1. For example, we can assume that equilibration occurs and solve equation (4.12) for $\alpha(t_1)$. If $0 < \alpha(t_1) \leq 1$, the value is accepted, and if $\alpha(t_1) > 1$, the calculated value is rejected and equation (4.13) is solved instead.

One important point to make here is that in the above, we are considering Bohr's assumption [112, 122], which states that when blood passes through the exchange zone, the alveolar oxygen partial pressure $P_O(t)$ is assumed to be constant; this is a valid assumption because the transit time of blood is much shorter than the breathing period. In addition to $P_O(t)$, the diffusive properties of the respiratory membrane are also be taken to be constant during blood transit time. This assumption will also be applied when modeling carbon dioxide in section 4.3.

4.3 Carbon Dioxide Transport

Carbon dioxide is transported in the blood as a dissolved gas in plasma and as bicarbonate. Considering the same control volume used for oxygen transport above, we apply mass conservation on both mentioned forms of carbon dioxide, which yields:

$$\frac{V_{bc}}{\tau}\left[\xi_C\Big(P_{bCe}(t)-P_{bCi}\Big)+\tilde{C}_e(t)-\tilde{C}_i\right]=\frac{\kappa A(t)\xi_C}{\Psi_C(t)+h(t)/D_{hC}+\zeta e(t)/D_{wC}}\Big(P_C(t)-P^*_{bC}(t)\Big), \tag{4.14}$$

where P_{bCi} is the fixed partial pressure of carbon dioxide at the capillary bed inlet and equal to 45 mmHg [115]. $P_{bCe}(t)$ is the partial pressure of carbon dioxide at the outlet of the capillary bed, and $\tilde{C}_i$ and $\tilde{C}_e(t)$ are the bicarbonate concentrations at the inlets and exits of the capillary bed respectively. Following [116], if we assume that bicarbonate equilibrates quickly, we can take $\tilde{C}$ to be quasi-steady, and relate it to P_{bC} by:

$$\tilde{C}=\frac{K_1}{K_{-1}[H^+]}\xi_C P_{bC}, \tag{4.15}$$

where $[H^+]$ is the concentration of hydrogen ions in the blood and is considered constant, and K_1 and K_{-1} are the forward and backward rates of the chemical reaction:
$CO_2+H_2O\underset{K_{-1}}{\overset{K_1}{\rightleftharpoons}}HCO_3^-+H^+$.

Equation (4.14) can then be written as:

$$\frac{V_{bc}}{\tau}\left(1+\frac{K_1}{K_{-1}[H^+]}\right)\Big(P_{bCe}(t)-P_{bCi}\Big)=\frac{\kappa A(t)}{\Psi_C(t)+h(t)/D_{hC}+\zeta e(t)/D_{wC}}\Big(P_C(t)-P^*_{bC}(t)\Big). \tag{4.16}$$

Figure 40-6 in [115][2] represents how the carbon dioxide partial pressure normally changes along the capillary. We choose $\beta(t)$ to define the carbon dioxide equilibration ratio, which is the length required for carbon dioxide equilibration divided by the capillary length L_c. We exploit the exponential nature of the curve to express $P_{bC}(s,t)$ at a fixed time as:

$$P_{bC}(s,t)=P_C(t)+\Big(P_{bCi}-P_C(t)\Big)\left(\frac{\epsilon P_C(t)}{P_{bCi}-P_C(t)}\right)^{s/\beta(t)L_c}, \tag{4.17}$$

where ϵ is a small parameter defined by

$$\epsilon=\frac{P_{bC}(\beta L_c,t)}{P_C(t)}-1. \tag{4.18}$$

It is set to 0.001, which means that full equilibration occurs at the location where $P_C(t)$ is 99.9% of the carbon dioxide partial pressure in the capillary. Both cases of partial and full

[2]Figure is not reproduced here because permission to reproduce was not requested.

equilibration (figures 4.4 and 4.5) can be lumped together here. We use equation (4.17) to find $P_{bCe}(t)$ and $P^*_{bC}(t)$:

$$P_{bCe}(t) = P_C(t) + \Big(P_{bCi} - P_C(t)\Big)\left(\frac{\epsilon P_C(t)}{P_{bCi} - P_C(t)}\right)^{1/\beta(t)},$$

$$P^*_{bC}(t) = P_C(t) + \beta(t)\frac{P_{bCi} - P_C(t)}{ln\Big(\frac{\epsilon P_C(t)}{P_{bCi} - P_C(t)}\Big)}\left(\left(\frac{\epsilon P_C(t)}{P_{bCi} - P_C(t)}\right)^{1/\beta(t)} - 1\right).$$

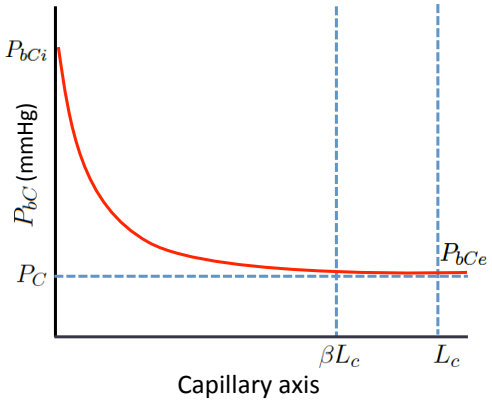

Figure 4.4: Full Equilibration of Carbon Dioxide.

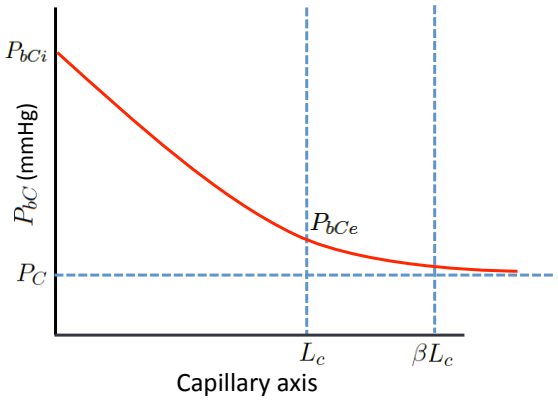

Figure 4.5: Partial Equilibration of Carbon Dioxide.

Given the small difference between the magnitudes of P_{bCi} and $P_C(t)$ (≈ 5 mmHg), back diffusion of carbon dioxide might occur for a short period of time over the course of breathing if $P_C(t)$ exceeds P_{bCi}. In that case, if we also assume $P_{bC}(s,t)$ to have an exponential form, we get the following relations:

$$P_{bC}(s,t) = P_C(t) + \Big(P_{bCi} - P_C(t)\Big)\left(\frac{\epsilon P_C(t)}{P_C(t) - P_{bCi}}\right)^{s/\beta(t)L_c}, \tag{4.19}$$

$$P_{bCe}(t) = P_C(t) + \Big(P_{bCi} - P_C(t)\Big)\left(\frac{\epsilon P_C(t)}{P_C(t) - P_{bCi}}\right)^{1/\beta(t)},$$

$$P^*_{bC}(t) = P_C(t) + \beta(t)\frac{P_{bCi} - P_C(t)}{ln\Big(\frac{\epsilon P_C(t)}{P_C(t) - P_{bCi}}\Big)}\left(\left(\frac{\epsilon P_C(t)}{P_C(t) - P_{bCi}}\right)^{1/\beta(t)} - 1\right).$$

The formulation of the alveolar model is now complete. We next couple the equations derived in chapters 3 and 4 to study different cases of breathing. This is covered in chapter 5.

Chapter 5

Alveolar Model - Results and Discussion

In this chapter, the alveolar model developed in chapters 3 and 4 is used to study different aspects of breathing that shed light on the importance of surfactants.

First, we present a base case where we show and discuss the different outputs of the alveolar model. Next, we study how the alveolus behaves in multiple test cases related to breathing. These include holding breath, impairing gas exchange, and breathing on the summit of Mount Everest. The case of lung collapse caused by the absence of surfactants from the lung is also shown.

The remainder of the chapter is devoted to showing the importance of the surfactant system during breathing. We do so by varying different surfactant properties and analyzing how gas exchange between the alveolus and the passing blood stream is affected. Changing the adsorption, desorption and diffusion charactesitics of surfactants are all considered. In addition, the effect of the interfacial resistance on gas exchange is examined. Also, expressions to evaluate the microscale work of breathing at the level of the alveolus are derived in this chapter and used when comparing different surfactants. The model is also used to study the roles that the different surfactant components play in breathing. The performance of each surfactant fraction is evaluated based on the area it offers for gas exchange and the microscale breathing work that it requires. Breathing cadence and the depth at which we breathe are two very important factors. For any given surfactant, the alveolar model affords the chance to build diagrams that we label as *Operating Breathing Space* diagrams. Every point on such diagram represents a mode of breathing (combination of breathing period and pleural pressure amplitude). For each mode, the breathing work exerted per minute and the available area for gas exchange are given.

The set of model parameters used is each case presented below is shown in appendix C. It is worth noting that in sections 5.1 to 5.3, exchange of surfactants between the bulk and

the interface is governed by Langmuir kinetics at all times. This corresponds to the first regime of the pulmonary surfactant model presented in section 2.4. We believe that doing so makes it clearer to understand the effect of the different surfactant properties (k_a, D_s, etc.). In the remainder of the chapter, when physiological pulmonary surfactants are studied, the full pulmonary surfactant model of section 2.4 is used (all three regimes).

5.1 Base Case

In this section, we show the main outputs of the model. All shown results are obtained after steady state solution is reached. We plot the outputs of the 18^{th} and 19^{th} periods. We first show how the mass fractions of the different components of the gas mixture in the alveolus, namely oxygen, carbon dioxide and nitrogen, vary with time.

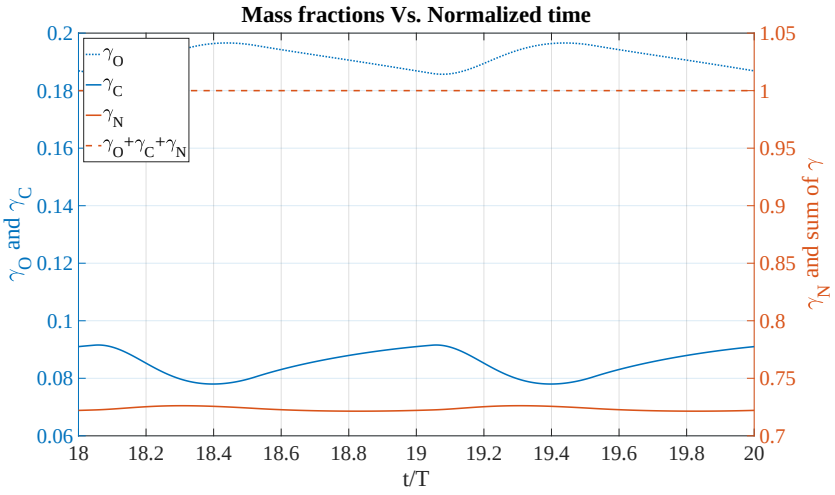

Figure 5.1: Variation of the mass fractions of the components of the alveolar gas mixture over a breathing cycle.

Next, the alveolar radius is shown to oscillate between $152\mu m$ and $170\mu m$, which corresponds to around 11% radial expansion, or 25% area expansion. This is in agreement with the literature findings about the expansion of the lung area during breathing, which is recorded to be in the range of $20 - 30\%$ [9].

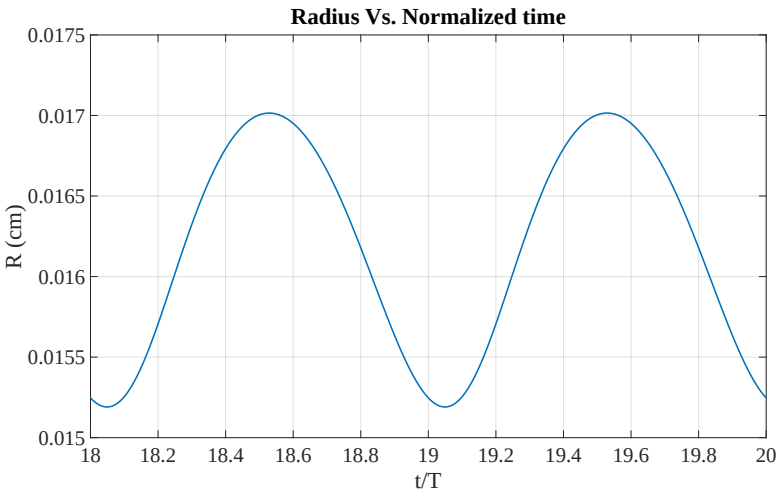

Figure 5.2: Variation of the alveolar radius over a breathing cycle. It is shown to increase by 11% during inhalation.

The interfacial surfactant concentration $\Gamma(t)$ is shown in figure 5.3 along with $\Gamma_{eq}(t)$. Figure 5.4 shows snapshots of the (steady-state) periodic variation of surfactant bulk concentration in the hypophase, over the course of a period of expansion/contraction. Time runs in order of increasing curve density from pale gray to black. The bulk surfactant field is plotted with respect to the three different Lagrangian and Eulerian mappings discussed in appendix B.

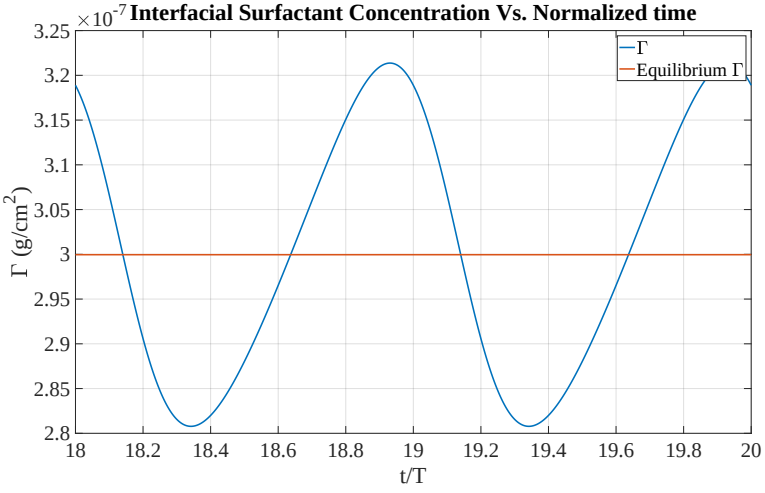

Figure 5.3: Interfacial surfactant concentration variation during breathing. Adsorption and desorption occur as indicated by the relative magnitudes of $\Gamma(t)$ and $\Gamma_{eq}(t)$.

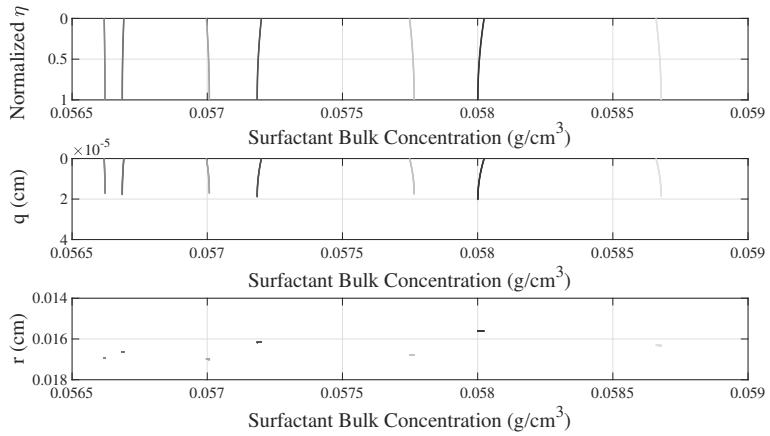

Figure 5.4: Top figure shows the Lagrangian description of the surfactant bulk concentration at various breathing times. Middle figure shows the Eulerian description, where the hypophase-gas interfaces are superposed for each curve at depth 0; change in hypophase thickness is clear. Bottom figure shows the bulk surfactant concentration as a function of the spatial radial coordinate r. The three mappings are explained in appendix B

.

The total number of surfactants is also plotted to verify the conservation of the surfactant species during the exchange between the bulk and the interface.

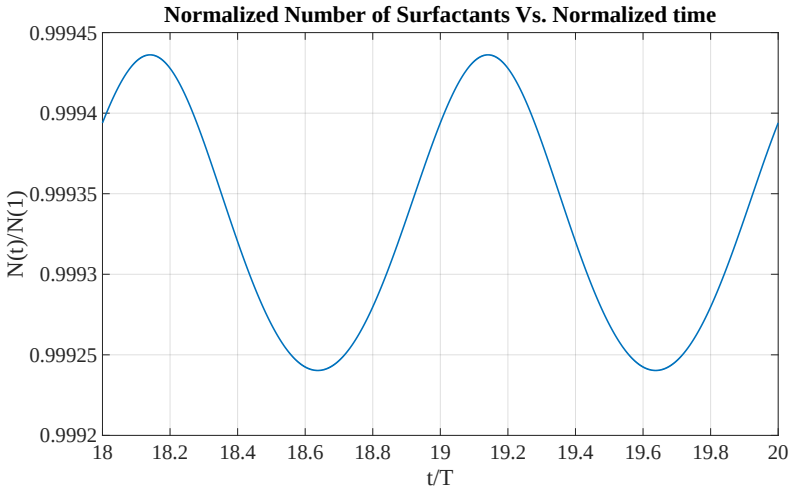

Figure 5.5: Number of surfactants is conserved over the course of breathing.

As previously discussed, surfactant dynamics affect the surface tension values at the interface. The resulting surface tension is plotted against the interfacial area in figure 5.6. Hysteresis occurs because of the different rates of surfactant adsorption and desorption during expansion and contraction of the alveolus. This hysteresis is believed to be the major source of the hysteresis observed in respiratory pressure-volume diagrams. It is important

to emphasize that pulmonary surfactants are able to decrease surface tension further as explained in section 2.4. As mentioned previously, in this set of results, we only include the first regime of the pulmonary surfactant model, and so a big decrease in surface tension is not captured when the surfactant film compresses. The interfacial resistance due to surfactants populating the interface is also plotted in figure 5.7. As can be seen, the interfacial resistance is at a maximum when the interfacial surfactant concentration is highest.

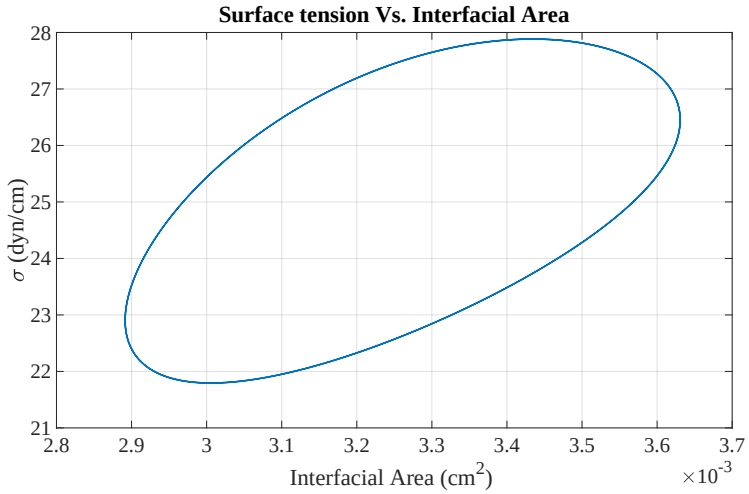

Figure 5.6: Hysteresis is apparent when surface tension is plotted against interfacial area.

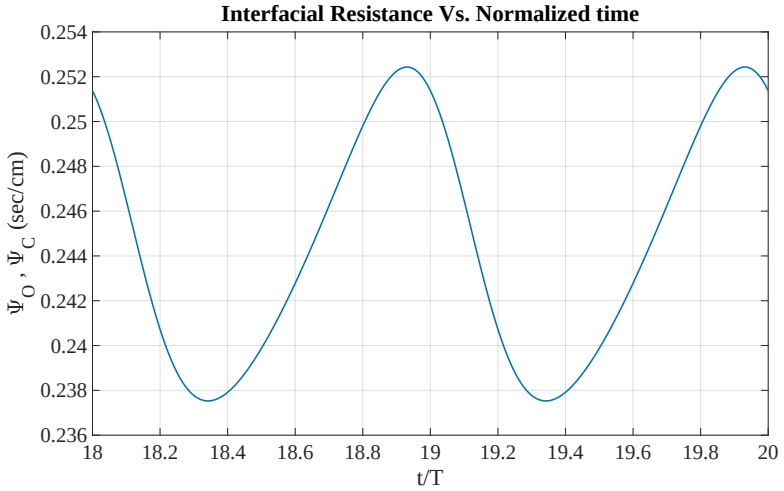

Figure 5.7: Interfacial resistance variation according to the model given in equation (4.4)

..

In addition to surface tension, the hoop stress in the alveolar wall affects the elastic recoil of the lung. The hoop stress variation with time as obtained from the model developed in

section 3.5 is plotted in figure 5.8. The values of the stress obtained is of the same order of those reported in the literature [94, 95, 123].

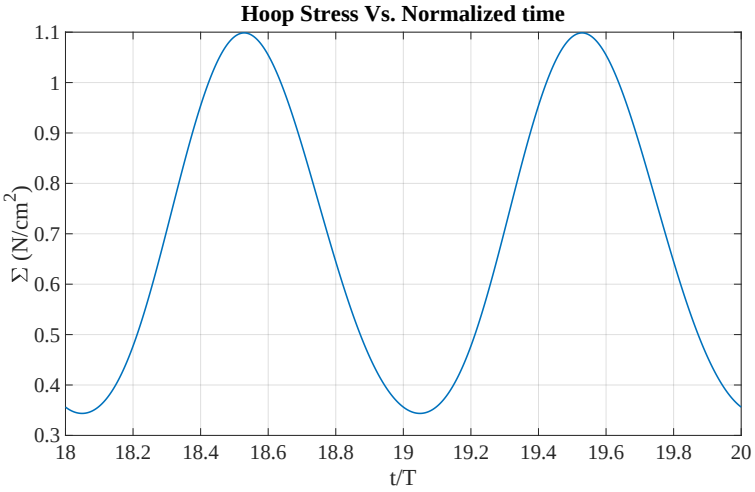

Figure 5.8: Variation of hoop stress with time.

Below, we show the behavior of some of the variables related to gas exchange between the alveolus and the passing bloodstream. Figure 5.9 shows how the partial pressure of oxygen in the alveolus and the homogenized oxygen partial pressure in the blood stream vary with time. Also, it is apparent from the relative magnitudes of both partial pressures that oxygen diffuses from the alveolus to the blood at all times over the course of a breathing period. This large difference is mainly due to the action of hemoglobin molecules that act as sinks to oxygen and maintain a pressure gradient between the alveolus and passing blood. The values of $P_O(t)$ here and throughout the dissertation are of similar magnitudes to those reported in the literature [121], [124].

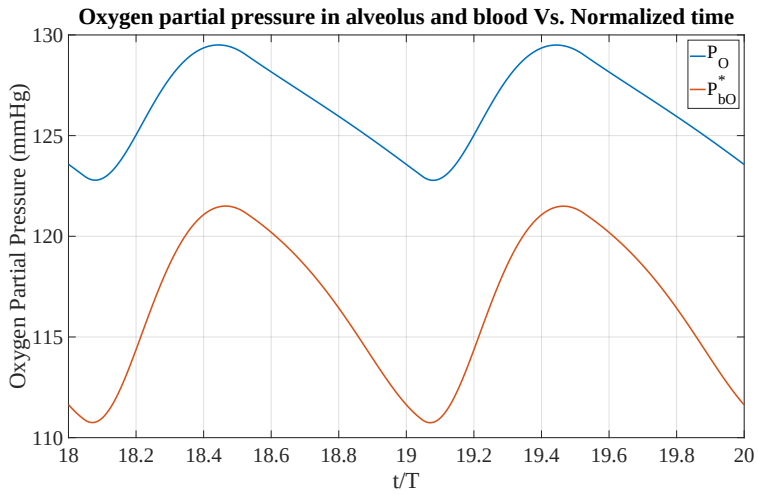

Figure 5.9: Alveolar and blood (homogenized) oxygen partial pressure over a breathing cycle. A large pressure gradient between the alveolus and passing blood stream exists.

In addition, the partial pressure of oxygen at the exit of the capillaries is plotted in figure 5.14. Because hemoglobin saturation occurs at an oxygen partial pressure of about 100 mmHg as shown in figure 4.3, all blood leaving the alveolus has enough oxygen to distribute to body tissues. It also appears that in this case, oxygen in the blood is equilibrating with that in the alveolus before exiting. The fraction of the capillary length that the blood traverses before reaching equilibration is shown in figure 5.11. It is worth noting that α is lowest at maximum alveolar radius and minimum interfacial resistance. In other words, oxygen is equilibrating faster when larger area is available for gas exchange and when resistance to gas transfer is lowest. The average measured values of α are around 1/3, which is around the same order of the model predicted one [112]. As seen later, when different parameters are considered in certain cases, α can retain values closer to the measured ones. The mass flux of oxygen is also shown in figure 5.12.

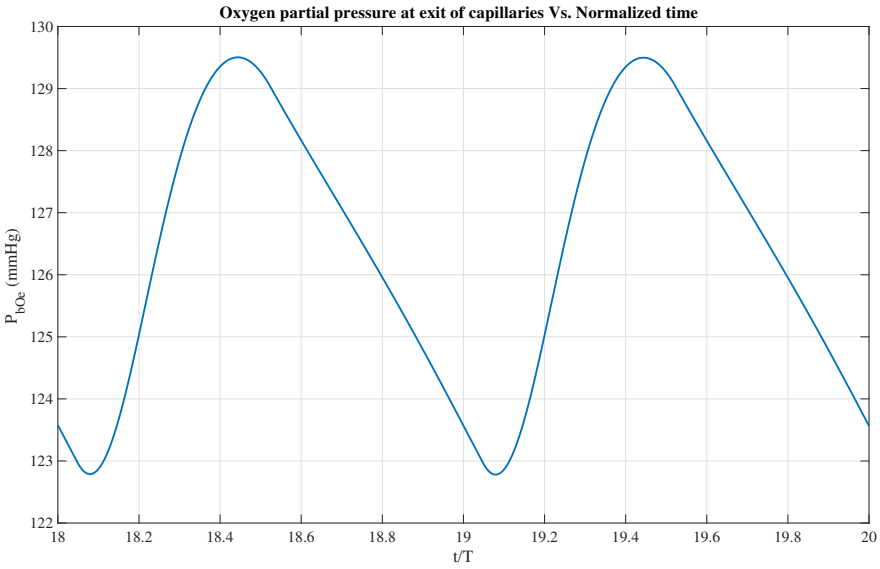

Figure 5.10: Partial pressure of oxygen at capillary exit is equilibrated with that in the alveolus.

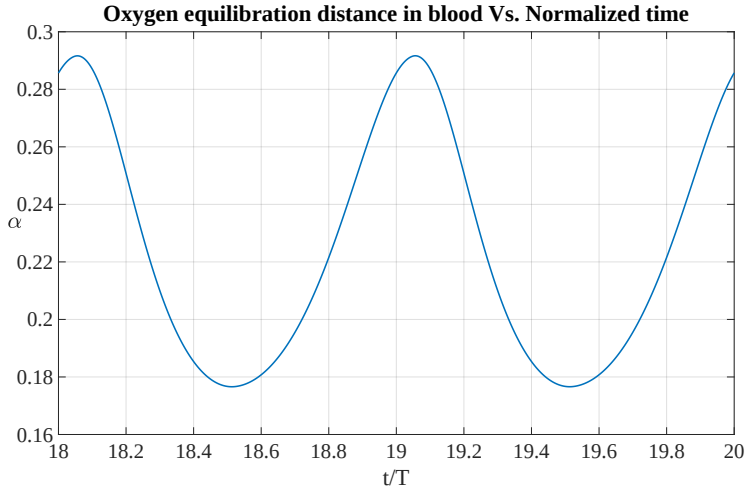

Figure 5.11: $\alpha(t)$ is smaller than one signaling equilibration of oxygen pressure over the course of breathing.

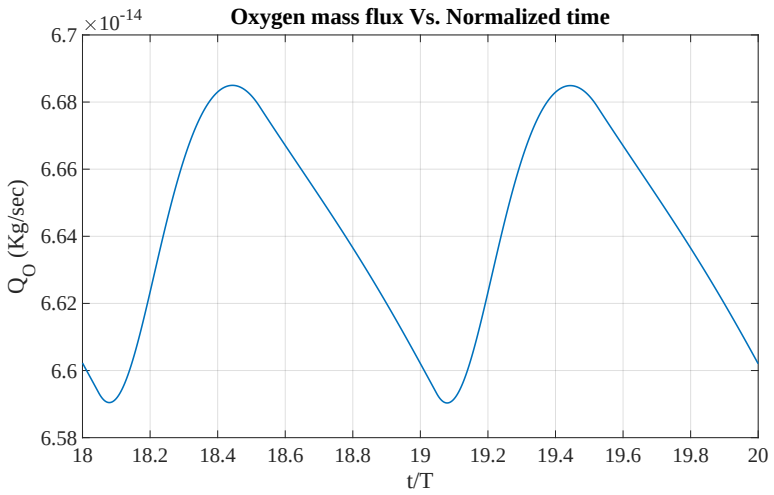

Figure 5.12: Oxygen flux from alveolus to blood passing through the exchange zone.

Figure 5.13 shows the time variation of the partial pressure of carbon dioxide in the alveolus and the homogenized carbon dioxide partial pressure in the blood stream. Like oxygen, the calculated values of carbon dioxide here and throughout are similar to those measured and reported in literature [121, 124]. Unlike oxygen however, a very slight margin exists between the carbon dioxide partial pressures in the alveolus and the blood. In some cases, back diffusion from the alveolus to the blood might occur. This only happens for very short fractions of the breathing period, and the net carbon dioxide transfer over a period is always from the blood to the alveolus.

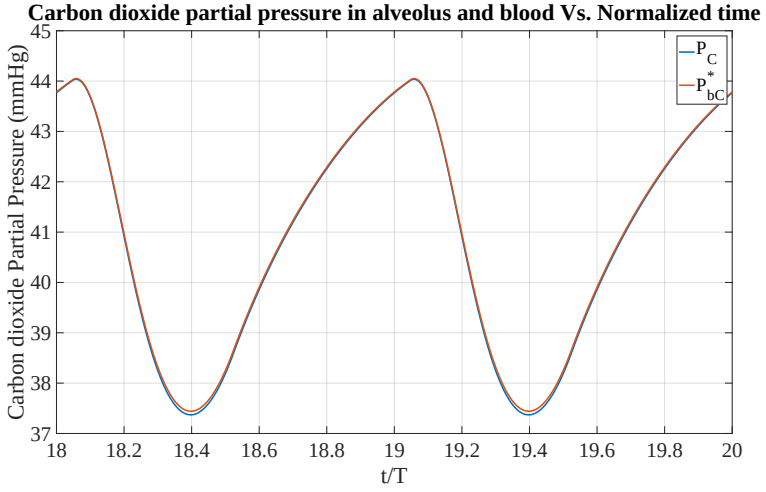

Figure 5.13: Partial pressure of carbon dioxide in alveolus and blood (homogenized) over a breathing cycle. A minor pressure gradient between the alveolus and passing blood stream exists.

The pressure of carbon dioxide at the exit of capillaries and the carbon dioxide equili-

bration ratio β are also plotted. Our model predicts much lower values of β as compared to α. This is an agreement with [125], where it is stated that the diffusional equilibration of carbon dioxide is much faster than that of oxygen. The actual value of β however needs further investigation. The carbon dioxide mass flux is also plotted.

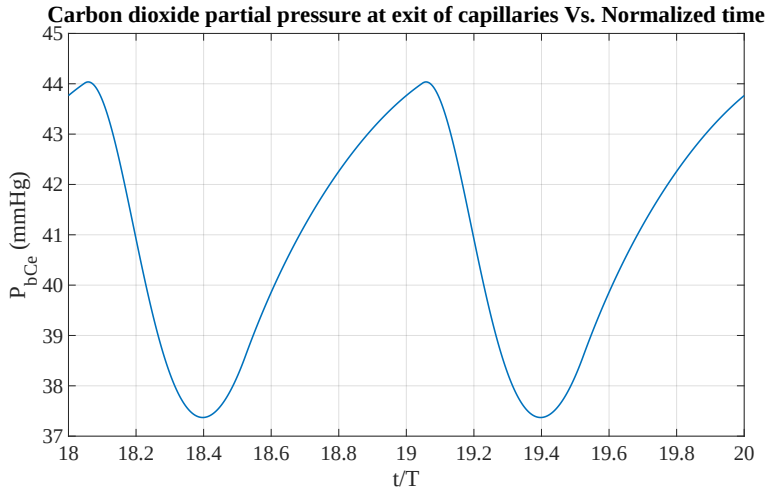

Figure 5.14: Partial pressure of carbon dioxide at capillary exit is equilibrated with that in the alveolus.

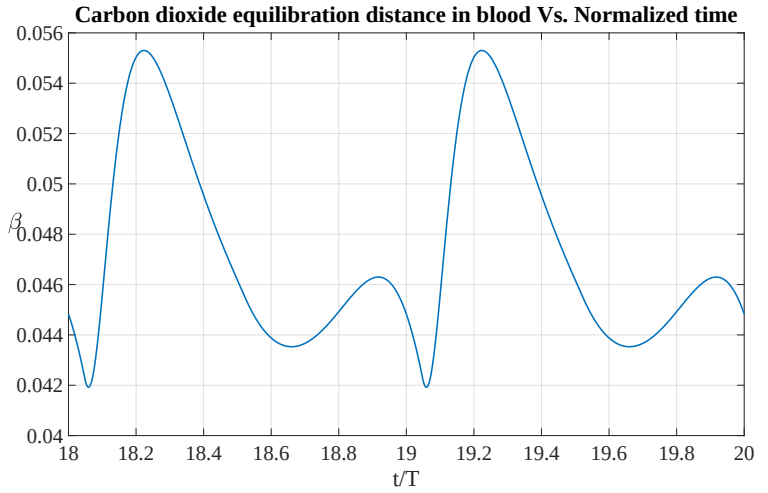

Figure 5.15: $\beta(t)$ is smaller than one signaling equilibration of carbon dioxide pressure over the course of breathing.

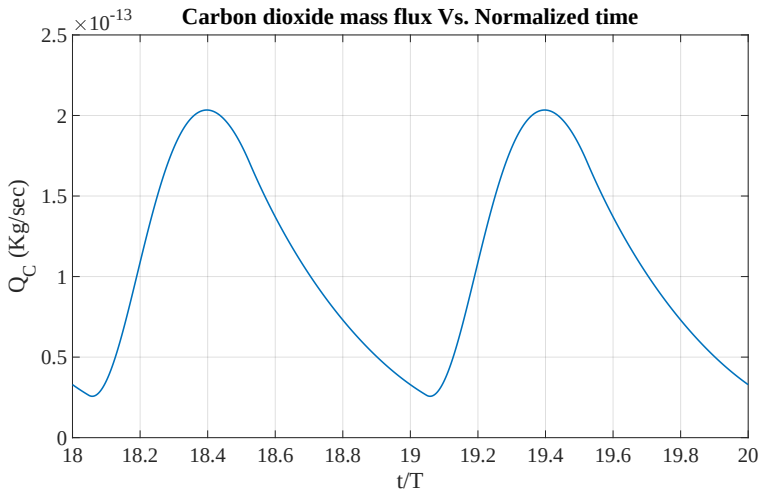

Figure 5.16: Carbon dioxide flux from alveolus to blood passing through the exchange zone.

5.2 Case Studies

In this section, the alveolar model is used to study interesting scenarios related to breathing such as holding breath, and breathing at high altitudes. It is important to note that in what remains of chapter 5, the constitutive relation of the alveolar wall stress given by equation (3.39) is replaced by that of an ideal spring. More information is provided in appendix C.

5.2.1 Holding Breath

The effect of holding breath is studied. We do so by suppressing changes in the pleural pressure at the end of inhalation. As can be seen in figure 5.17, the radius increases due to inhalation and then reaches a maximum constant value. At that instant, the pressure differential across the alveolus and the forces due to the elastic recoil are in equilibrium.

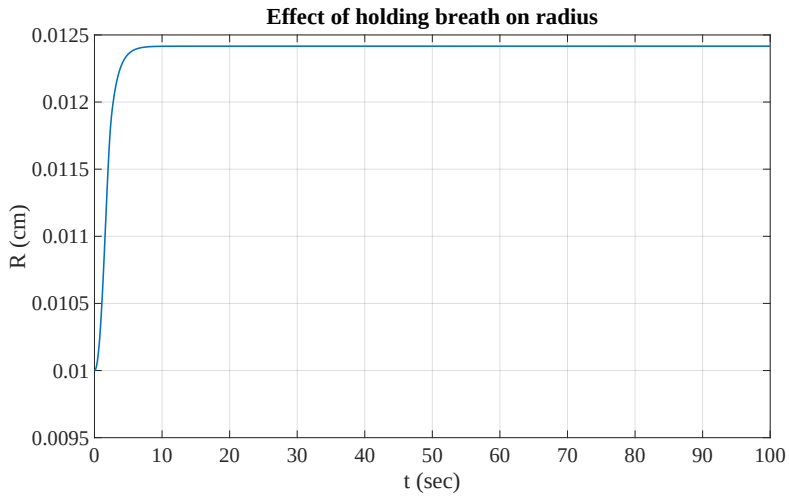

Figure 5.17: Alveolar radius increases with inhalation and then becomes constant because of holding the breath.

As expected, over the course of time, the alveolar oxygen partial pressure decays to that at the capillary entrance. Subsequently, oxygen flux from the alveolus to the blood stream decays to zero.

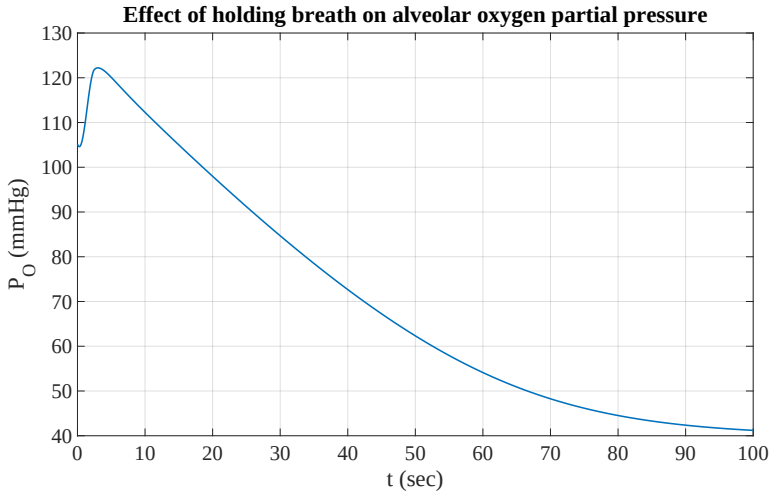

Figure 5.18: When holding breath, oxygen partial pressure in the alveolus decays to that at the capillary inlet.

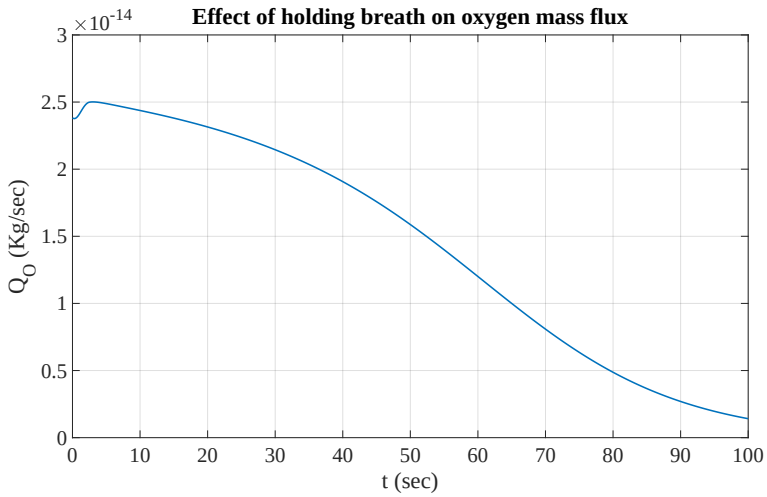

Figure 5.19: Oxygen diffusion drops to zero when holding breath because of the elimination of the pressure gradient in oxygen between the alveolus and the passing blood stream.

Similar trends are observed for carbon dioxide. The carbon dioxide partial pressure in the alveolus converges to that at the capillary inlet, and the carbon dioxide flux drops to zero.

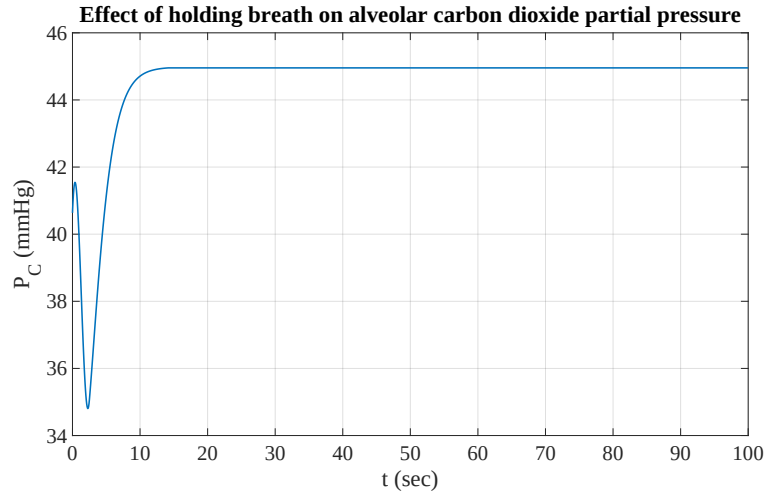

Figure 5.20: When holding breath, carbon dioxide partial pressure in the alveolus converges to that at the capillary inlet.

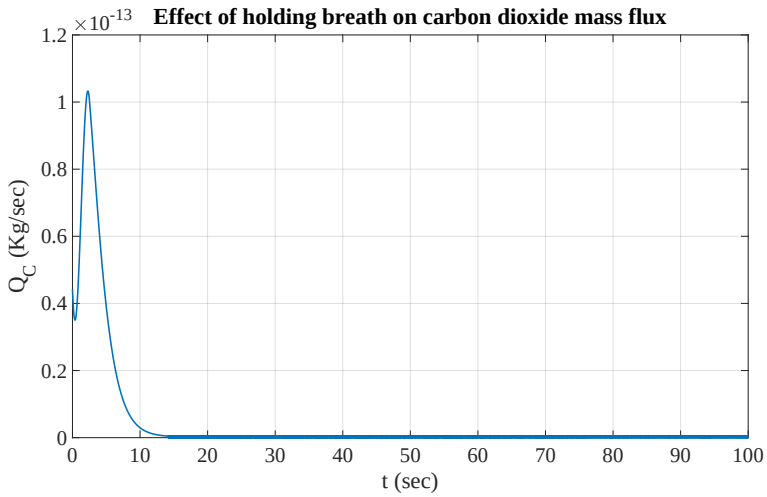

Figure 5.21: Carbon dioxide diffusion drops to zero when holding breath because of the elimination of the pressure gradient in carbon dioxide between the alveolus and the passing blood stream.

5.2.2 Suppressing Gas Exchange

Now, we model the case where gas exchange is impaired in the lung. We suppress gas exchange by setting the fraction of the alveolar area participating in gas exchange κ to a near zero value. As expected, the partial pressure of oxygen builds up and converges to the maximum value $\overline{\gamma_O}\frac{M_G}{M_O}(P_{atm} - P_V)$. The partial pressure of oxygen at the alveolar exit is also plotted and shown to have very minor oscillations above the value corresponding to the partial pressure at the capillaries' inlet. The two values are not exactly the same because κ was not set to exactly zero. Another variable worth looking at is α, which shoots to very high magnitudes due to the absence of gas exchange, and consequently absence of equilibration.

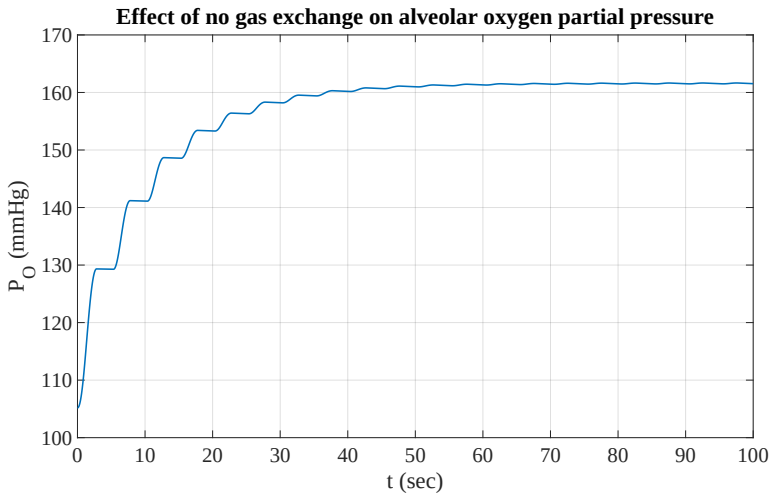

Figure 5.22: When gas exchange is suppressed, oxygen partial pressure in the alveolus converges to its maximum value set by the oxygen mass fraction at the alveolar opening $\overline{\gamma_O}$.

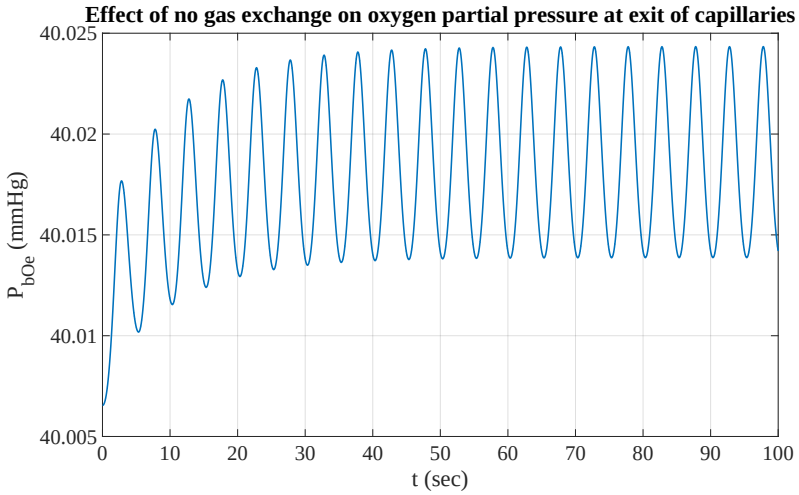

Figure 5.23: Oxygen partial pressure at capillary exit is almost equal to that at capillary inlet.

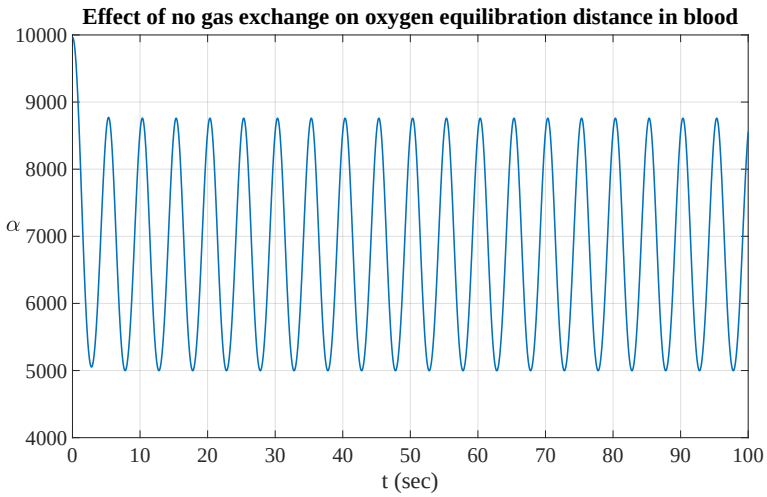

Figure 5.24: Oxygen equilibration ratio $\alpha(t)$ shoots to high magnitudes due to absence of gas exchange.

The same behavior is observed for carbon dioxide. Its partial pressure in the alveolus converges to $\overline{\gamma_C}\frac{M_G}{M_C}(P_{atm} - P_V)$, and its partial pressure at the capillary exit is very close to that at the capillary inlet. β has a similar behavior as α.

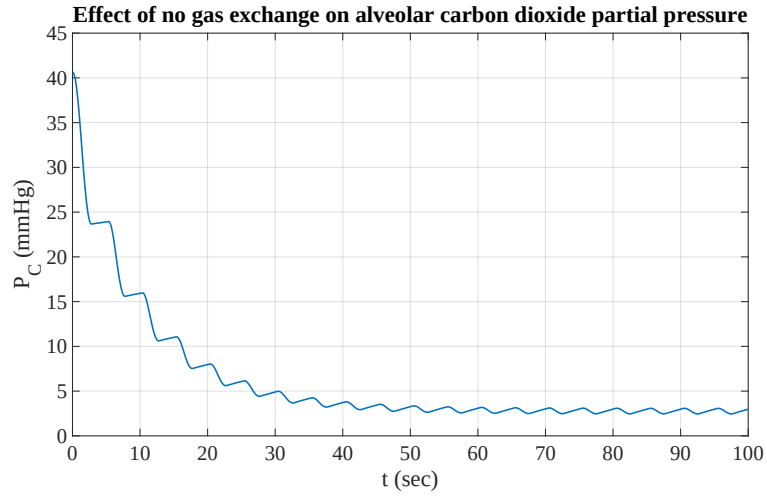

Figure 5.25: When gas exchange is suppressed, carbon dioxide partial pressure in the alveolus converges to the value set by the carbon dioxide mass fraction at the alveolar opening $\overline{\gamma_C}$.

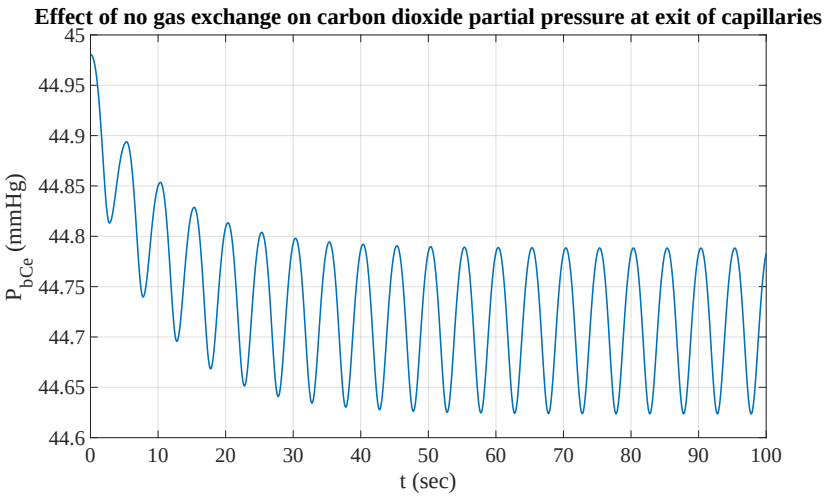

Figure 5.26: Carbon dioxide partial pressure at capillary exit is almost equal to that at capillary inlet.

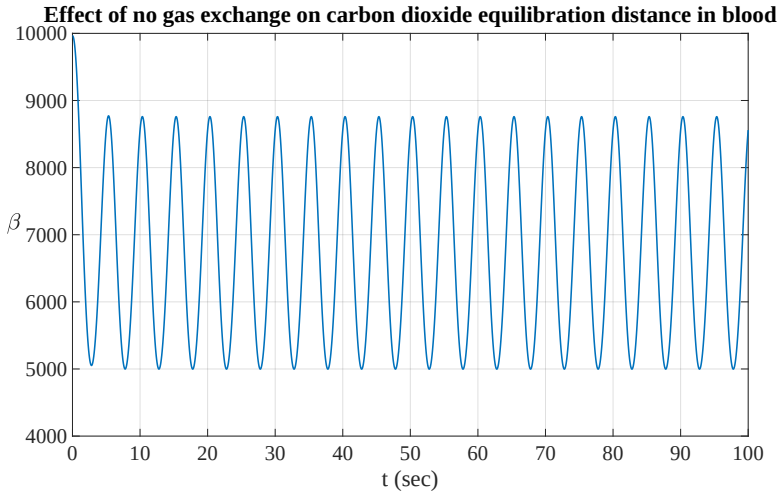

Figure 5.27: Carbon dioxide equilibration ratio $\beta(t)$ shoots to high magnitudes due to absence of gas exchange.

5.2.3 Breathing at the Summit of Mount Everest

In this section, we study the effect of breathing at high altitudes. We consider the summit of mount Everest as an example and inspect how certain variables pertaining to gas exchange vary when humans breathe in such location. Figure 5.28 shows the estimated oxygen partial pressure in the alveolus and blood for a breathing period of five seconds. The homogenized partial pressure of oxygen in the blood passing through the exchange zone is shown to oscillate around 26 mmHg. This is consistent with the measure values reported in [126]. Referring to figure 4.3 that shows the hemoglobin saturation model used earlier, we observe

that only 50% of hemoglobin is saturated with oxygen. This offers an explanation to why climbers of mount Everest often suffer from hypoxia.

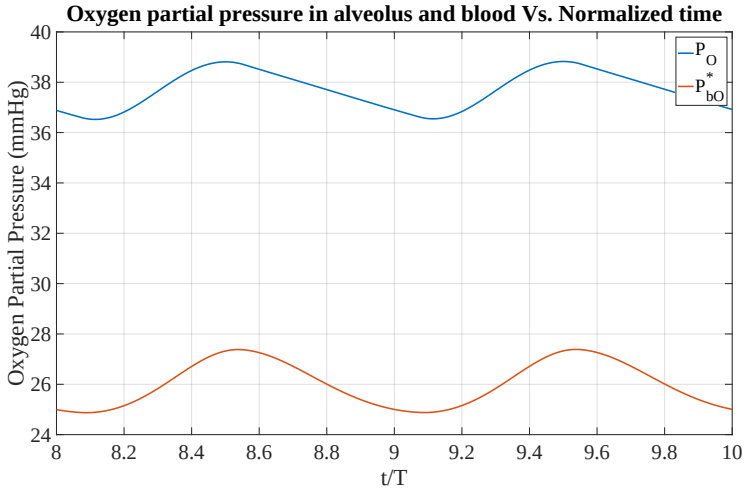

Figure 5.28: Avelolar partial pressures of oxygen in the alveolus and blood are much lower than those observed when breathing at the coast. This is mainly due to the difference in atmospheric pressure between the two locations and consequently the difference in oxygen content in air.

The effect of breathing at a faster rate is also simulated to test its effect on oxygen levels in the blood. Results show that when the breathing period is reduced from 5 to 0.5 seconds, a substantial increase in oxygen flux from the alveolus to the blood occurs (figure 5.29). This causes an increase in the oxygen partial pressure from an average of 30 mmHg to 34 mmHg at capillary exit as can be seen in figure 5.30. This increase in oxygen partial pressure corresponds to an increase from 58% to 66% in hemoglobin saturation.

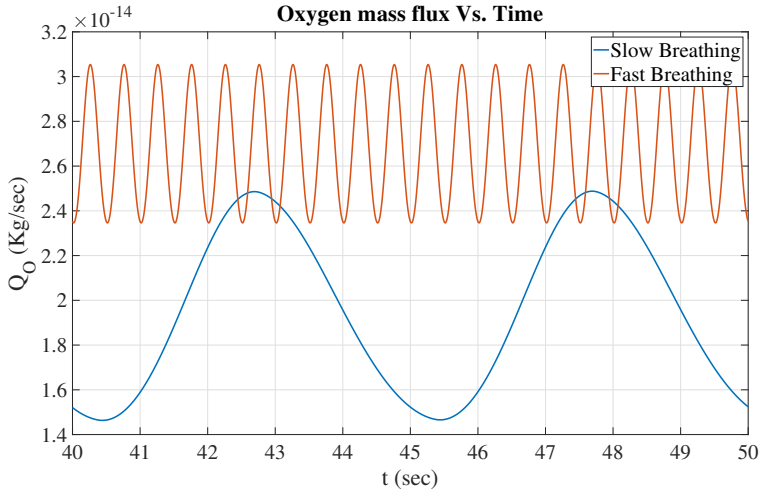

Figure 5.29: Faster breathing leads to an increased oxygen flux from alveolus to capillary bed.

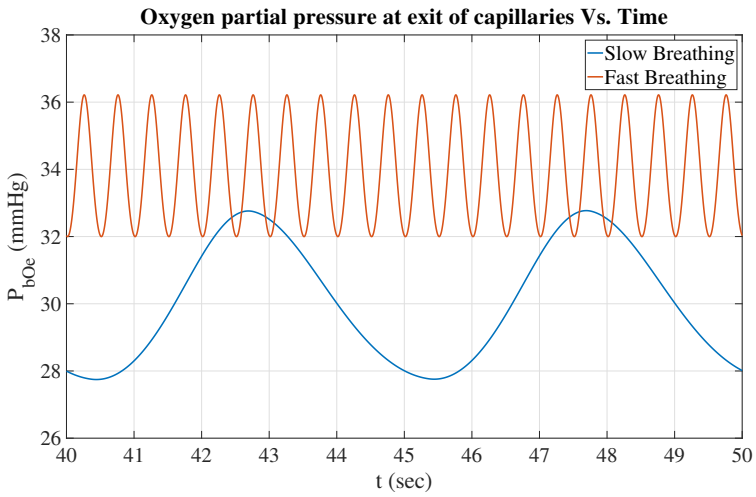

Figure 5.30: The increased oxygen flux results in higher oxygen partial pressures at capillary exit in the case of fast breathing. This is accompanied by a 6 % increase in hemoglobin saturation.

5.2.4 Missing Surfactants

In section 5.3, the effect of the surfactant system's different time scales on breathing will be studied. First, we would like to investigate what happens in the case of surfactants missing from the lung. We set the surface tension value to be constant at 70 (dyn/cm) as shown in figure 5.31. As the pleural pressure drops for inhalation to occur, the elastic recoil due to the high surface tension forces counteracts the increase in the alveolar radius. High surface tension causes the internal pressure of the gas mixture inside the alveolus to build up (figure 5.32) to values that are at least an order of magnitude higher than those achieved in regular breathing ($\approx \pm 1$ cmH_2O). The high elastic recoil consequently causes the alveolus to collapse as seen in figure 5.33.

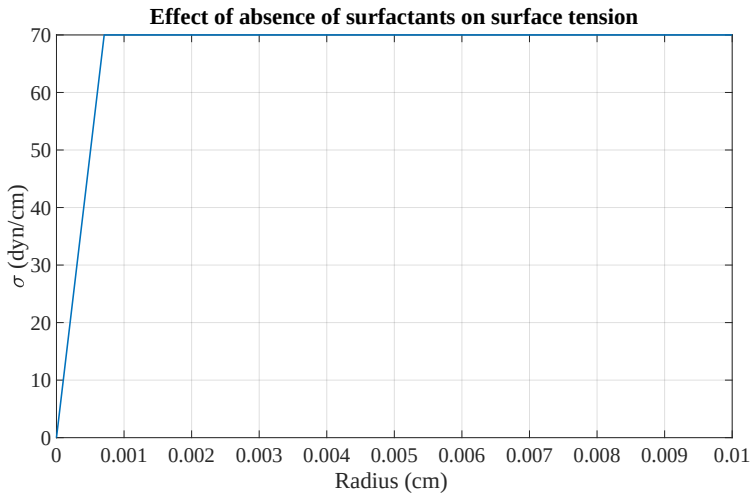

Figure 5.31: Surface tension is set to 70 (dyn/cm) when surfactants are missing. Start of breathing is on the right end of the figure at $R = 0.01$ cm. Surface tension value drops to zero because of alveolar collapse as shown in figure 5.33.

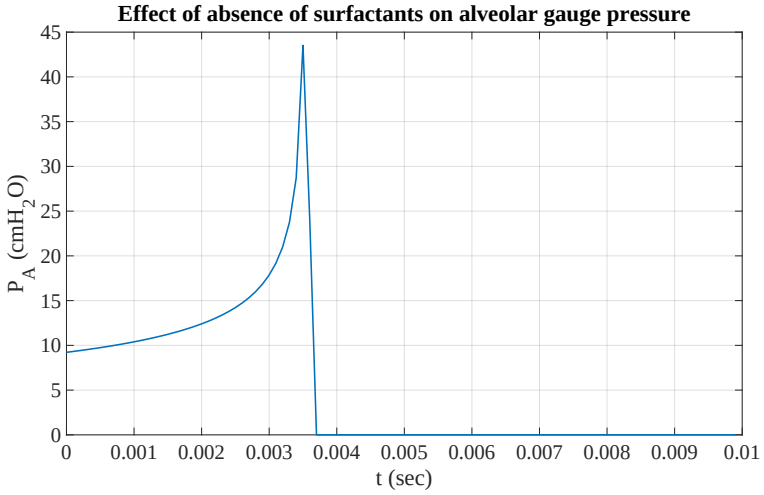

Figure 5.32: Elastic recoil is large because of large surface tension. This leads to an enormous pressure buildup inside the alveolus.

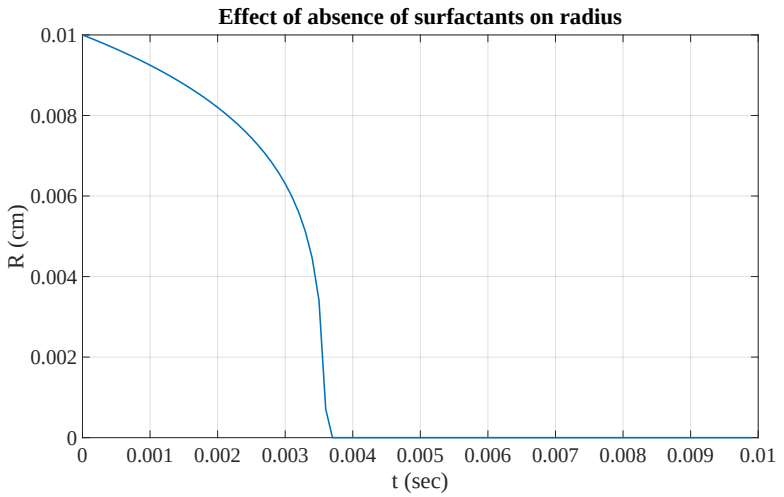

Figure 5.33: Large alveolar pressure causes air to exit the alveolus leading to its collapse.

5.3 Effect of Surfactant Properties

In this section, we perform test cases to show the impact of surfactants on the mechanics of breathing. All parameters in the model are kept fixed and only those corresponding to the surfactant system are varied. First, three surfactants with varying P_1 and P_2 are tested. P_1 and P_2 were defined in subsection 2.3.2 as the ratios of breathing timescale to adsorption time scale, and breathing timescale to desorption timescale respectively. Next, we study the effect of varying P_3, defined in section2.3.2 as the ratio of breathing timescale to diffusion timescale. At the end of this section, we analyze the effect of the interfacial resistance on breathing.

5.3.1 Effect of Adsoroption and Desorption

We vary the adsorption and desorption constants k_a and k_d for three surfactants, and study their effect on our model. Table 5.1 shows the used values of k_a and k_d. The ratio of k_a to k_d, the total number of surfactants, and the breathing and diffusion timescales in the three cases are kept constant. Hence, only the ratios of timescales P_1 and P_2 are varied.

Values of k_a and k_d			
Surfactant	k_a (ml/(g sec))	k_d (1/sec)	$\frac{k_a}{k_d}$(ml/g)
Surfactant A	3	0.000025	120000
Surfactant B	30	0.00025	120000
Surfactant C	300	0.0025	120000

Table 5.1: Values of adsorption and desorption coefficients of the three considered surfactants.

The interfacial surfactant concentration is plotted in figure 5.34. The shown behavior of the surfactants is similar to the one reported in figure 2.16.

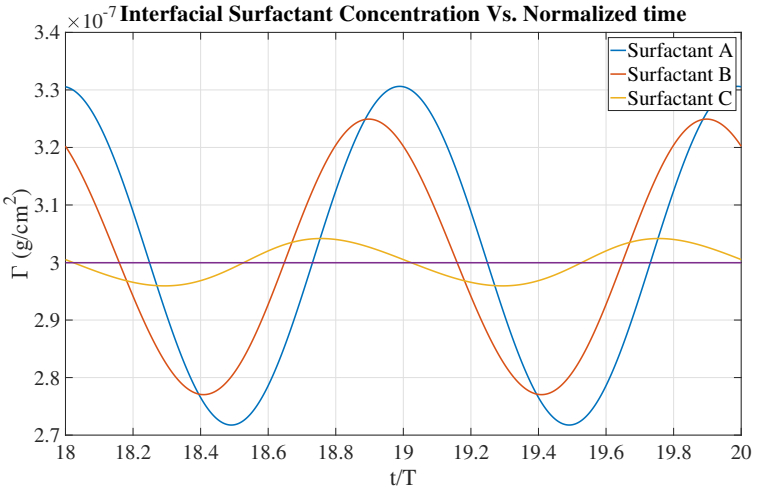

Figure 5.34: Interfacial surfactant concentration of surfactant C deviates the least from Γ_{eq} because of its large adsorption and desorption coefficients.

The resulting surface tension for the three surfactants is plotted in figure 5.35. Because the interfacial concentration of surfactant C deviates only slightly from Γ_{eq}, the corresponding surface tension is approximately always equal to the equilibrium surface tension value $\sigma_{eq} = 25$ dyn/cm. The surface tension of surfactant A on the other hand deviates from σ_{eq} the most, as expected. Figure 5.36 shows how the alveolar radius changes for each surfactant. It is interesting to note that surfactant C allows the largest alveolar expansion because it attains the lowest surface tension value during inhalation as compared to surfactants A and B. However, surfactant C also causes the lowest alveolar radius value because it has the highest surface tension value during exhalation as shown in figure 5.35. This is not desirable as it may cause alveolar instability and collapse. As explained in section 2.4, pulmonary surfactants have the ability to freeze below σ_{eq}, which suppresses their desorption from the interface and causes a large decrease of surface tension. This will be explored later in section 5.5.

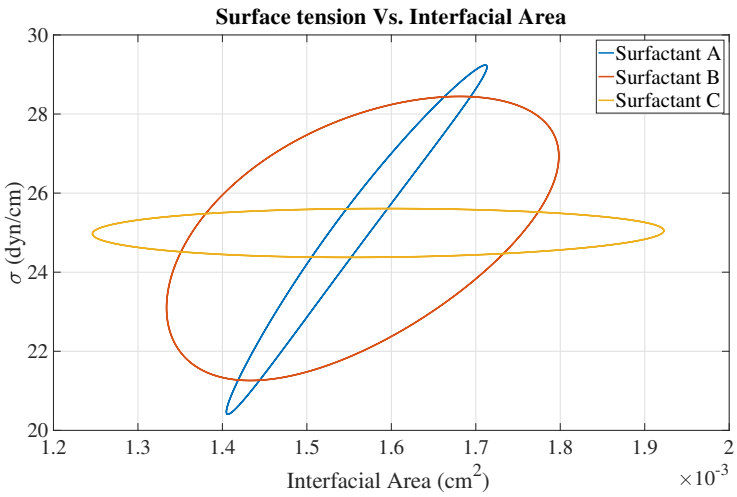

Figure 5.35: Hysteresis of surface tension loops decreases with increasing k_a and k_d. Surface tension converges to Γ_{eq} as k_a and k_d increase.

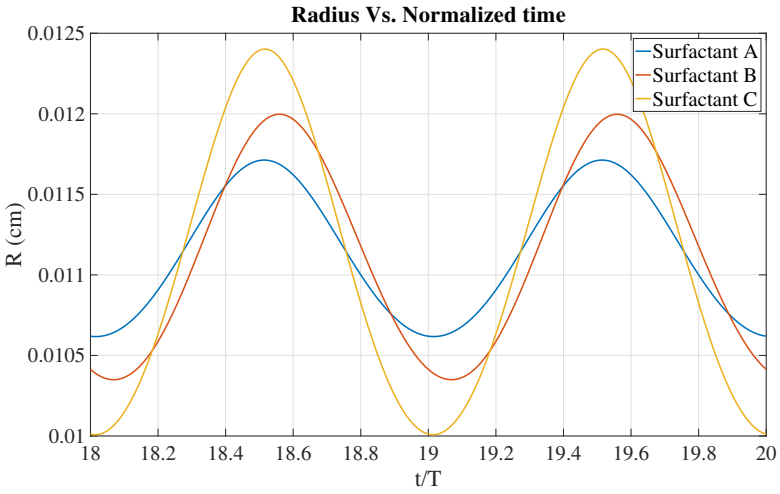

Figure 5.36: Surfactant A leads to the smallest alveolar expansion during inhalation due to high surface tension. At end of exhalation, surfactant C results in the smallest alveolar radius which is apparent from its high surface tension in figure 5.35.

As for the effect of surfactants on gas exchange, we see that the highly adsorbing and desorbing surfactant C results in the highest oxygen and carbon dioxide fluxes because it provides the largest area for gas exchange.

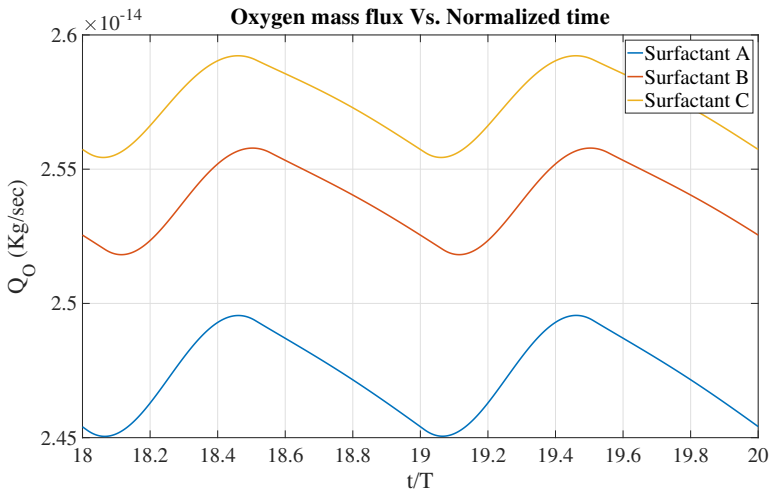

Figure 5.37: Surfactant A results in the lowest oxygen flux, and surfactant C results in the highest. This is consistent with the relative magnitudes of the areas for gas exchange offered by each surfactant.

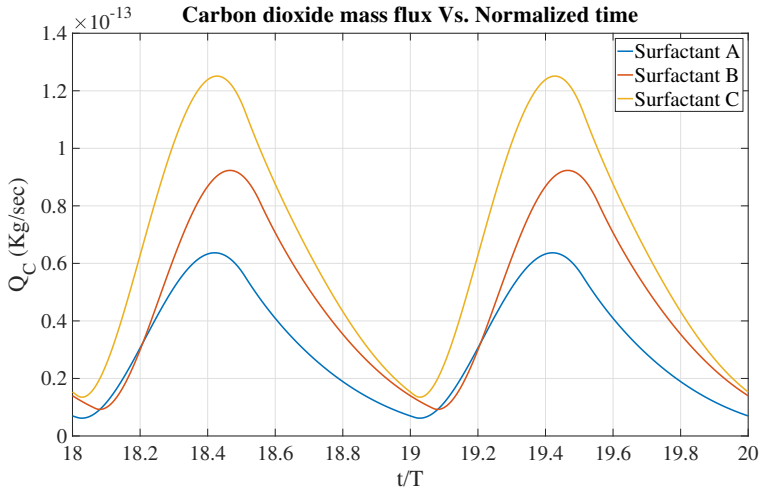

Figure 5.38: As in the case of oxygen, the flux of carbon dioxide is largest for the highly adsorbing surfactant C.

Furthermore, a larger gas flux results in a higher oxygen partial pressure and a lower carbon dioxide partial pressure at the capillary exit, which is desirable.

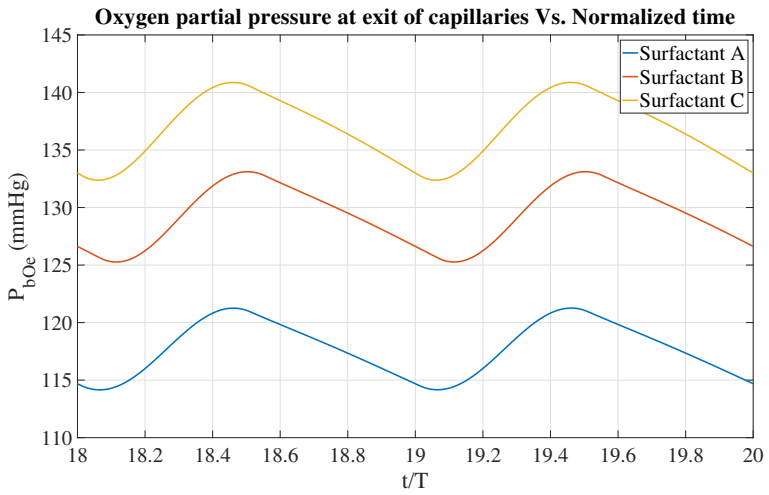

Figure 5.39: Oxygen partial pressure at capillary exit is higher for the case of larger oxygen flux.

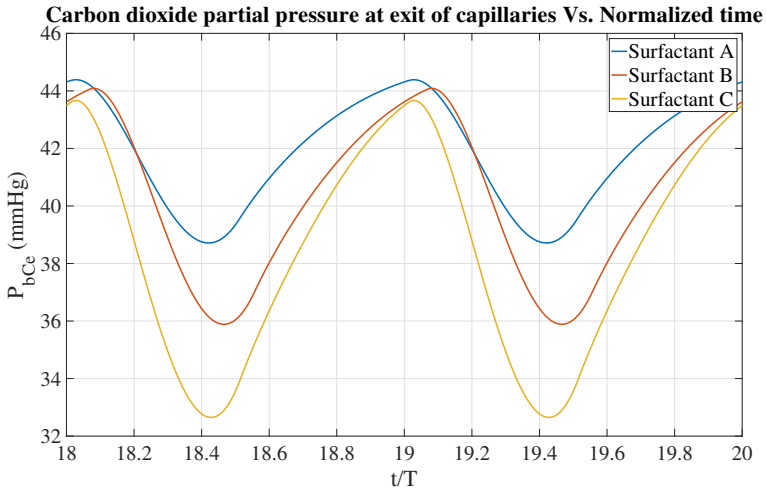

Figure 5.40: Carbon dioxide partial pressure at capillary exit is higher for the case of larger carbon dioxide flux.

We also examine the fraction of the capillary length that is traversed by the blood before reaching hemoglobin saturation. We find that hemoglobin saturation is fastest for surfactant C. This is preferable because it provides a large margin for blood to be saturated with oxygen in case there was a disease causing lower flux.

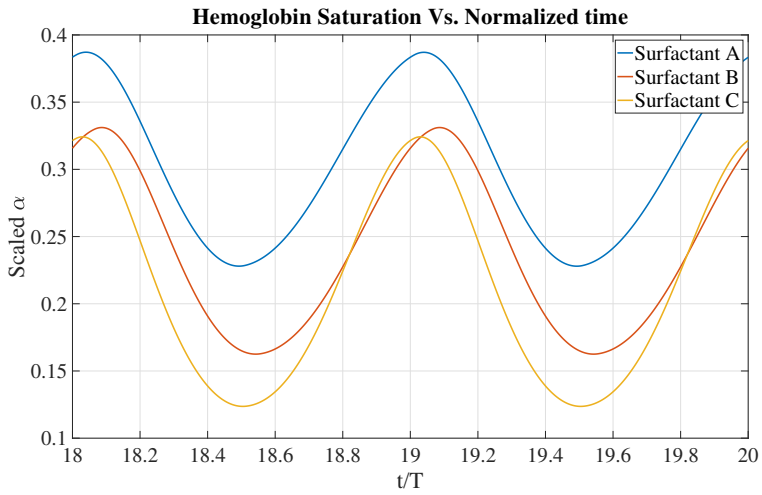

Figure 5.41: The distance traveled by blood before hemoglobin saturation is shortest for the surfactant resulting in highest oxygen flux (surfactant C).

It might seem from these results that a faster adsorbing and desorbing surfactant is the best choice in reference to breathing. However, it is important to note two main disadvantages of such surfactants. First, the low alveolar area reached at the end of exhalation causes pressure buildup in the alveolus. In the case of our alveolar model that is composed of one alveolus, this high pressure causes an increase in the pressure gradient between the alveolus and the blood stream and hence a larger flux. In the real case however, alveoli are connected, and a pressure buildup in one alveolus might lead to the gas mixture leaving it to another alveolus, or in other words alveolar collapse. Second, the fast adsorbing and desorbing surfactant had the largest amplitude in the radial oscillations. This as will be shown later in section 5.5 leads to a higher work of breathing, or energy expenditure, which is not desirable. Hence, we would like to stress the point that the main goal of this section was to explain how the relative timescales pertaining to adsorption and desorption may affect surfactant dynamics and gas exchange. However, other factors such as avoiding alveolar collapse and minimizing the work of breathing should be considered when comparing surfactants. This will be elucidated in section 5.5.

5.3.2 Diffusion

Now we turn to studying the effect of surfactant diffusion on breathing. To do so, we consider two surfactants with varying diffusion coefficients. The first surfactant has $D_s = 10^{-8}$ (cm^2/sec) and represents the fast diffusion case, while the other has $D_s = 10^{-12}$ (cm^2/sec) and respresents the slow diffusion case; all other surfactant properties are similar. In other words, the ratio of time scales P_3 defined in subsection 2.3.2 is the only varied quantity in this case and is equal to $P_3 = 79.61$ for fast diffusion and $P_3 = 0.007961$ for slow diffusion. We first examine the bulk concentration profiles for the two surfactants at different times as seen in figures 5.42 and 5.43. In the case of slow diffusion, the concentration at the bottom of the

hypophase is always constant. However, in the subphase, the surfactant concentration varies significantly due to surfactant adsorption and desorption. This leads to the depletion of the subphase from surfactants at times which causes a delay in the adsorption mechanics, and consequently lower values of $\Gamma(t)$. This is usually termed a diffusion limited case. In the case when surfactants diffuse at a faster rate, the subphase is always enriched with surfactants that are ready to adsorb to the interface as shown in figure 5.43.

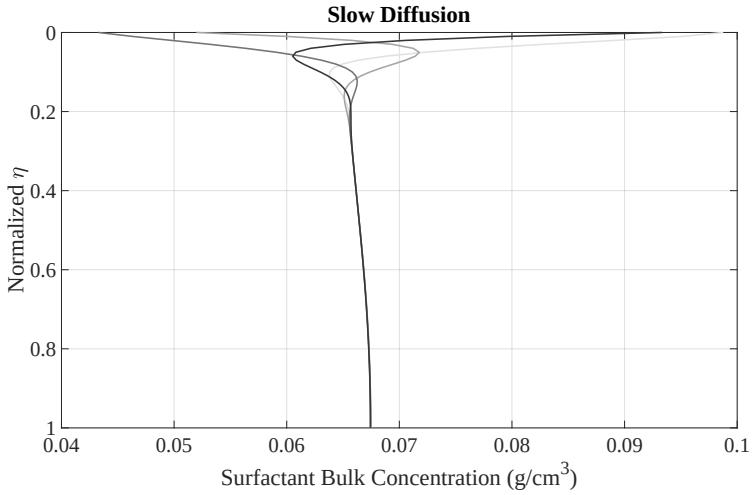

Figure 5.42: Slow diffusion prevents surfactants traveling from the bulk bottom to reach the subphase over a course of a breathing period. This limits the supply of surfactants to the interface.

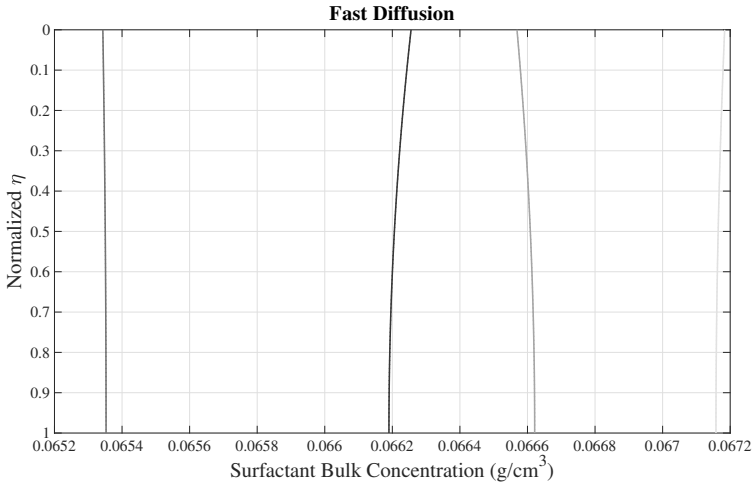

Figure 5.43: Subphase is constantly replenished by surfactants diffusing quickly from the bulk bottom.

The impact of the diffusion constant can be understood when observing the interfacial surfactant concentration, or equivalently the existing surface tension. The surface tension

caused by the slowly diffusing surfactant is higher than that of the fast diffusing one at all times. This causes the alveolar radius to be smaller in the slow diffusion case as seen in figure 5.46.

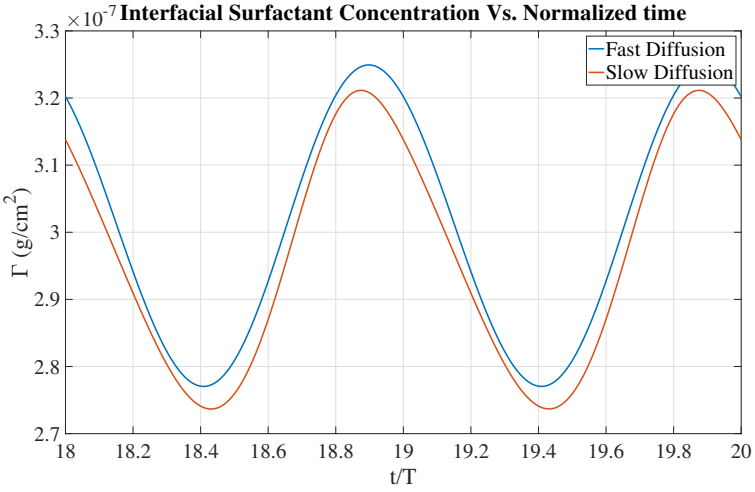

Figure 5.44: Interfacial surfactant concentration is higher for the highly diffusinve surfactant.

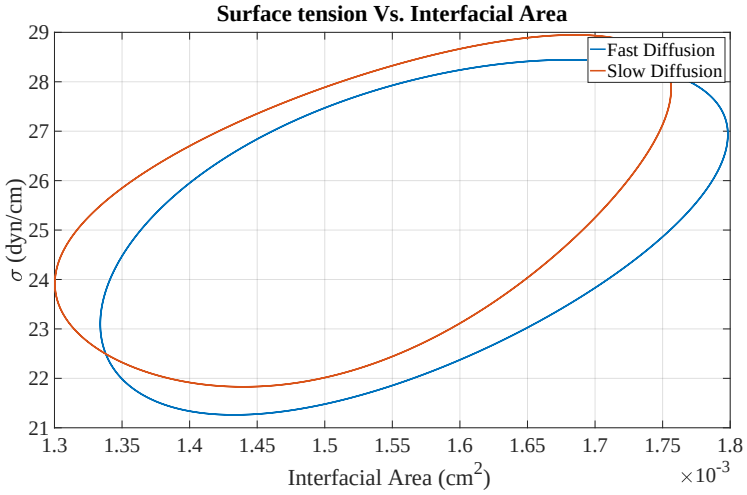

Figure 5.45: The higher interfacial concentration caused by the fast diffusing surfactant leads to lower surface tension values.

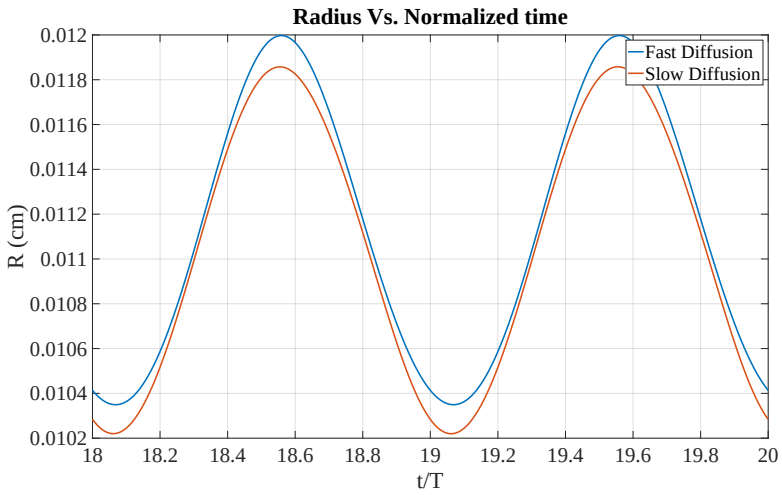

Figure 5.46: Higher elastic recoil exists in the case of the slowly diffusing surfactant. This leads to smaller alveolar area expansion.

The effect of the diffusion coefficient on the partial pressures of oxygen and carbon dioxide at the capillaries' exit is plotted in figures 5.47 and 5.48.

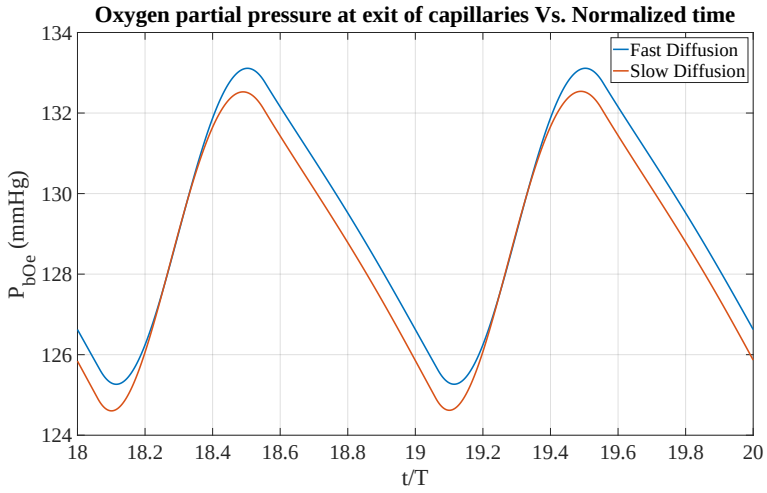

Figure 5.47: Surfactant Diffusion affects oxygen partial pressure at capillary exit.

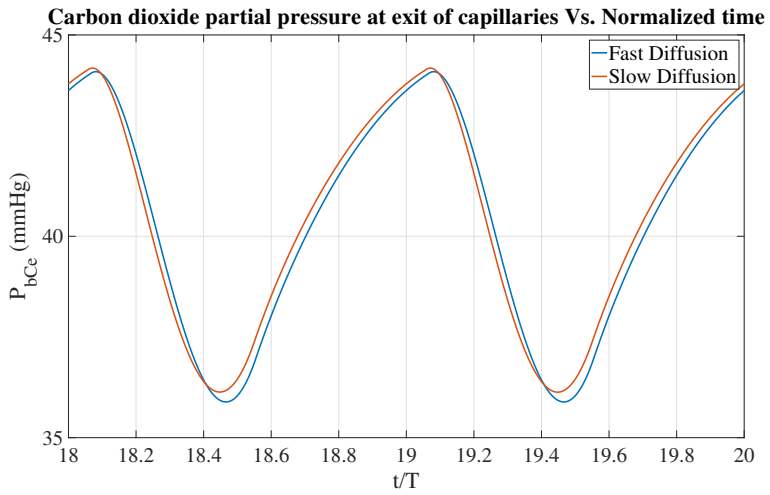

Figure 5.48: Surfactant Diffusion affects carbon dioxide partial pressure at capillary exit.

5.3.3 Interfacial Resistance

The interfacial resistance model that we extracted from [81] was not particularly for a fresh extract of a native pulmonary surfactant. Hence, we are not very sure how much it fits our current model. However, due to paucity of data, we used it as a preliminary model. To test the possible effects of the surfactant interfacial resistance on some aspects of breathing, we compare three hypothetical cases of interfacial resistance models that are shown in figure 5.49. We choose high interfacial resistance values as an attempt to model pulmonary alveolar proteinosis, where accumulation of surfactant in the alveolar airspaces impedes gas exchange [42].

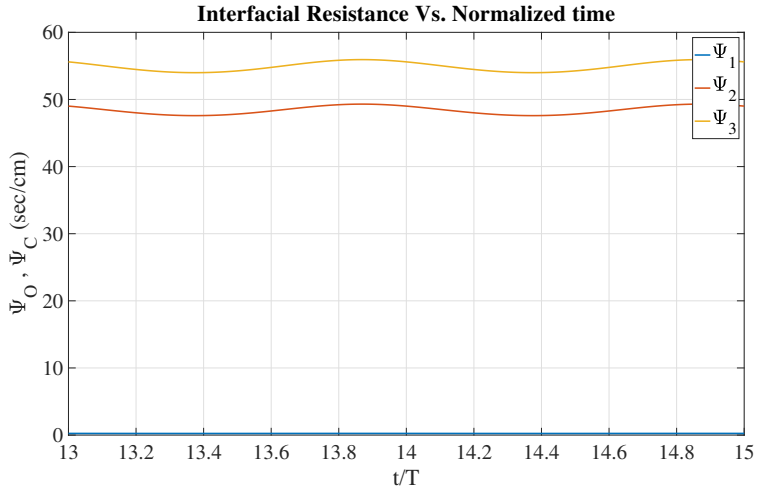

Figure 5.49: Interfacial Resistance vs. Time

Looking at the oxygen flux first, we find that a high interfacial resistance can cause a substantial decrease in the amount of oxygen being transferred from the alveolus to the passing bloodstream.

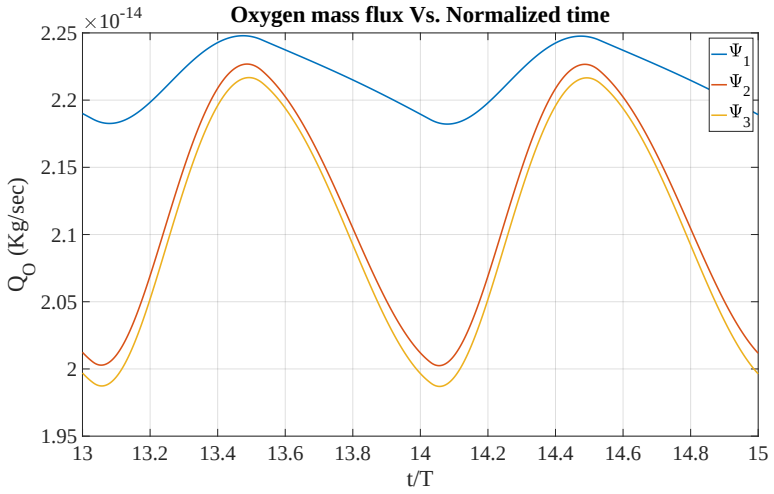

Figure 5.50: High interfacial resistance impedes oxygen diffusion, which can be seen in the decrease of the oxygen flux $Q_O(t)$.

The effect of the interfacial resistance on the oxygen flux can be problematic, and this is clarified by looking at the oxygen partial pressure at the capillaries' exit for the three considered cases shown in figure 5.51. As mentioned previously, hemoglobin saturation occurs when the oxygen partial pressure in the blood is around 100 mmHg. When comparing the three cases, we observe that hemoglobin saturation is only reached for the case when interfacial resistance is very low (Ψ_1). For the two other interfacial resistance models, blood exits the capillaries for the majority of the breathing period with unsaturated hemoglobin. This decreases the oxygen transfer to the body tissues.

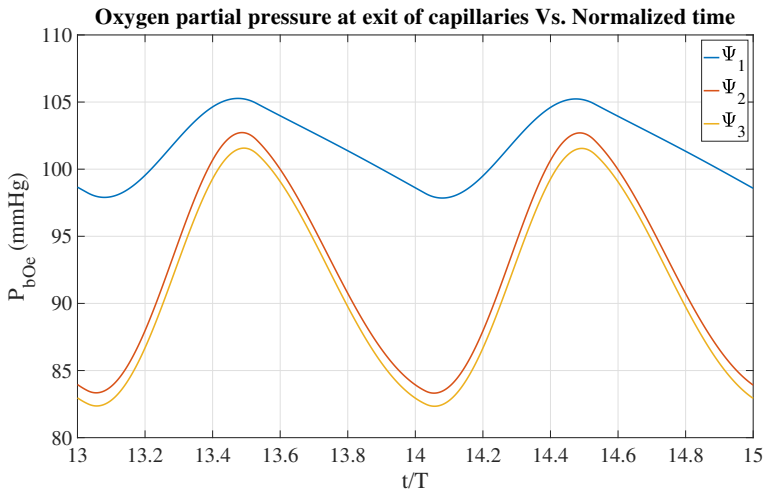

Figure 5.51: Hight interfacial resistance causes oxygen partial pressure at capillary exit to be lower than the required one for hemoglobin saturation ($\approx$ 100 mmHg).

It is clear that interfacial resistance due to the presence of surfactants at the interface can have an important effect on gas exchange. However, one might argue that the low oxygen pressures at the exit of the capillaries is due to low oxygen pressures in the alveolus. For this reason, we plot the alveolar oxygen partial pressures for the three cases (figure 5.52), and we see that their values are above the desired 100 mmHg. We also plot the oxygen equilibration ratio $\alpha(t)$ in figure 5.53, and verify that oxygen equilibration occurs for the case of Ψ_1 ($\alpha(t) < 1$), and that for the other two cases (Ψ_2 and Ψ_3), equilibration does not occur ($\alpha(t) > 1$).

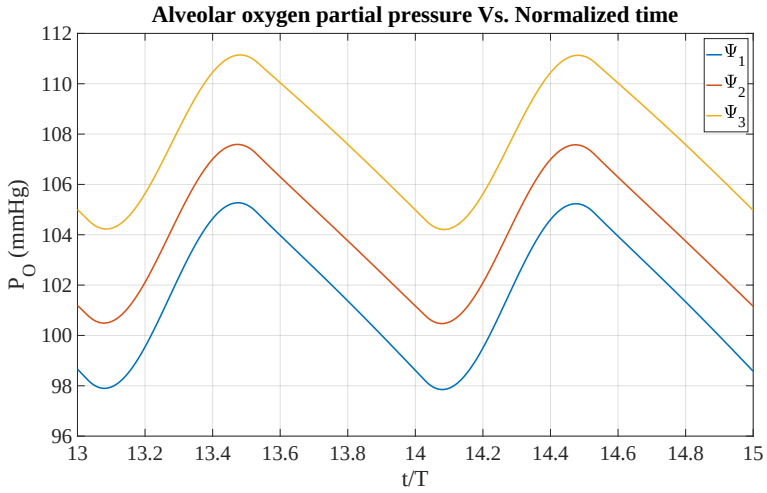

Figure 5.52: Oxygen partial pressures in alveolus are at normal values. Equilibration with the blood does not occur in the case of Ψ_2 and Ψ_3 as can be seen by comparing the pressures with those given in figure 5.51.

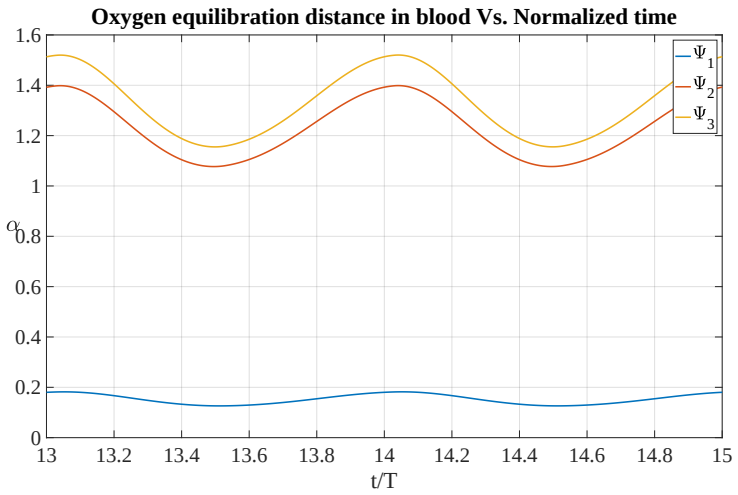

Figure 5.53: Oxygen equilibration ratio $\alpha(t)$ is shown for the three interfacial resistance modesl. $\alpha(t) < 1$ only in the case of Ψ_1.

5.4 Microscale Work of Breathing

As mentioned in section 5.3, quantifying the work of breathing is important when comparing surfactants. We define the microscale work of breathing as the inhalation work that has to be done to inflate the alveolus from its resting state to its maximum expanded state. This will occur over a half breathing period. The work of inhalation is split into three components that correspond to the expansion of the hypophase, expansion of the alveolar wall, and expansion of the hypophase surface (air-water interface).

Expansion of the Hypophase

The hypophase is modeled as a viscous fluid with the stress tensor $\boldsymbol{T}$ given by $\boldsymbol{T} = -\overline{P}_h \boldsymbol{I} + 2\mu_h \boldsymbol{D}$, where the strain rate tensor $\boldsymbol{D}$ has already been defined. The stress power per unit volume is given by $\boldsymbol{T}.\boldsymbol{D}$ which yields:

$$\boldsymbol{T}.\boldsymbol{D} = (-\overline{P}_h \boldsymbol{I} + 2\mu_h \boldsymbol{D}) \cdot \boldsymbol{D} = -\overline{P}_h \mathrm{tr}(\boldsymbol{D}) + 2\mu_h \boldsymbol{D} \cdot \boldsymbol{D}, \tag{5.1}$$

where $\mathrm{tr}(\boldsymbol{D})$ is equal to zero because the fluid is incompressible. Thus, the stress power per unit volume is found to be equal to:

$$\boldsymbol{T}.\boldsymbol{D} = \frac{12\mu_h R^4(t)\dot{R}^2(t)}{r^6}. \tag{5.2}$$

Integrating over the volume of the fluid, we get the total stress power at time t.

$$\int_{V(t)} \boldsymbol{T}.\boldsymbol{D}\, dV = \int_{R(t)-h(t)}^{R(t)} \frac{12\mu_h R^4(t)\dot{R}^2(t)}{r^6} 4\pi r^2 dr = 16\pi\mu_h R^4(t)\dot{R}^2(t)\Big(\frac{1}{(R(t)-h(t))^3} - \frac{1}{R^3(t)}\Big). \tag{5.3}$$

For $h(t)/R(t) << 1$, the result can be simplified to $\int_{V(t)} \boldsymbol{T}.\boldsymbol{D}\ dV = 48\pi\mu_h\dot{R}^2(t)h(t)$.
To find the work it takes to expand the hypophase when inhaling, we integrate the stress power over the half breathing period corresponding to inhalation. Hence, if t_1 is the start of inhalation and t_2 marks its end, the total work to expand the hypophase is:

$$W_{hypo} = \int_{t_1}^{t_2} 48\pi\mu_h\dot{R}^2(t)h(t)dt. \tag{5.4}$$

Expansion of the Alveolar Wall

The stress tensor in the alveolar wall is defined by $\boldsymbol{T} = \sigma_r \boldsymbol{e_r}\otimes\boldsymbol{e_r} + \Sigma(t)(\boldsymbol{e_\theta}\otimes\boldsymbol{e_\theta} + \boldsymbol{e_\phi}\otimes\boldsymbol{e_\phi})$, where σ_r is the radial stress to be found and $\Sigma(t)$ is the average hoop stress in the alveolar wall and is a function of time only ($\sigma_{\theta\theta} = \sigma_{\phi\phi} = \Sigma(t)$). The dependence of $\Sigma(t)$ on time is given by equation (3.39). Using the local equilibrium equations in spherical coordinates, we find that σ_r satisfies the following differential equation:

$$\frac{\partial\sigma_r}{\partial r} + \frac{1}{r}(2\sigma_r - 2\Sigma) = 0. \tag{5.5}$$

Solving the above equation and applying the boundary condition $\sigma_r = -\overline{P}_{pl}(t)$ at $r = R(t) + e(t)$, we get that

$$\sigma_r(r,t) = -(\overline{P}_{pl}(t) + \Sigma(t))\frac{(R(t)+e(t))^2}{r^2} + \Sigma(t). \tag{5.6}$$

The strain rate tensor of the solid is the same as that of the fluid since they both undergo the same isochoric deformation. Thus the stress power per unit volume is equal to:

$$\boldsymbol{T}.\boldsymbol{D} = \Big(-(\overline{P}_{pl}(t) + \Sigma(t))\frac{(R(t)+e(t))^2}{r^2} + \Sigma(t)\Big)\Big(\frac{-2R^2(t)\dot{R}(t)}{r^3}\Big) + \frac{2\Sigma(t)R^2(t)\dot{R}(t)}{r^3}, \tag{5.7}$$

which can be simplified to:

$$\boldsymbol{T}.\boldsymbol{D} = 2(\overline{P}_{pl}(t) + \Sigma(t))(R(t)+e(t))^2\frac{R^2(t)\dot{R}(t)}{r^5}. \tag{5.8}$$

Integrating over the volume of the alveolar wall, we get the total stress power at time t.

$$\begin{aligned}\int_{V(t)} \boldsymbol{T}.\boldsymbol{D}\ dV &= \int_{R(t)}^{R(t)+e(t)} 2(\overline{P}_{pl}(t) + \Sigma(t))(R(t)+e(t))^2\frac{R^2(t)\dot{R}(t)}{r^5}4\pi r^2 dr \\ &= 4\pi(\overline{P}_{pl}(t) + \Sigma(t))\dot{R}(t)((R(t)+e(t))^2 - R^2(t)).\end{aligned} \tag{5.9}$$

For $e(t)/R(t) << 1$, the above result can be simplified to $\int_{V(t)} \boldsymbol{T}.\boldsymbol{D}\ dV = 8\pi(\overline{P}_{pl}(t) + \Sigma(t))\dot{R}(t)R(t)e(t)$. To find the work it takes to expand the alveolar wall when inhaling, we

integrate the stress power over the half breathing period corresponding to inhalation. Hence, if inhalation starts at t_1 and ends at t_2, the total work to expand the alveolar wall is:

$$W_{wall} = \int_{t_1}^{t_2} 8\pi(\overline{P}_{pl}(t) + \Sigma(t))\dot{R}(t)R(t)e(t)dt. \tag{5.10}$$

Expansion of the Hypophase Interface

In order to expand the air-water interface, work has to be done against the surface tension that arises there. Following [127, 128], the interfacial work exerted during inhalation can be found by integrating the surface tension over the area of expansion. This part of the inhalation work is expressed as:

$$W_{interf} = \int_{A_I(t_1)}^{A_I(t_2)} \sigma dA_I^* \tag{5.11}$$

where, $A_I(t_1)$ is the interfacial area at the beginning of inhalation at time t_1 and $A_I(t_2)$ is the interfacial area at the end of inhalation at time t_2.

Total Work of Inhalation

The total work of inhalation is then equal to:

$$\begin{aligned} W_{inh} &= W_{hypo} + W_{wall} + W_{interf} \\ &= \int_{t_1}^{t_2} \left(48\pi\mu_h\dot{R}^2(t)h(t) + 8\pi\Big(\overline{P}_{pl}(t) + \Sigma(t)\Big)\dot{R}(t)R(t)e(t)\right)dt + \int_{A_I(t_1)}^{A_I(t_2)} \sigma dA_I^*. \end{aligned} \tag{5.12}$$

5.5 Endogenous Pulmonary Surfactant and its Fractions

As mentioned in section 1.2, pulmonary surfactant is a complex mixture of phospholipids ($70 - 80\%$), hydrophopic and hydrophobic proteins (10%), and neutral lipids (10%). In acute respiratory distress syndrome (ARDS), surfactant extracts have shown lower levels of phospholipids and proteins [129], but it is not very clear how each component of pulmonary surfactant contributes to this disease [130]. Ingenito et al. extracted fresh calf lung surfactant by lavage and isolated its components by centrifuge [65]. Experiments were performed on the different surfactant portions using a pulsating-bubble surfactometer and a set of surfactant properties was extracted for multiple combination of the fractions. The results obtained from [65, 130] are summarized in table 5.2.

In the beginning of this section, we use our developed model to study the effect of each surfactant fraction on breathing. This is important because identifying the performance

of each component can give insight on the development of exogenous surfactants to treat ARDS. At the end of the section, we compare the surfactant extracted from calf (CLS) with a derivative of porcine lung surfactant (Curosurf).

5.5.1 Role of Pulmonary Surfactant Fractions

The roles of the different components of a fresh calf surfactant are investigated using our developed model. To do so, we first use the full mixture of the calf lung surfactant (CLS), referred to as native surfactant in [65], and study its effect on breathing. The performance of the surfactant is evaluated based on the area it provides for gas exchange and on the amount of work that has to be exerted when breathing. Next, we reconstruct the native surfactant by adding its components discretely. We evaluate the performance of the phospholipid (PL) portion first, then add the hydrophobic apoproteins (HA). Next, the hydrophilic apoprotein[1] SP-A is added, followed by the addition of neutral lipids (NL). At every step, the effect of the added surfactant fraction can be understood. Table 5.2 contains the values of the properties of the different surfactant fractions [130]. The diffusion coefficient $D_s = 10^{-6}$ cm^2/sec of CLS also obtained from [130] was used for all fractions. All variables in table 5.2 were defined in sections 2.4 and 3.4, except σ_{min}, which is the minimum surface tension in a dynamic system reached during squeeze out of surfactants.

Surfactant Parameter Values					
Surfactant	k_a (ml/(g.min))	$\frac{k_a}{k_d}$ (ml/g)	$\overline{\sigma}$ (dyn/cm)	Y (dyn/cm)	σ_{min} (dyn/cm)
Native	$6 * 10^5$	$1.2 * 10^5$	22	140	1
PL	$0.02 * 10^5$	$1.2 * 10^5$	22	65	20
PL+HA	$3.5 * 10^5$	$1.3 * 10^5$	22	50	1
PL+HA+SP-A	$4 * 10^5$	$1.4 * 10^5$	22	110	1
PL+HA+SP-A+NL	$5 * 10^5$	$1.4 * 10^5$	22	125	1

Table 5.2: Parameter values of surfactant fractions under study [130].

We first use our model to study the case of an alveolus coated with the native surfactant. Figure 5.54 shows the alveolar radius variation for that case. Surface tension is also plotted against the interfacial area for this case in figure 5.55. All results are shown after steady state is reached. Figures 5.54 and 5.55 will be compared to those generated by the model when the alveolus is coated with the different surfactant fractions. This provides insight on the role of each surfactant component.

[1]Information about SP-D is not available.

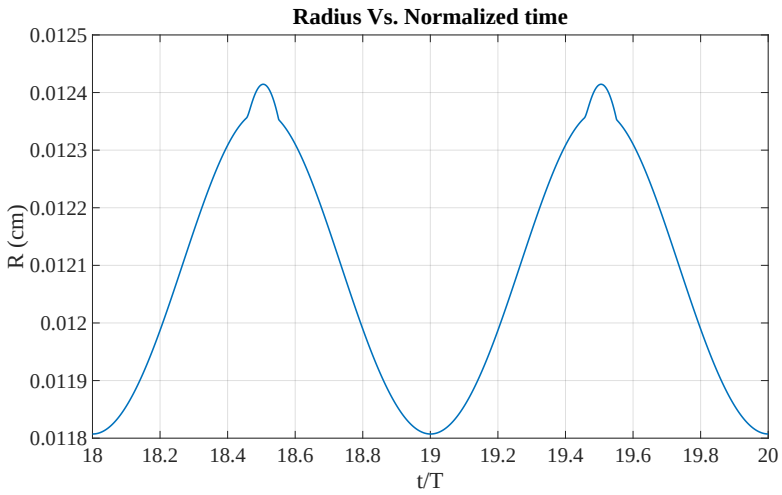

Figure 5.54: Variation in alveolar radius for an alveolus coated with native surfactant.

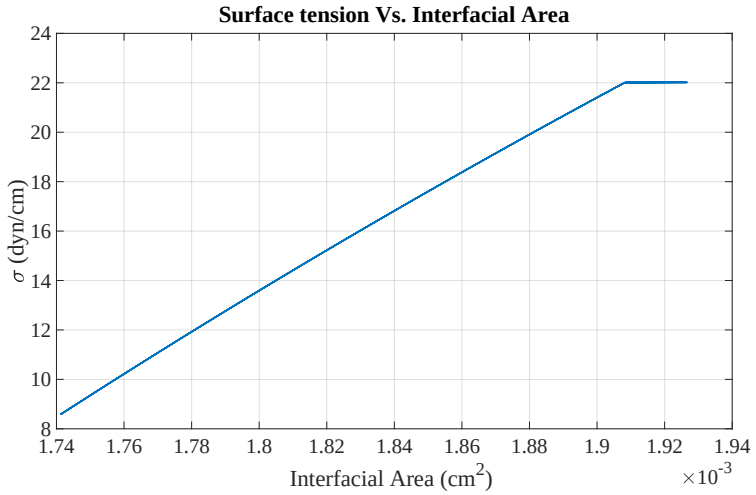

Figure 5.55: Variation of surface tension over a breathing period for an alveolus coated with native surfactant.

Phospholipid

Now, the alveolus is only coated with the phospholipid portion of the surfactant. The resulting alveolar radius variation resulting from our model is compared to that of the native surfactant and shown in figure 5.56.

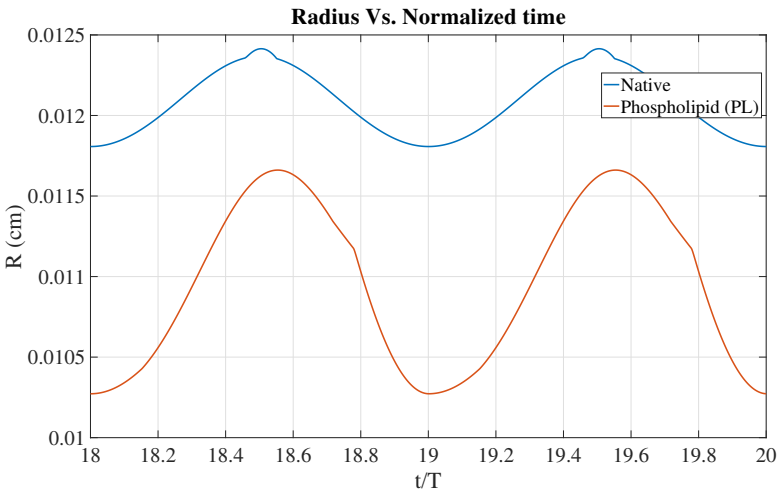

Figure 5.56: Smaller radii and larger oscillations result when the alveolus is only coated with PL.

First, we observe that in the case of the native surfactant, the radius varies from 118 μm to 125 μm, while the phospholipid portion alone causes oscillations between 103 μm to 117 μm. This can be explained when looking at the surface tension of the two cases shown in figure 5.57. The native surfactant prevents the surface tension to increase beyond its equilibrium value due to its fast adsorption. However, for the phospholipid, surface tension rises above the equilibrium value by 27%. This explains the difference in the maximum alveolar radius for each surfactant. Looking at the other end of figure 5.55, we notice that the native surfactant behaves as an insoluble surfactant below the equilibrium surface tension, which suppresses desorption and causes a big drop in surface tension[2]. However, the phospholipid portion cannot withstand compression and is squeezed out of the interface in the early stages of exhalation. The low surface tension value caused by the native surfactant explains the large radius at the end of exhalation, and likewise the failure of the phospholipid to decrease surface tension results in a relatively low radius at the end of the breathing cycle.

[2]Squeeze out is not reached with the model parameters used.

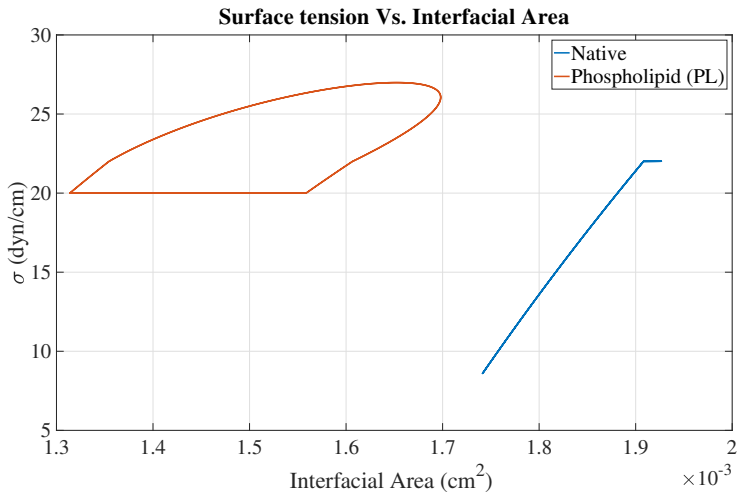

Figure 5.57: Variation of surface tension over a breathing period for an alveolus coated with PL. Squeeze out occurs and keeps surface tension at high values.

The total number of surfactants normalized by its initial value is plotted for the case of phospholipid to show conservation of surfactants during all three regimes including squeeze out.

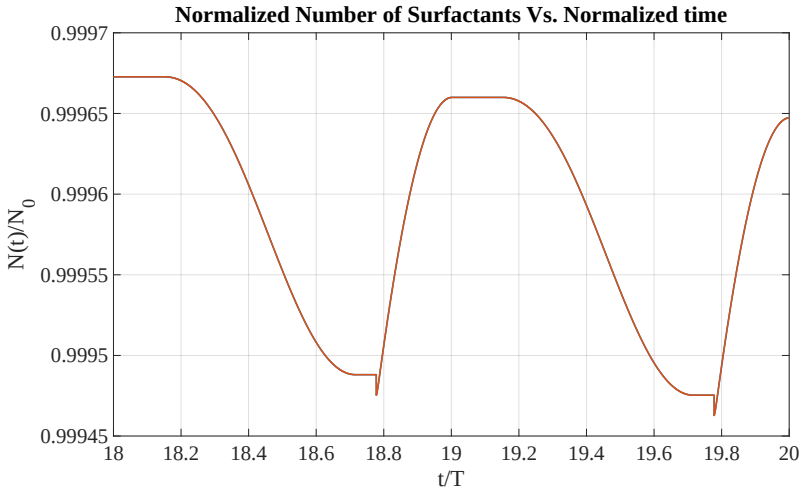

Figure 5.58: Total number of surfactants is conserved.

In table 5.3, we document the average area available for gas exchange, the interfacial work of inhalation, and the total work of inhalation for each surfactant. Work quantities were calculated following the procedure given in section 5.4. As expected from figure 5.56, the native surfactant provides a larger average area as compared to PL; this leads to more efficient gas exchange. What is very interesting however is that this is achieved with less total work than that exerted when the phospholipid alone is present. Hence, the native

surfactant behaves, i.e adsorbs, desorbs, diffuses, etc. in such a way to decrease the surface tension by a large amount over a breathing cycle, which causes the alveolus to have smaller oscillations around a large area, hence decreasing the total work of breathing and enhancing the gas exchange.

Area for Gas Exchange and Work of Inhalation			
Surfactant	Average Area for Gas Exchange ($10^5 \mu m^2$)	Interfacial Work (10^{-8}N.cm)	Total Work (10^{-6}N.cm)
Native	1.84	3	1.39
PL	1.5	9.59	3.42

Table 5.3: Area provided for gas exchange and work of breathing are presented for the native surfactant and PL. PL provides less area for gas exchange and requires more breathing effort.

We next explore the effect of adding the hydrophobic apoproteins to the phospholipid portion.

Phospholipid and Hydrophobic Apoproteins

Figure 5.59 shows the effect of adding the hydrophobic apoproteins to the phospholipid portion on the alveolar oscillations. More area for gas exchange is recovered and this can be attributed to the lower surface tension values attained in this case as seen in figure 5.60. It appears however that the rate at which surface tension decreases when the surfactant film compresses is slower than that of the native surfactant. As will be shown next, this rate is recovered when the hydrophilic apoprotein SP-A is added. In addition to providing more area for gas exchange, hydrophobic apoproteins decrease the inhalation work during breathing. This is tabulated in table 5.4. Another very important aspect is that the hydrophobic apoproteins keep the alveolus inflated at a large area at the end of exhalation. This prevents pressure buildup and the collapse of the alveolus into a neighboring one; this effect was not seen in the case of PL alone.

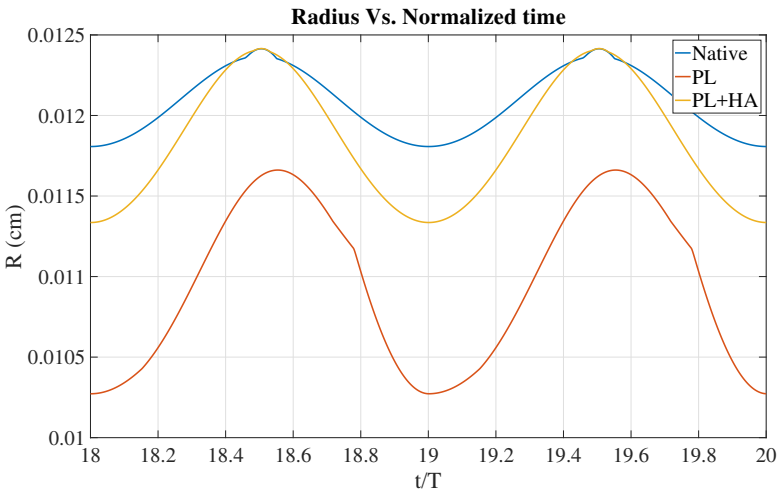

Figure 5.59: Adding HA to PL restores most of the area for gas exchange provided by the native surfactant.

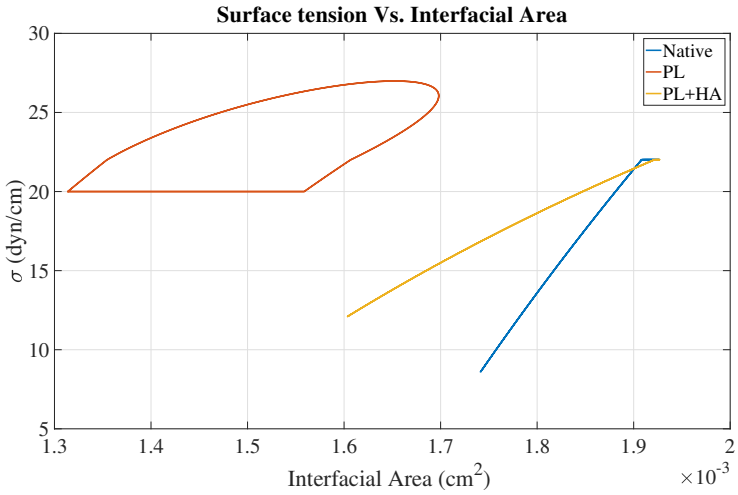

Figure 5.60: Hydrophobic apoproteins delay surfactant squeezeout. Rate of surface tension decrease with film compression is not fully restored.

Area for Gas Exchange and Work of Inhalation			
Surfactant	Average Area for Gas Exchange ($10^5 \mu m^2$)	Interfacial Work (10^{-8}N.cm)	Total Work (10^{-6}N.cm)
Native	1.84	3	1.39
PL	1.5	9.59	3.42
PL+HA	1.74	5.6	2.5

Table 5.4: Hydrophobic apoproteins HA are added to PL. This restores most of the area for gas exchange, and decreases the breathing effort. In addition, this decreases the risk of alveolar collapse caused by a pressure buildup in the alveolus.

Phospholipid, Hydrophobic and Hydrophilic Apoproteins

The addition of the hydrophilic apoprotein SP-A to the phospholipid and hydrophobic proteins increases the rate at which surface tension decreases during exhalation (compression of surfactant film). This leads to a larger area for gas exchange and lower breathing work. Results are shown in figures 5.61 and 5.62, and table 5.5.

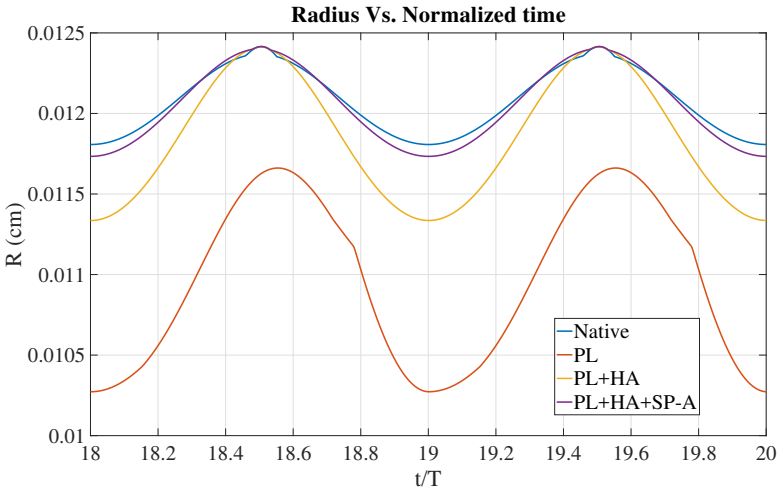

Figure 5.61: Almost all gas exchange area is restored when apoprotein SP-A is added to the PL+HA mixture.

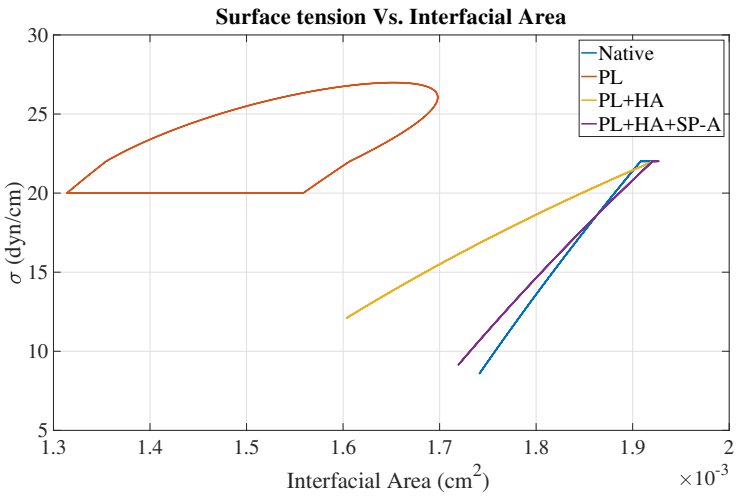

Figure 5.62: The rate at which surface tension decreases upon film compression increases with the addition of SP-A.

Area for Gas Exchange and Work of Inhalation			
Surfactant	Average Area for Gas Exchange ($10^5 \mu m^2$)	Interfacial Work (10^{-8}N.cm)	Total Work (10^{-6}N.cm)
Native	1.84	3	1.39
PL	1.5	9.59	3.42
PL+HA	1.74	5.6	2.5
PL+HA+SP-A	1.82	3.3	1.56

Table 5.5: Hydrophilic apoprotein SP-A is added to the mixture. A further increase in the average area for gas exchange and a larger decrease in the breathing work is observed. This is consistent with the damping of the alveolar oscillations shown in figure 5.61 and the increase in their average value.

Phospholipid, Hydrophobic and Hydrophilic Apoprotein, and Neutral Lipids

When neutral lipids are added to the mixture, very minor changes are observed. Nonetheless, the case of the native surfactant is almost fully recovered. The slight difference between the native surfactant and the reconstructed one might be due to experimental error when obtaining the surfactant parameters k_a, k_d, etc. Another possibility for this slight deviation can be attributed to the absence of apoprotein SP-D in the reconstruction of the surfactant.

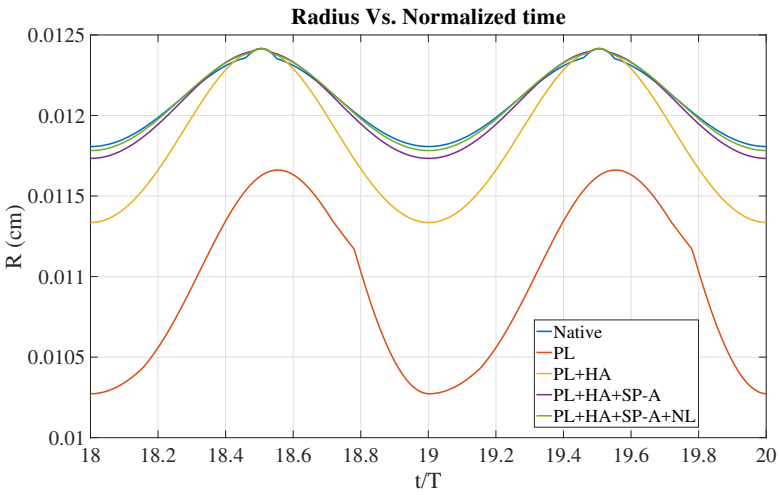

Figure 5.63: Minor differences can be seen with the addition of neutral lipids. Difference between the fully reconstructed mixture and the native surfactant might be due to absence of apoprotein SP-D.

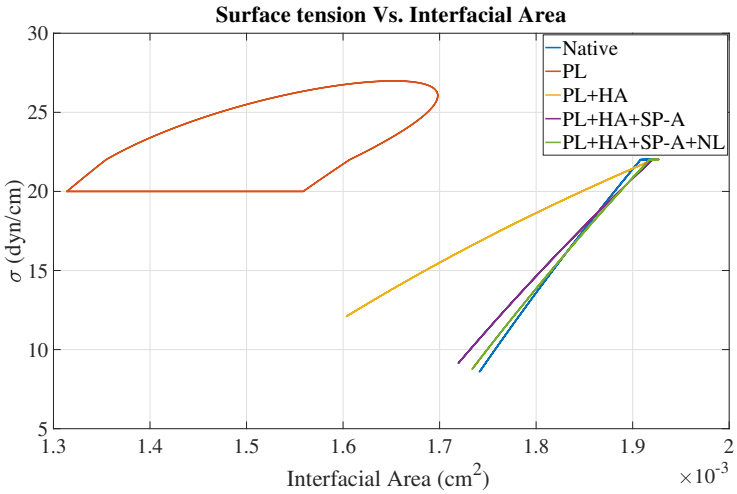

Figure 5.64: Surface tension over a breathing period for an alveolus coated with the fully reconstructed mixture almost coincides with that of the native surfactant.

Area for Gas Exchange and Work of Inhalation			
Surfactant	Average Area for Gas Exchange ($10^5 \mu m^2$)	Interfacial Work (10^{-8}N.cm)	Total Work (10^{-6}N.cm)
Native	1.84	3	1.39
PL	1.5	9.59	3.42
PL+HA	1.74	5.6	2.5
PL+HA+SP-A	1.82	3.3	1.56
PL+HA+SP-A+NL	1.83	3.07	1.45

Table 5.6: Surfactant mixture is fully reconstructed with the addition of neutral lipids. Very minor differences are observed in the performances of the native surfactant and the fully reconstructed mixture.

Next, we compare different surfactants that are extracted from calves and porcine like animals.

5.5.2 CLS vs Curosurf

Two known surfactants are compared. The first is extracted from calves and is termed CLS, while the other is extracted from porcine like animals and is referred to as Curosurf. The multiple properties of the two surfactant types are shown in table 5.7. In addition, the diffusion coefficients of CLS and Curosurf are 10^{-6} and 10^{-9} (cm^2/sec) respectively [130].

Surfactant Parameter Values of CLS and Curosurf					
Surfactant	k_a(ml/(g min))	$\frac{k_a}{k_d}$(ml/g)	$\overline{\sigma}$(dyn/cm)	Y (dyn/cm)	σ_{min} (dyn/cm)
CLS	$6 * 10^5$	$1.2 * 10^5$	22	140	1
Curosurf	$0.07 * 10^5$	$1 * 10^5$	25	100	1

Table 5.7: Parameter values of CLS and Curosurf [130].

As can be seen from figure 5.65, the model predicted alveolar expansion of CLS is higher than that of Curosurf. Looking at the comparison of the surface tension plots of both surfactants, we notice that CLS leads to lower surface tension values. This is mainly due to the higher k_a and D_s of CLS. This result is consistent with our findings in subections 5.3.1 and 5.3.2.

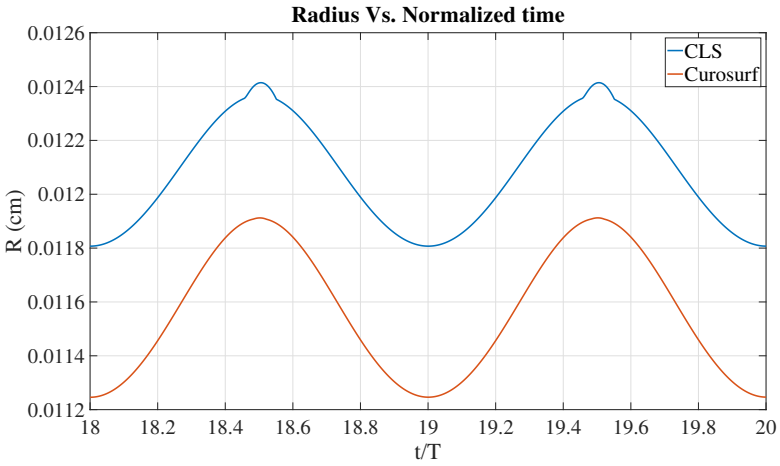

Figure 5.65: Area provided by CLS is considerably larger than that provided by Curosurf.

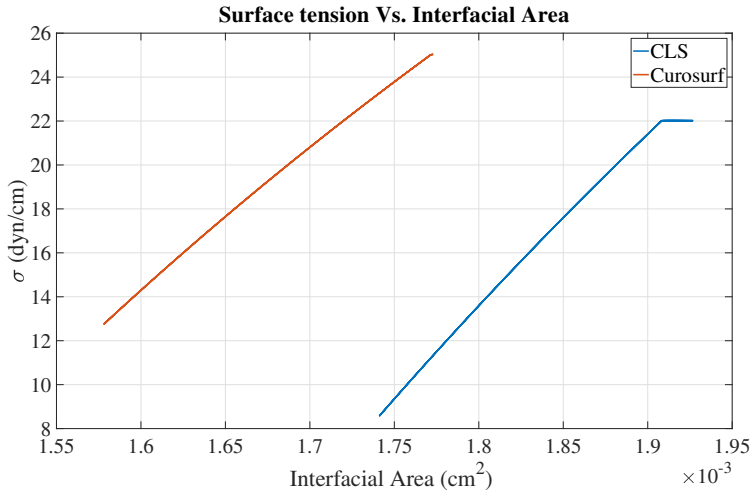

Figure 5.66: The lower surface tension values achieved by CLS cause a smaller elastic recoil of the alveolus, which explains the difference in the radii shown in figure 5.65.

We also examine the oxygen partial pressure at capillary exit. For the majority of the cycle, this pressure is higher for CLS because of the larger gas exchange area that it provides. We notice however that the pressure resulting from Curosurf exceeds that of CLS in some fractions of the breathing period. We hypothesize that this is due to pressure buildup in the alveolus resulting from the smaller alveolar area offered by Curosurf. The pressure buildup increases the flux of oxygen and may lead to higher partial pressure at capillary exit. In the real lung however, alveoli are not isolated from one another, and a high pressure buildup can cause the alveolus to empty into another one. This leads to alveolar collapse and does not enhance gas diffusion. Because our model consists of just one alveolus, we cannot model

such effect. The average area offered by each surfactant and the breathing work exerted are shown in table 5.8.

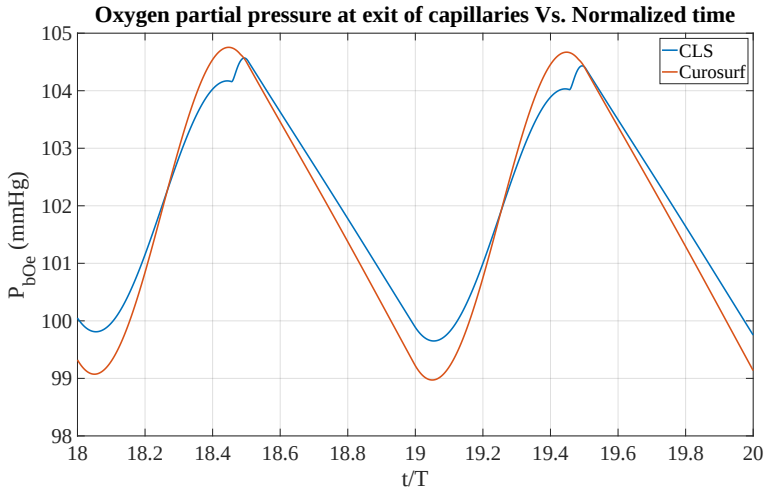

Figure 5.67: The larger area for gas exchange provided by CLS causes oxygen partial pressure at capillary exit to be higher for most of the breathing cycle.

Area for Gas Exchange and Work of Inhalation of CLS and Curosurf			
Surfactant	Average Area for Gas Exchange ($10^5 \mu m^2$)	Interfacial Work (10^{-8}N.cm)	Total Work (10^{-6}N.cm)
CLS	1.84	3	1.39
Curosurf	1.68	3.72	1.57

Table 5.8: CLS provides larger area for gas exchange and decreases breathing effort as compared to Curosurf.

5.6 Operating Breathing Space

In this section, we show some results related to the inhalation work and the gas flux during breathing and how they are affected by surfactants. In all presented results, the gas flux and work are computed over a minute of breathing; we refer to these quantities as gas flux per minute and work per minute respectively. The results in figures 5.68 to 5.71 correspond to the same soluble surfactant that we refer to as Surfactant A (SA). All model parameters used in this section can be found in appendix C. Figure 5.68 shows how the oxygen flux per minute and the inhalation work per minute vary when humans breathe at different breathing cadences (periods). At low periods, maximum oxygen flux can be attained but more inhalation work should be exerted. This is similar to the case of humans exercising; we breath faster and do more work. This is also similar to artificial ventilation where machines

are operated at lower periods and provide maximum gas flux by doing the work themselves [131]. As the period of breathing increases, breathing work decreases and reaches a plateau. Oxygen flux is also shown to decrease with breathing period. Figure 5.69 is a similar plot for carbon dioxide exchange.

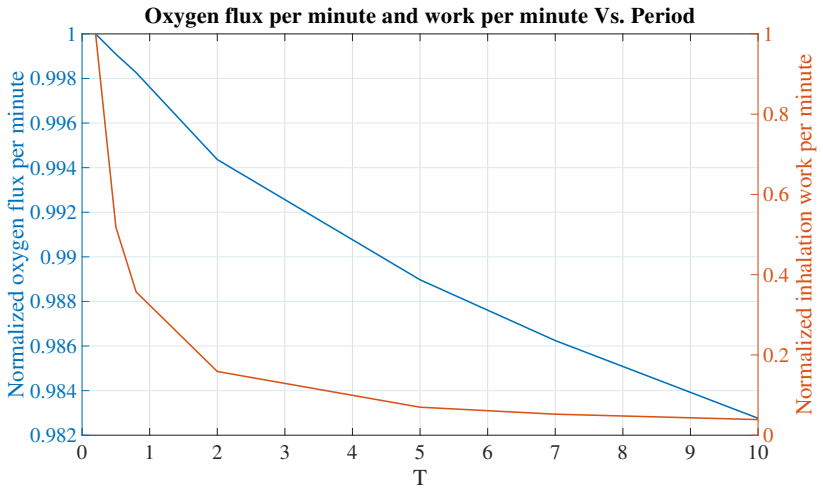

Figure 5.68: At low periods, maximum inhalation work per minute is exerted, and maximum oxygen exchange occurs. As the breathing period increases, both work per minute and oxygen flux per minute decrease.

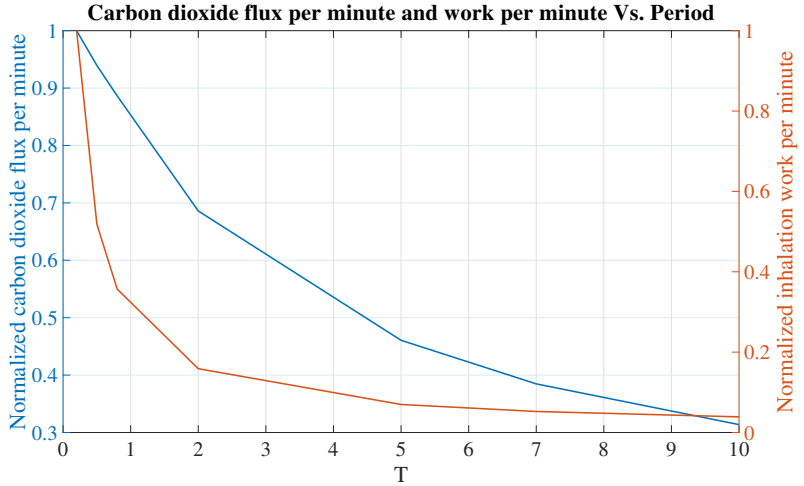

Figure 5.69: Carbon dioxide diffusion is similar to that of oxygen. As the breathing period increases, the drop in carbon dioxide flux is much bigger than that of oxygen.

The decrease in flux per minute and work per minute can be explained when examining figure 5.70. On this plot, we show the difference between the maximum and minimum values of the alveolar radius for every period after steady state is reached. This difference increases with T, but the steepness of its slope decreases as the period increases. This causes the

breathing work and the gas flux over a period to head towards reaching a plateau. As period increases however, the number of cycles in a minute decreases, which causes the flux per minute and work per minute to decrease with larger periods. The behavior of the difference between the maximum and minimum values of the alveolar radius can be explained by looking at how the subphase concentration[3] varies at different periods. Since the surfactants reside in a small layer of fluid, there is a limit to the surfactant amount that can be provided from the bulk to the interface; this motivates the introduction of a novel concept that we refer to as *Surfactant Limited Reservoir*. In this case, the subphase concentration is dropping by around 20%, which is limiting the supply of surfactants to the interface, which hinders larger alveolar expansion.

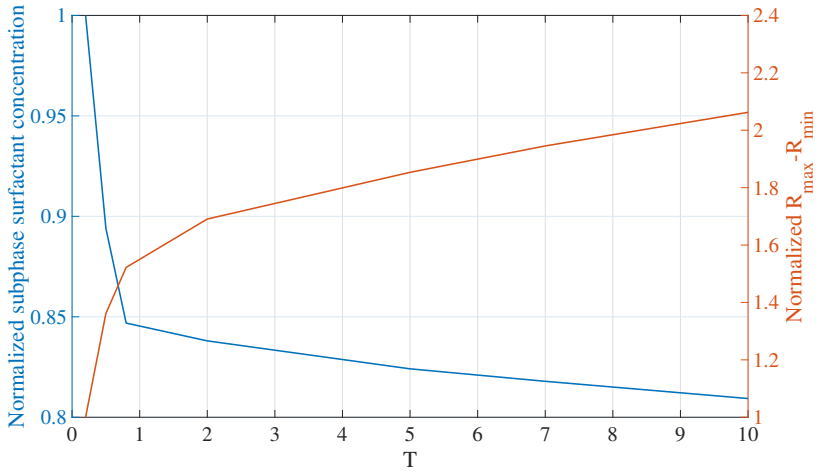

Figure 5.70: Subphase concentration drops by about 20%. This causes the subphase to be depleted from surfactants which hinders surfactant adsorption to the interface. This leads in a decrease in the rate at which the alveolus expands, which is shown by the decrease in the slope of the difference in alveolar radii.

Instead of just studying how changing the breathing period affects the gas flux and inhalation work, we also examined the effect of changing the amplitude of the pleural pressures (how deep we breath). For every surfactant, we construct a diagram that we refer to as *Operating Breathing Space* diagram. Such diagram is made of lines of constant breathing periods (black) and lines of constant pleural pressure amplitudes (red). Every point of intersection of a red and black line represents a mode of breathing. At a chosen breathing mode, the vertical axis of the diagram reads the average area available for gas exchange, while the horizontal one gives the inhalation work exerted over a minute. Figure 5.71 also offers different paths that a person can follow in order to increase gas flux without exerting more work.

[3]The subphase shown is evaluated at maximum alveolar radius.

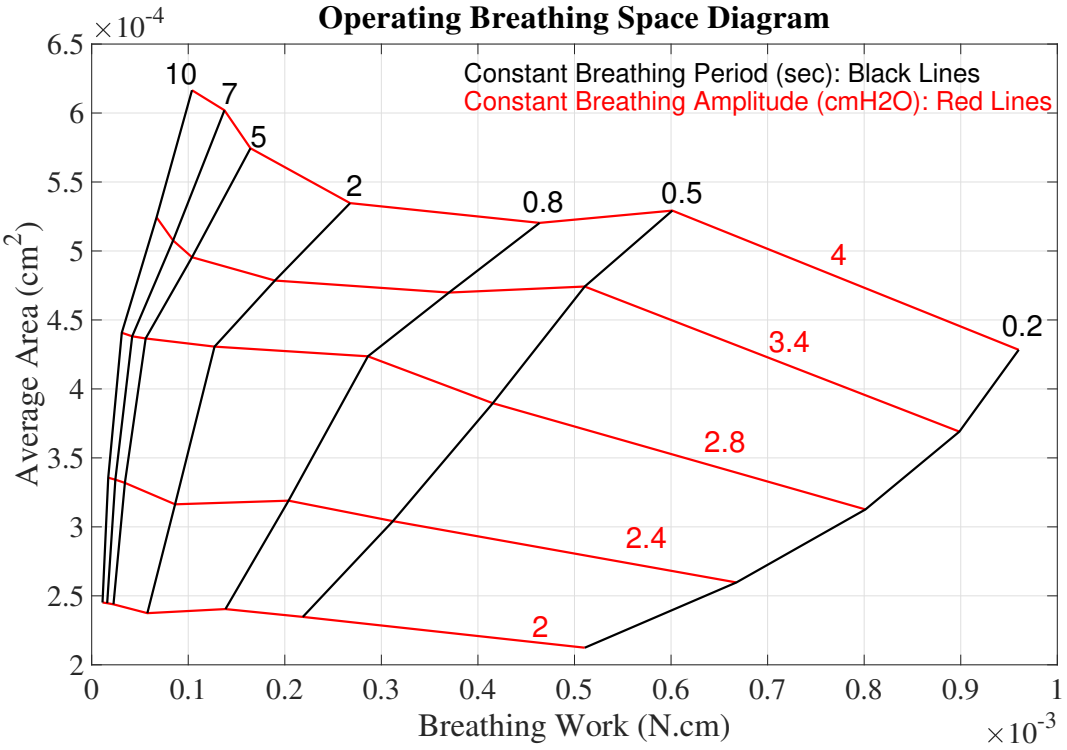

Figure 5.71: This diagram spans the multiple modes of breathing. It provides the average area available for gas exchange and the inhalation work exerted over a minute of breathing for different breathing modes.

As mentioned earlier, every *Operating Breathing Space* diagram corresponds to one surfactant. The diagram in figure 5.71 for example corresponds to the mentioned surfactant SA. We now build an operating breathing diagram for surfactant SB with an adsorption coefficient[4] that is 3 times lower than that of SA. As can be seen from figure 5.72, the operating breathing diagram of SB shifts down and to the right. In other words, for the same mode of breathing, less area for gas exchange is provided and more work is exerted when SB is used instead of SA. Such diagrams are very useful when designing exogenous surfactants.

[4]The ratio of k_a and k_d is kept constant, so k_d is also decreased by a factor of 3.

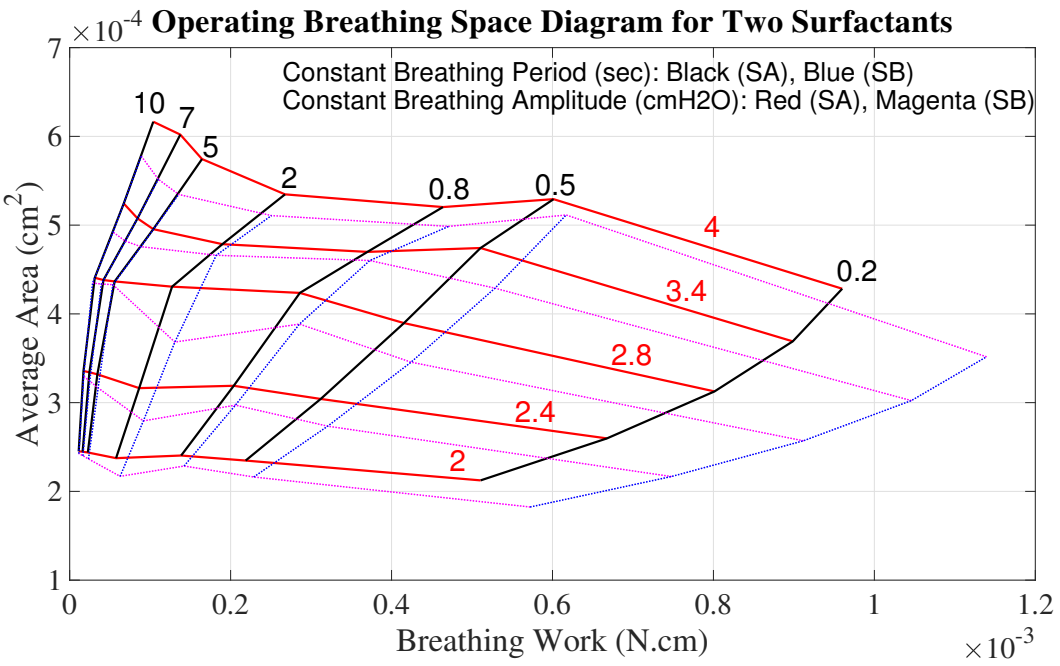

Figure 5.72: For the same breathing mode, surfactant SB provides less area for gas exchange and requires a larger breathing effort. This can be seen by the shift in the operating breathing space diagram (down and to the right).

While results in this section are still considered preliminary, and require more analysis before drawing definite conclusions, we believe that the novel idea of an *Operating Breathing Space* diagram is a step in the right direction regarding surfactant design. In other words, the alveolar model developed in this dissertation can be used to predict the breathing performance of an alveolus coated by different surfactants. For each surfactant, an *Operating Breathing Space* diagram can be constructed, and comparison among the different surfactants can be performed.

Next, the main outcomes of the dissertation are summarized in chapter 6. Limitations of the alveolar model, and ideas of future work are also presented.

Chapter 6

Conclusion

Essential to human survival is the constant replenishment of the body with oxygen and its depletion of carbon dioxide. This is done through breathing, an unconscious process that many of us take for granted. This seemingly simple and effortless activity for a healthy human requires complex interaction among multiple organs of the body. For example, the nervous, respiratory and cardiovascular systems all function simultaneously to ensure that breathing is effective and unhampered. The body however is prone to diseases and malfunctions. Any minor defect can have catastrophic effects and can lead to death. While research in the medical field is abundant and potent in treating the human body, we believe that engineers and mathematicians also have a contributing role. Our desire to advance human health has led us to study mathematically a complex mixture found in the lungs that is responsible for many deaths per year when it is dysfunctional. This mixture is referred to as pulmonary surfactant, and is found in a thin fluid layer that coats the inside of lung alveoli. We devoted this dissertation to the mathematical investigation of the determinative contributions of pulmonary surfactants to breathing. Our findings can improve treatments and consequently decrease the high mortality that accompanies respiratory distress syndrome, a well-known health condition that affects premature infants and adults, and that is caused by surfactant dysfunction.

Before developing a model to investigate the role of surfactant molecules in breathing, we simplified the alveolar geometry to a flat sheet coated by a thin fluid layer that is contaminated with surfactants as seen in chapter 2. This simple geometry allowed us to explore the interplay between the different transport modes that surfactants undergo, namely adsorption, desorption and diffusion. Several boundary value problems were solved for both a static and a deforming sheet. In addition, to the authors' best knowledge, it is the first time that a Lagrangian technique was applied to solve the surfactant transport problem in a constrained domain.

The knowledge gained from chapter 2 on pulmonary surfactant dynamics was then used in a mathematical model developed in chapters 3 and 4 that aimed at understanding the

effects that surfactants have on breathing. The model that we developed focused on the alveolus, where oxygen delivery and carbon dioxide removal to and from the blood occur. To our best knowledge, the developed model is the first to allow the simultaneous investigation of alveolar mechanics and gas exchange, as both are affected by surfactant dynamics. In addition, interfacial resistance that results from surfactants crowding air-water interfaces was incorporated in our model. Because breathing requires mechanical movement of multiple body parts, work has to be exerted during the process. Work of breathing is important to consider as breathing effort can be enormously affected by bodily malfunctions. Futhermore, it has been recorded that some infants stop breathing from fatigue when faced with excessive respiratory demands [132]. For this reason, we also derive an expression for the microscale work of breathing at the level of the alveolus and use it to compute the inhalation effort required when a certain surfactant is used. Another novel aspect of the model is the computation of the free motion of the alveolar boundary for a specific surfactant coating. In most research works in the literature, motion is prescribed and surfactant behavior is analyzed. Here however, pleural pressure is prescribed, and the resulting motion of the alveolar boundary is found by considering multiple phenomena such as surfactant transport in the hypophase and its ability to decrease surface tension. In the next section, we summarize the main takeaways from the dissertation.

6.1 Main Takeaways

We present a short summary of the main takeaways from this document that provide insight on breathing in general, and on the role of pulmonary surfactant.

The model was used to simulate multiple case studies related to breathing. When we hold our breath, oxygen in the alveolus diffuses to the blood passing through the exchange zone until its partial pressure in the alveolus equilibrates with that at the capillary inlet. Our model shows that it takes about a minute and a half for that to occur. At the same time, carbon dioxide diffuses out of the blood, but cannot be expelled out of the body while we hold our breath. With time, carbon dioxide partial pressure in the alveolus equilibrates with that at the capillary inlet. The model predicted a time span of 10 seconds before equilibration of carbon dioxide occured. Similar orders of magnitude for both oxygen and carbon dioxide are found in the literature [121]. Another aspect that we investigated was breathing at high altitudes such as at the summit of mount Everest. Our model predicted that the homogenized oxygen partial pressure in the blood is about 26 mmHg. This is consistent with the measured values reported in [126]. Using the model that we used for hemoglobin saturation shown in figure 4.3, we observe that only 50% of hemoglobin is saturated with oxygen, which explains the suffering of climbers from hypoxia. The effect of breathing at a faster rate was then simulated to test its effect on oxygen levels in the blood of mount Everst climbers. Results showed that fast breathing at a period of 0.5 seconds (compared to 5 seconds previously) increased oxygen flux from the alveolus to the blood and caused an

increase in the oxygen partial pressure from an average of 30 mmHg to 34 mmHg at capillary exit as can be seen in figure 5.30. This increase in oxygen partial pressure corresponds to an increase from 58% to 66% in hemoglobin saturation.

Surfactant deficiency or absence from the lung, which is a leading cause in the death of premature infants was also tested using our model. The high surface tension present in this case increases the elastic recoil of the lung and causes a pressure buildup inside the alveolus. This leads to the ejection of the gas mixture out of the alveolus and consequently alveolar collapse. This unfavorable behavior of alveolar collapse is the best example to illustrate the importance of surfactants on breathing. In chapter 2, surfactant transport in the hypophase was shown to be controlled by three non-dimensional parameters that represent ratios of the times scales of breathing, surfactant diffusion, adsorption, and desorption. Different values of the non-dimensional parameters were tested in the alveolar model. We mention here the main findings. Fast[1] adsorption of surfactants to the interface is necessary for large alveolar expansion and consequently effective gas exchange. Slow adsorption would result in high surface tension during inhalation and larger resistance to inflation. Fast surfactant diffusion in the bulk was also shown to be favorable to breathing. Slow diffusion resulted in the depletion of the subphase from surfactants, which decreased their ability to adsorb to the interface and to lower surface tension. Consequently, slow diffusion resulted in lower oxygen partial pressure at capillary exit. In the case of surfactant desorption, it was shown that a slower process is advantageous to breathing. Fast desorbing surfactants cause the surface tension to be high during exhalation. This causes pressure buildup in the alveolus as its radius decreases, and might lead to alveolar collapse. However, as explained in section 2.4, when the interfacial concentration of surfactants exceeds the maximum equilibrium concentration in a static system $\overline{\Gamma}$, pulmonary surfactants behave as insoluble surfactants. This causes the interfacial surfactant concentration to increase at a faster rate, which is accompanied by a decrease in surface tension to near zero values. The interfacial resistance of surfactants was also shown to have a considerable effect on gas exchange.

We next turned to using our model to understand the effect of every surfactant fraction on breathing. This was enabled thanks to the excellent experimental work in [130]. Our model showed that the phospholipid fraction did not offer much area for gas exchange and required a large breathing effort as compared to a fresh native surfactant. We conclude that the phospholipid portion of pulmonary surfactant cannot be used on its own as a viable surfactant. Such result was also reported in [20]. The addition of hydrophobic apoprotein SP-B and SP-C to phospholipid enormously improved its breathing contribution. Around 90% of the gas exchange area provided by the native surfactant was recovered and the breathing effort was reduced by 27%. The main underlying reason behind that positive change was the delay of surfactant film squeeze-out. However, the rate at which surface tension decreased was still much lower than that of the native surfactant. The addition of the hydrophilic sur-

[1] All comparisons here are done relative to the breathing cadence.

factant SP-A recovered that rate and led to a further 37% decrease in breathing work. The gas exchange area was almost fully recovered. Our model could not predict the main role of neutral lipids as no considerable effect was observed after their addition to the mixture. The model was also used to compare calf and porcine extract of surfactants, where it was shown that the calf extract is more efficient, mainly because of its adsorptive and diffusive properties.

Finally, we introduced the novel concept of an *Operating Breathing Space* diagram that corresponds to a specific surfactant. The average area available for gas exchange and the inhalation work of breathing over a minute are the main outputs of such diagram. In addition, the diagram spans multiple modes of breathing that we define by a combination of a breathing period and pleural pressure amplitude. Such diagrams are very important when designing surfactants.

6.2 Limitations and Future Work

The alveolar model presented in this dissertation provides valuable information regarding surfactant dynamics and breathing but suffers from multiple limitations and shortcomings.

The main weakness of this model is the considered geometry. The shape of the alveolus is not perfectly spherical as was considered in this dissertation. In fact, it was suggested that the surface of an alveolus has a polyhedral shape, giving it the form of a honeycomb [123]. Nonetheless, assuming a spherical geometry facilitated the modeling of different aspects of breathing. Another drawback that is also related to geometry is the fact that alveoli are not isolated as considered in this dissertation. In the real lung, alveoli are interconnected and found in the form of small clusters. This allows the exchange of gases between the different alveoli, an effect that was not considered here. In other words, the interplay of an alveolus with neighboring ones was not included in our model, and the implications of missing this effect on the values of oxygen and carbon dioxide fluxes need further investigation. A preliminary step towards remedying that would be extending the current model to a system formed by two interconnected alveoli.

Other modifications that will be implemented in the future to improve the alveolar model comprise but are not limited to including the rheological properties of the hypophase as done in [133], and also including Marangoni flows arising by the nonuniform surfactant distribution on the interface as performed in [134]. Another notable improvement for this model would be to include multilayer collapse and surfactant respreading to the pulmonary surfactant model presented in section 2.4. Such surfactant model was presented in [67]. Another significant limitation of our work was the absence of a validated constitutive model for the stresses in the alveolar wall from the literature. Current work is being conducted in collaboration with a biomechanics group at UC Berkeley to derive a constitutive relation for

the alveolar wall that can be implemented in this model to replace equation (3.39). Further investigation of the novel idea of an *Operating Breathing Space* diagram is also needed. We look to develop and implement an optimization procedure that helps us determine the most efficient surfactant under specific breathing conditions. Finally, the lack of experimental data to validate some of the results presented in this thesis is another major drawback.

In conclusion, the alveolar model developed in this dissertation elucidated many contributing actions of surfactants on breathing. Such findings can be used to improve the manufacturing of exogenous surfactants utilized in clinical applications and can hopefully decrease the mortality rates associated with surfactant related health conditions such as respiratory distress syndrome.

Bibliography

[1] D. D. Chiras, *Human Body Systems*, 2nd edition. Jones & Bartlett Publishers, May 2013, ISBN: 978-1-4496-4793-3.

[2] T. S. Pittman and K. R. Zeigler, "Basic Human Needs", in *Social Psychology,: Handbook of Basic Principles*, 2nd edition, Guilford Publications, 2013, pp. 473–489, ISBN: 978-1-4625-1486-1.

[3] V. Fanelli and V. M. Ranieri, "Mechanisms and clinical consequences of acute lung injury", *Annals of the american thoracic society*, vol. 12 Suppl 1, S3–8, Mar. 2015, ISSN: 2325-6621. DOI: 10.1513/AnnalsATS.201407-340MG.

[4] G. D. Rubenfeld, E. Caldwell, E. Peabody, J. Weaver, D. P. Martin, M. Neff, E. J. Stern, and L. D. Hudson, "Incidence and Outcomes of Acute Lung Injury", *New england journal of medicine*, vol. 353, no. 16, pp. 1685–1693, Oct. 2005, ISSN: 0028-4793. DOI: 10.1056/NEJMoa050333.

[5] W. A. Carlo and N. Ambalavanan, "Respiratory distress syndrome (hyaline membrane disease)", in *Nelson textbook of pediatrics*, 19th edition, 2011, pp. 581–590.

[6] N. Tam, *Respiratory System: A Tutorial Study Guide*. PublishDrive, Jun. 2015, ISBN: 978-1-301-80538-9.

[7] *5 Functions of Respiratory System*, www.visiblebody.com/learn/respiratory/5-functions-of-respiratory-system. (visited on 11/30/2017).

[8] R. Kara, *The Respiratory System*, 1st edition. Britannica Educational Publishing, 2011, pp. 18–38, ISBN: 978-1-61530-147-8.

[9] C. C. Hsia, D. M. Hyde, and E. R. Weibel, "Lung structure and the intrinsic challenges of gas exchange", *Comprehensive physiology*, 2016.

[10] *Respiratory System*, www.innerbody.com/anatomy/respiratory. (visited on 11/30/2017).

[11] J. P. T. Ward, J. Ward, and R. M. Leach, *The Respiratory System at a Glance*. John Wiley & Sons, Nov. 2011, pp. 12–14, ISBN: 978-1-118-29373-7.

[12] M. Ochs, J. R. Nyengaard, A. Jung, L. Knudsen, M. Voigt, T. Wahlers, J. Richter, and H. J. G. Gundersen, "The number of alveoli in the human lung", *American journal of respiratory and critical care medicine*, vol. 169, no. 1, pp. 120–124, 2004.

[13] O. D. Chuquimia, D. H. Petursdottir, N. Periolo, and C. Fernández, "Alveolar epithelial cells are critical in protection of the respiratory tract by secretion of factors able to modulate the activity of pulmonary macrophages and directly control bacterial growth", *Infection and immunity*, vol. 81, no. 1, pp. 381–389, 2013.

[14] P. O. Nkadi, T. A. Merritt, and D.-A. M. Pillers, "An Overview of Pulmonary Surfactant in the Neonate: Genetics, Metabolism, and the Role of Surfactant in Health and Disease", *Molecular genetics and metabolism*, vol. 97, no. 2, pp. 95–101, Jun. 2009, ISSN: 1096-7192. DOI: 10.1016/j.ymgme.2009.01.015.

[15] D. A. Edwards, H. Brenner, and D. T. Wasan, *Interfacial transport processes and rheology*. Butterworth-Heinemann Series in Chemical Engineering, Elsevier, 2013.

[16] C. G. Cochrane, "Pulmonary surfactant in allergic inflammation: New insights into the molecular mechanisms of surfactant function", *American journal of physiology-lung cellular and molecular physiology*, vol. 288, no. 4, pp. L608–L609, 2005.

[17] J. Mazela, T. A. Merritt, J. Gadzinowski, and S. Sinha, "Evolution of pulmonary surfactants for the treatment of neonatal respiratory distress syndrome and paediatric lung diseases", *Acta paediatrica*, vol. 95, no. 9, pp. 1036–1048, 2006.

[18] M. M. Fyrillas and A. J. Szeri, "Dissolution or growth of soluble spherical oscillating bubbles: The effect of surfactants", *Journal of fluid mechanics*, vol. 289, pp. 295–314, 1995.

[19] J. Hildebran, J Goerke, and J. Clements, "Pulmonary surface film stability and composition", *Journal of applied physiology*, vol. 47, no. 3, pp. 604–611, 1979.

[20] F. Possmayer, "The role of surfactant-associated proteins.", *The american review of respiratory disease*, vol. 142, no. 4, pp. 749–752, 1990.

[21] R. H. Notter, "Biophysical behavior of lung surfactant: Implications for respiratory physiology and pathophysiology.", in *Seminars in perinatology*, vol. 12, 1988, pp. 180–212.

[22] F. Possmayer, K. Nag, K. Rodriguez, R. Qanbar, and S. Schrch, "Surface activity in vitro: Role of surfactant proteins", *Comparative biochemistry and physiology. part a, molecular & integrative physiology*, vol. 129, no. 1, pp. 209–220, May 2001, ISSN: 1095-6433.

[23] E. J. A. Veldhuizen and H. P. Haagsman, "Role of pulmonary surfactant components in surface film formation and dynamics", *Biochimica et biophysica acta (bba) - biomembranes*, vol. 1467, no. 2, pp. 255–270, Aug. 2000, ISSN: 0005-2736. DOI: 10.1016/S0005-2736(00)00256-X.

[24] J. Goerke and J. A. Clements, "Alveolar surface tension and lung surfactant", *Comprehensive physiology*, 1986.

[25] K. v. Neergaard, "Neue auffassungen über einen grundbegriff der atemmechanik", *Zeitschrift für die gesamte experimentelle medizin*, vol. 66, no. 1, pp. 373–394, 1929.

[26] E. P. Radford Jr, "Method for estimating respiratory surface area of mammalian lungs from their physical characteristics.", *Proceedings of the society for experimental biology and medicine*, vol. 87, no. 1, pp. 58–61, 1954.

[27] E. Radford, "Recent studies of mechanical properties of mammalian lungs", *Tissue elasticity*, vol. 177, 1957.

[28] J. Mead and C. Collier, "Relation of volume history of lungs to respiratory mechanics in anesthetized dogs", *Journal of applied physiology*, vol. 14, no. 5, pp. 669–678, 1959.

[29] J Mead, J. Whittenberger, and E. Radford, "Surface tension as a factor in pulmonary volume-pressure hysteresis", *Journal of applied physiology*, vol. 10, no. 2, pp. 191–196, 1957.

[30] R. Pattle, "Properties, function, and origin of the alveolar lining layer", *Proceedings of the royal society of london b: Biological sciences*, vol. 148, no. 931, pp. 217–240, 1958.

[31] J. A. Clements, "Surface tension of lung extracts", *Proceedings of the society for experimental biology and medicine*, vol. 95, no. 1, pp. 170–172, 1957.

[32] J. A. Clements, E. S. Brown, and R. P. Johnson, "Pulmonary surface tension and the mucus lining of the lungs: Some theoretical considerations", *Journal of applied physiology*, vol. 12, no. 2, pp. 262–268, 1958.

[33] E. S. Brown, R. P. Johnson, and J. A. Clements, "Pulmonary surface tension", *Journal of applied physiology*, vol. 14, no. 5, pp. 717–720, 1959.

[34] E. S. Brown, "Isolation and assay of dipalmityl lecithin in lung extracts", *American journal of physiology–legacy content*, vol. 207, no. 2, pp. 402–406, 1964.

[35] M. E. Avery and J. Mead, "Surface properties in relation to atelectasis and hyaline membrane disease", *Ama journal of diseases of children*, vol. 97, no. 5_PART_I, pp. 517–523, 1959.

[36] M. E. Avery, "On replacing the surfactant", *Pediatrics*, vol. 65, no. 6, pp. 1176–1177, 1980.

[37] M. Hailman, T. A. Merritt, H. Schneider, B. L. Epstein, F. Mannino, D. K. Edwards, and L. Gluck, "Isolation of human surfactant from amniotic fluid and a pilot study of its efficacy in respiratory distress syndrome", *Pediatrics*, vol. 71, no. 4, pp. 473–482, 1983.

[38] M. Ikegami, T. Hesterberg, M. Nozaki, and F. H. Adams, "Restoration of lung pressure-volume characteristics with surfactant: Comparison of nebulization versus instillation and natural versus synthetic surfactant", *Pediatric research*, vol. 11, no. 3, pp. 178–182, 1977.

[39] C. Morley, N Miller, A. Bangham, and J. Davis, "Dry artificial lung surfactant and its effect on very premature babies", *The lancet*, vol. 317, no. 8211, pp. 64–68, 1981.

[40] K. Altirkawi, "Surfactant therapy: The current practice and the future trends", *Sudanese journal of paediatrics*, vol. 13, no. 1, p. 11, 2013.

[41] A. Dushianthan, R. Cusack, V. Goss, A. D. Postle, and M. P. W. Grocott, "Clinical review: Exogenous surfactant therapy for acute lung injury/acute respiratory distress syndrome–where do we go from here?", *Critical care (london, england)*, vol. 16, no. 6, p. 238, Nov. 2012, ISSN: 1466-609X. DOI: 10.1186/cc11512.

[42] J. Perez-Gil and T. E. Weaver, "Pulmonary surfactant pathophysiology: Current models and open questions", *Physiology (bethesda, md.)*, vol. 25, no. 3, pp. 132–141, Jun. 2010, ISSN: 1548-9221. DOI: 10.1152/physiol.00006.2010.

[43] L. A. Creuwels, L. M. van Golde, and H. P. Haagsman, "The pulmonary surfactant system: Biochemical and clinical aspects", *Lung*, vol. 175, no. 1, pp. 1–39, 1997, ISSN: 0341-2040.

[44] B. A. Hills, "An alternative view of the role(s) of surfactant and the alveolar model", *Journal of applied physiology (bethesda, md.: 1985)*, vol. 87, no. 5, pp. 1567–1583, Nov. 1999, ISSN: 8750-7587.

[45] S Schurch, M. Lee, and P. Gehr, *Pulmonary surfactant: Surface properties and function of alveolar and airway surfactant*. Nov. 1992, vol. 64, DOI: 10.1351/pac199264111745.

[46] R. H. Notter and P. E. Morrow, "Pulmonary surfactant: A surface chemistry viewpoint", *Annals of biomedical engineering*, vol. 3, no. 2, pp. 119–159, Jun. 1975, ISSN: 0090-6964, 1573-9686. DOI: 10.1007/BF02363067.

[47] J. Goerke, "Pulmonary surfactant: Functions and molecular composition", *Biochimica et biophysica acta (bba) - molecular basis of disease*, vol. 1408, no. 2, pp. 79–89, Nov. 1998, ISSN: 0925-4439. DOI: 10.1016/S0925-4439(98)00060-X.

[48] Y. Y. Zuo, R. A. W. Veldhuizen, A. W. Neumann, N. O. Petersen, and F. Possmayer, "Current perspectives in pulmonary surfactant–inhibition, enhancement and evaluation", *Biochimica et biophysica acta*, vol. 1778, no. 10, pp. 1947–1977, Oct. 2008, ISSN: 0006-3002. DOI: 10.1016/j.bbamem.2008.03.021.

[49] S. Rugonyi, S. C. Biswas, and S. B. Hall, "The Biophysical Function of Pulmonary Surfactant", *Respiratory physiology & neurobiology*, vol. 163, no. 1-3, pp. 244–255, Nov. 2008, ISSN: 1569-9048. DOI: 10.1016/j.resp.2008.05.018.

[50] R. W. Walters, R. R. Jenq, and S. B. Hall, "Distinct steps in the adsorption of pulmonary surfactant to an air-liquid interface", *Biophysical journal*, vol. 78, no. 1, pp. 257–266, Jan. 2000, ISSN: 0006-3495. DOI: 10.1016/S0006-3495(00)76589-1.

[51] J. Hohlfeld, H. Fabel, and H. Hamm, "The role of pulmonary surfactant in obstructive airways disease", *The european respiratory journal*, vol. 10, no. 2, pp. 482–491, Feb. 1997, ISSN: 0903-1936.

[52] H. P. Haagsman, A. Hogenkamp, M. van Eijk, and E. J. A. Veldhuizen, "Surfactant collectins and innate immunity", *Neonatology*, vol. 93, no. 4, pp. 288–294, 2008, ISSN: 1661-7819. DOI: 10.1159/000121454.

[53] P. S. Kingma and J. A. Whitsett, "In defense of the lung: Surfactant protein A and surfactant protein D", *Current opinion in pharmacology*, vol. 6, no. 3, pp. 277–283, Jun. 2006, ISSN: 1471-4892. DOI: 10.1016/j.coph.2006.02.003.

[54] Y. Kuroki, M. Takahashi, and C. Nishitani, "Pulmonary collectins in innate immunity of the lung", *Cellular microbiology*, vol. 9, no. 8, pp. 1871–1879, Aug. 2007, ISSN: 1462-5814. DOI: 10.1111/j.1462-5822.2007.00953.x.

[55] J. R. Wright, "Immunoregulatory functions of surfactant proteins", *Nature reviews. immunology*, vol. 5, no. 1, pp. 58–68, Jan. 2005, ISSN: 1474-1733. DOI: 10.1038/nri1528.

[56] C. B. Daniels and S. Orgeig, "Pulmonary surfactant: The key to the evolution of air breathing", *News in physiological sciences: An international journal of physiology produced jointly by the international union of physiological sciences and the american physiological society*, vol. 18, pp. 151–157, Aug. 2003, ISSN: 0886-1714.

[57] S. Baoukina and D. P. Tieleman, "Computer simulations of lung surfactant", *Biochimica et biophysica acta*, vol. 1858, no. 10, pp. 2431–2440, 2016, ISSN: 0006-3002. DOI: 10.1016/j.bbamem.2016.02.030.

[58] J. B. Grotberg, "Pulmonary Flow and Transport Phenomena", *Annual review of fluid mechanics*, vol. 26, no. 1, pp. 529–571, 1994. DOI: 10.1146/annurev.fl.26.010194.002525.

[59] J. B. Grotberg, "Respiratory fluid mechanics and transport processes", *Annual review of biomedical engineering*, vol. 3, pp. 421–457, 2001, ISSN: 1523-9829. DOI: 10.1146/annurev.bioeng.3.1.421.

[60] J. B. Grotberg, "Respiratory fluid mechanics", *Physics of fluids*, vol. 23, no. 2, Feb. 2011, ISSN: 1070-6631. DOI: 10.1063/1.3517737.

[61] G. Putz, J. Goerke, S. Schrch, and J. A. Clements, "Evaluation of pressure-driven captive bubble surfactometer", *Journal of applied physiology (bethesda, md.: 1985)*, vol. 76, no. 4, pp. 1417–1424, Apr. 1994, ISSN: 8750-7587.

[62] G. Putz, J. Goerke, H. W. Taeusch, and J. A. Clements, "Comparison of captive and pulsating bubble surfactometers with use of lung surfactants", *Journal of applied physiology (bethesda, md.: 1985)*, vol. 76, no. 4, pp. 1425–1431, Apr. 1994, ISSN: 8750-7587.

[63] S. Schrch, H. Bachofen, and F. Possmayer, "Surface activity in situ, in vivo, and in the captive bubble surfactometer", *Comparative biochemistry and physiology. part a, molecular & integrative physiology*, vol. 129, no. 1, pp. 195–207, May 2001, ISSN: 1095-6433.

[64] D. R. Otis, E. P. Ingenito, R. D. Kamm, and M. Johnson, "Dynamic surface tension of surfactant TA: Experiments and theory", *Journal of applied physiology (bethesda, md.: 1985)*, vol. 77, no. 6, pp. 2681–2688, Dec. 1994, ISSN: 8750-7587.

[65] E. P. Ingenito, L. Mark, J. Morris, F. F. Espinosa, R. D. Kamm, and M. Johnson, "Biophysical characterization and modeling of lung surfactant components", *Journal of applied physiology (bethesda, md.: 1985)*, vol. 86, no. 5, pp. 1702–1714, May 1999, ISSN: 8750-7587.

[66] J. Morris, E. P. Ingenito, L. Mark, R. D. Kamm, and M. Johnson, "Dynamic behavior of lung surfactant", *Journal of biomechanical engineering*, vol. 123, no. 1, pp. 106–113, Feb. 2001, ISSN: 0148-0731.

[67] M. Krueger and D. Gaver, "A Theoretical Model of Pulmonary Surfactant Multilayer Collapse under Oscillating Area Conditions", *Journal of colloid and interface science*, vol. 229, no. 2, pp. 353–364, Sep. 2000, ISSN: 1095-7103. DOI: 10.1006/jcis.2000.7029.

[68] H.-H. Wei, S. W. Benintendi, D. Halpern, and J. B. Grotberg, "Cycle-induced flow and transport in a model of alveolar liquid lining", *Journal of fluid mechanics*, vol. 483, pp. 1–36, May 2003, ISSN: 1469-7645, 0022-1120. DOI: 10.1017/S0022112003003859.

[69] H.-H. Wei, H. Fujioka, R. B. Hirschl, and J. B. Grotberg, "A model of flow and surfactant transport in an oscillatory alveolus partially filled with liquid", *Physics of fluids*, vol. 17, no. 3, p. 031 510, Mar. 2005, ISSN: 1070-6631. DOI: 10.1063/1.1830487.

[70] M. S. Borgas and J. B. Grotberg, "Monolayer flow on a thin film", *Journal of fluid mechanics*, vol. 193, pp. 151–170, Aug. 1988, ISSN: 1469-7645, 0022-1120. DOI: 10.1017/S0022112088002095.

[71] F. F. Espinosa and R. D. Kamm, "Thin layer flows due to surface tension gradients over a membrane undergoing nonuniform, periodic strain", *Annals of biomedical engineering*, vol. 25, no. 6, pp. 913–925, Dec. 1997, ISSN: 0090-6964.

[72] R. Levy and M. Shearer, "The Motion of a Thin Liquid Film Driven by Surfactant and Gravity", *Siam journal on applied mathematics*, vol. 66, no. 5, pp. 1588–1609, Jan. 2006, ISSN: 0036-1399. DOI: 10.1137/050637030.

[73] T. A. Siebert and S. Rugonyi, "Influence of Liquid-Layer Thickness on Pulmonary Surfactant Spreading and Collapse", *Biophysical journal*, vol. 95, no. 10, pp. 4549–4559, Nov. 2008, ISSN: 0006-3495. DOI: 10.1529/biophysj.107.127654.

[74] R. V. Craster and O. K. Matar, "Surfactant transport on mucus films", *Journal of fluid mechanics*, vol. 425, pp. 235–258, Dec. 2000, ISSN: 1469-7645, 0022-1120. DOI: 10.1017/S0022112000002317.

[75] V. Suresh and J. B. Grotberg, "The effect of gravity on liquid plug propagation in a two-dimensional channel", *Physics of fluids*, vol. 17, no. 3, p. 031 507, Mar. 2005, ISSN: 1070-6631. DOI: 10.1063/1.1863853.

[76] Y. Zheng, J. C. Anderson, V. Suresh, and J. B. Grotberg, "Effect of gravity on liquid plug transport through an airway bifurcation model", *Journal of biomechanical engineering*, vol. 127, no. 5, pp. 798–806, Oct. 2005, ISSN: 0148-0731.

[77] F. F. Espinosa and R. D. Kamm, "Meniscus formation during tracheal instillation of surfactant.", *Journal of applied physiology (bethesda, md. : 1985)*, vol. 85, no. 1, pp. 266–272, Jul. 1998, ISSN: 8750-7587.

[78] D. R. Otis, M. Johnson, T. J. Pedley, and R. D. Kamm, "Role of pulmonary surfactant in airway closure: A computational study", *Journal of applied physiology (bethesda, md.: 1985)*, vol. 75, no. 3, pp. 1323–1333, Sep. 1993, ISSN: 8750-7587.

[79] D. Halpern and J. B. Grotberg, "Surfactant effects on fluid-elastic instabilities of liquid-lined flexible tubes: A model of airway closure", *Journal of biomechanical engineering*, vol. 115, no. 3, pp. 271–277, Aug. 1993, ISSN: 0148-0731.

[80] Y. Y. Zuo, D. Li, E. Acosta, P. N. Cox, and A. W. Neumann, "Effect of surfactant on interfacial gas transfer studied by axisymmetric drop shape analysis-captive bubble (ADSA-CB)", *Langmuir: The acs journal of surfaces and colloids*, vol. 21, no. 12, pp. 5446–5452, Jun. 2005, ISSN: 0743-7463. DOI: 10.1021/la050281u.

[81] Y. Y. Zuo, E. Acosta, P. N. Cox, D. Li, and A. W. Neumann, "Effect of Compressed Bovine Lipid Extract Surfactant Films on Oxygen Transfer", *Langmuir*, vol. 23, no. 3, pp. 1339–1346, Jan. 2007, ISSN: 0743-7463. DOI: 10.1021/la061608+.

[82] M. N. Möller, Q. Li, M. Chinnaraj, H. C. Cheung, J. R. Lancaster Jr, and A. Denicola, "Solubility and diffusion of oxygen in phospholipid membranes", *Biochimica et biophysica acta (bba) - biomembranes*, vol. 1858, no. 11, pp. 2923–2930, Nov. 2016, ISSN: 0005-2736. DOI: 10.1016/j.bbamem.2016.09.003.

[83] C. Åberg, E. Sparr, M. Larsson, and H. Wennerström, "A theoretical study of diffusional transport over the alveolar surfactant layer", *Journal of the royal society interface*, vol. 7, no. 51, pp. 1403–1410, Oct. 2010, ISSN: 1742-5689. DOI: 10.1098/rsif.2010.0082.

[84] E. J. M. Campbell, *The respiratory muscles and the mechanics of breathing*. Lloyd-Luke, 1958.

[85] J. G. McFadyen, D. R. Thompson, and L. D. Martin, "Applied respiratory physiology", in *Pediatric critical care medicine*, Springer, 2014, pp. 3–18.

[86] O. Chowdhury, P. Bhat, G. F. Rafferty, S. Hannam, A. D. Milner, and A. Greenough, "In vitro assessment of the effect of proportional assist ventilation on the work of breathing", *European journal of pediatrics*, vol. 175, no. 5, pp. 639–643, May 2016, ISSN: 1432-1076. DOI: 10.1007/s00431-015-2673-7.

[87] A. Tulaimat, A. Patel, M. Wisniewski, and R. Gueret, "The validity and reliability of the clinical assessment of increased work of breathing in acutely ill patients", *Journal of critical care*, vol. 34, no. Supplement C, pp. 111–115, Aug. 2016, ISSN: 0883-9441. DOI: 10.1016/j.jcrc.2016.04.013.

[88] J. C. Anderson, A. L. Babb, and M. P. Hlastala, "Modeling soluble gas exchange in the airways and alveoli", *Annals of biomedical engineering*, vol. 31, no. 11, pp. 1402–1422, 2003.

[89] R. H. Notter, *Lung surfactants: Basic science and clinical applications*. Marcel Dekker, 2000.

[90] P. K. Kundu, I. M. Cohen, and D. R. Dowling, *Fluid Mechanics, Fifth Edition*, 5th edition. Waltham, MA: Academic Press, 2012, ISBN: 978-0-12-382100-3.

[91] C.-H. Chang and E. I. Franses, "Adsorption dynamics of surfactants at the air/water interface: A critical review of mathematical models, data, and mechanisms", *Colloids and surfaces a: Physicochemical and engineering aspects*, vol. 100, pp. 1–45, 1995.

[92] P Tchoreloff, A Gulik, B Denizot, J. Proust, and F Puisieux, "A structural study of interfacial phospholipid and lung surfactant layers by transmission electron microscopy after blodgett sampling: Influence of surface pressure and temperature", *Chemistry and physics of lipids*, vol. 59, no. 2, pp. 151–165, 1991.

[93] J. E. H. Bunt, L. J. Zimmermann, J. Darcos Wattimena, R. H. van Beek, P. J. SAUER, and V. P. Carnielli, "Endogenous surfactant turnover in preterm infants measured with stable isotopes", *American journal of respiratory and critical care medicine*, vol. 157, no. 3, pp. 810–814, 1998.

[94] G. N. Maksym and J. H. Bates, "A distributed nonlinear model of lung tissue elasticity", *Journal of applied physiology*, vol. 82, no. 1, pp. 32–41, 1997.

[95] D. Vawter, Y. Fung, and J. West, "Constitutive equation of lung tissue elasticity", *J. biomech. eng*, vol. 101, no. 1, pp. 38–45, 1979.

[96] D Stamenovic and T. Wilson, "A strain energy function for lung parenchyma", *Journal of biomechanical engineering*, vol. 107, no. 1, pp. 81–86, 1985.

[97] S. Rausch, C. Martin, P. Bornemann, S Uhlig, and W. Wall, "Material model of lung parenchyma based on living precision-cut lung slice testing", *Journal of the mechanical behavior of biomedical materials*, vol. 4, no. 4, pp. 583–592, 2011.

[98] T Ashcroft, J. M. Simpson, and V Timbrell, "Simple method of estimating severity of pulmonary fibrosis on a numerical scale.", *Journal of clinical pathology*, vol. 41, no. 4, pp. 467–470, 1988.

[99] B. Birkelbach, D. Lutz, C. Ruppert, I. Henneke, E. Lopez-Rodriguez, A. Günther, M. Ochs, P. Mahavadi, and L. Knudsen, "Linking progression of fibrotic lung remodeling and ultrastructural alterations of alveolar epithelial type ii cells in the amiodarone mouse model", *American journal of physiology-lung cellular and molecular physiology*, vol. 309, no. 1, pp. L63–L75, 2015.

[100] C. Mühlfeld and M. Ochs, "Quantitative microscopy of the lung-a problem-based approach part 2: Stereological parameters and study designs in various diseases of the respiratory tract", *American journal of physiology-lung cellular and molecular physiology*, 2013.

[101] B. Yang, A. Jbaily, Y. Lu, A. J. Szeri, and G. D. O'Connell, "LUNG MICROMECHANICS OF PULMONARY FIBROSIS: A FINITE ELEMENT ANALYSIS", in *Summer Biomechanics, Bioengineering and Biotransport Conference*, Tucson, Arizona, Jun. 2017.

[102] S. A. Maas, B. J. Ellis, G. A. Ateshian, and J. A. Weiss, "Febio: Finite elements for biomechanics", *Journal of biomechanical engineering*, vol. 134, no. 1, p. 011 005, 2012.

[103] R. S. Harris, "Pressure-volume curves of the respiratory system", *Respiratory care*, vol. 50, no. 1, pp. 78–99, 2005.

[104] F. G. Hoppin, J. C. Stothert, I. A. Greaves, Y.-L. Lai, and J. Hildebrandt, "Lung recoil: Elastic and rheological properties", *Comprehensive physiology*, 1986.

[105] E. Roan and C. M. Waters, "What do we know about mechanical strain in lung alveoli?", *American journal of physiology-lung cellular and molecular physiology*, vol. 301, no. 5, pp. L625–L635, 2011.

[106] D. Rubenstein, W. Yin, and M. D. Frame, "Flow in the Lungs", in *Biofluid Mechanics: An Introduction to Fluid Mechanics, Macrocirculation, and Microcirculation*, Academic Press, Jul. 2015, pp. 327–353, ISBN: 978-0-12-801169-0.

[107] D. Rubenstein, W. Yin, and M. D. Frame, "Mass Transport and Heat Transfer in the Microcirculation", in *Biofluid Mechanics: An Introduction to Fluid Mechanics, Macrocirculation, and Microcirculation*, Academic Press, Jul. 2015, pp. 267–309, ISBN: 978-0-12-801169-0.

[108] F. Roughton and R. Forster, "Relative importance of diffusion and chemical reaction rates in determining rate of exchange of gases in the human lung, with special reference to true diffusing capacity of pulmonary membrane and volume of blood in the lung capillaries", *Journal of applied physiology*, vol. 11, no. 2, pp. 290–302, 1957.

[109] E. R. Weibel, B. Sapoval, and M. Filoche, "Design of peripheral airways for efficient gas exchange", *Respiratory physiology & neurobiology*, vol. 148, no. 1, pp. 3–21, 2005.

[110] J. E. Cotes, D. J. Chinn, and M. R. Miller, *Lung function: Physiology, measurement and application in medicine*. John Wiley & Sons, 2009.

[111] C. Hsia, C. Chuong, and R. Johnson, "Critique of conceptual basis of diffusing capacity estimates: A finite element analysis", *Journal of applied physiology*, vol. 79, no. 3, pp. 1039–1047, 1995.

[112] S. Martin and B. Maury, "Modeling of the oxygen transfer in the respiratory process", *Esaim: Mathematical modelling and numerical analysis*, vol. 47, no. 4, pp. 935–960, 2013.

[113] B. Maury, "Gas exchanges", in *The Respiratory System in Equations*, Springer, 2013.

[114] E. R. Weibel, C. R. Taylor, J. J. O'Neil, D. E. Leith, P. Gehr, H. Hoppeler, V. Langman, and R. V. Baudinette, "Maximal oxygen consumption and pulmonary diffusing capacity: A direct comparison of physiologic and morphometric measurements in canids", *Respiration physiology*, vol. 54, no. 2, pp. 173–188, 1983.

[115] A. C. Guyton and J. E. Hall, "Transport of oxygen and carbon dioxide in blood and tissue fluids", in *Textbook of medical physiology*, El Sevier Saunders, 2006, pp. 502–513.

[116] J. Keener and J. Sneyd, *Mathematical physiology: I: Cellular physiology*. Springer Science & Business Media, 2009.

[117] W. A. Eaton, E. Henry, J. Hofrichter, A. Mozzarelli, *et al.*, "Is cooperative oxygen binding by hemoglobin really understood?", *Nature structural biology*, vol. 6, no. 4, 1999.

[118] G. R. Kelman, "Digital computer subroutine for the conversion of oxygen tension into saturation.", *Journal of applied physiology*, vol. 21, no. 4, pp. 1375–1376, 1966.

[119] J. Monod, J. Wyman, and J.-P. Changeux, "On the nature of allosteric transitions: A plausible model", *Journal of molecular biology*, vol. 12, no. 1, pp. 88–118, 1965.

[120] A. J. Swan and M. H. Tawhai, "Evidence for minimal oxygen heterogeneity in the healthy human pulmonary acinus", *Journal of applied physiology*, vol. 110, no. 2, pp. 528–537, 2011.

[121] A. Ben-Tal, "Simplified models for gas exchange in the human lungs", *Journal of theoretical biology*, vol. 238, no. 2, pp. 474–495, 2006.

[122] C. Brighenti, G. Gnudi, and G. Avanzolini, "A simulation model of the oxygen alveolo–capillary exchange in normal and pathological conditions", *Physiological measurement*, vol. 24, no. 2, p. 261, 2003.

[123] S. Andreassen, K. L. Steimle, M. L. Mogensen, J. B. de la Serna, S. Rees, and D. S. Karbing, "The effect of tissue elastic properties and surfactant on alveolar stability", *Journal of applied physiology*, vol. 109, no. 5, pp. 1369–1377, 2010.

[124] J. Hughes, "Review series: Lung function made easy: Assessing gas exchange", *Chronic respiratory disease*, vol. 4, no. 4, pp. 205–214, 2007.

[125] J Piiper, M Meyer, and P Scheid, "Diffusion limitation in alveolar-capillary co2 transfer in human lungs: Experimental evidence from rebreathing equilibration", in *Biophysics and physiology of carbon dioxide*, Springer, 1980, pp. 359–365.

[126] M. P. Grocott, D. S. Martin, D. Z. Levett, R. McMorrow, J. Windsor, and H. E. Montgomery, "Arterial blood gases and oxygen content in climbers on mount everest", *New england journal of medicine*, vol. 360, no. 2, pp. 140–149, 2009.

[127] R Kowe, R. Schroter, F. Matthews, and D Hitchings, "Analysis of elastic and surface tension effects in the lung alveolus using finite element methods", *Journal of biomechanics*, vol. 19, no. 7, pp. 541–549, 1986.

[128] W. A. Wall, L. Wiechert, A. Comerford, and S. Rausch, "Towards a comprehensive computational model for the respiratory system", *International journal for numerical methods in biomedical engineering*, vol. 26, no. 7, pp. 807–827, 2010.

[129] T. Gregory, W. Longmore, M. Moxley, J. Whitsett, C. Reed, A. Fowler 3rd, L. Hudson, R. Maunder, C Crim, and T. Hyers, "Surfactant chemical composition and biophysical activity in acute respiratory distress syndrome.", *Journal of clinical investigation*, vol. 88, no. 6, p. 1976, 1991.

[130] J. S. Morris, "Characterization of the dynamic behavior of lung surfactant and its components", Master's thesis, Massachusetts Institute of Technology, 1998.

[131] A Greenough, J Pool, F Greenall, C Morley, and H Gamsu, "Comparison of different rates of artificial ventilation in preterm neonates with respiratory distress syndrome", *Acta paediatrica*, vol. 76, no. 5, pp. 706–712, 1987.

[132] J. G. McFadyen, D. R. Thompson, and L. D. Martin, "Applied respiratory physiology", in *Pediatric critical care medicine: Volume 2: Respiratory, cardiovascular and central nervous systems*, D. S. Wheeler, H. R. Wong, and T. P. Shanley, Eds. London: Springer London, 2014, pp. 3–18, ISBN: 978-1-4471-6356-5. DOI: 10.1007/978-1-4471-6356-5_1.

[133] L. W. Horn and S. H. Davis, "Apparent surface tension hysteresis of a dynamical system", *Journal of colloid and interface science*, vol. 51, no. 3, pp. 459–476, 1975.

[134] A. PODGÓRSKI and L. GRADOŃ, "An improved mathematical model of hydrodynamical self-cleansing of pulmonary alveoli", *The annals of occupational hygiene*, vol. 37, no. 4, pp. 347–366, 1993.

[135] M. G. Levitzky, *Pulmonary Physiology*, 7th edition. McGraw Hill Professional, Jan. 30, 2007, ISBN: 978-0-07-150874-2.

[136] R. J. LeVeque, *Finite difference methods for ordinary and partial differential equations: Steady-state and time-dependent problems*. SIAM, 2007.

[137] J. B. West, *Respiratory physiology: The essentials*. Lippincott Williams & Wilkins, 2012.

[138] Y. A. Cengel and M. A. Boles, *Thermodynamics: An Engineering Approach*, 8th edition. McGraw-Hill Education, Jan. 7, 2014, ISBN: 978-0-07-339817-4.

[139] S. M. Saad, Z. Policova, E. J. Acosta, and A. W. Neumann, "Effect of surfactant concentration, compression ratio and compression rate on the surface activity and dynamic properties of a lung surfactant", *Biochimica et biophysica acta (bba)-biomembranes*, vol. 1818, no. 1, pp. 103–116, 2012.

[140] A. A. Merrikh and J. L. Lage, "Effect of blood flow on gas transport in a pulmonary capillary", *Journal of biomechanical engineering*, vol. 127, no. 3, pp. 432–439, 2005.

Appendix A

Effective Resistance

In this section, we derive an expression for the effective resistance Ω that appears in equation (3.12). The purpose of doing so is to get an order of magnitude of Ω that can be used in the model. The bronchial tree is assumed to be symmetric with an incoming volumetric flux Q through the trachea. At every generation, the number of airways doubles and the flux is halved. This is shown in figure A.1. The pressure drop across every generation i is called

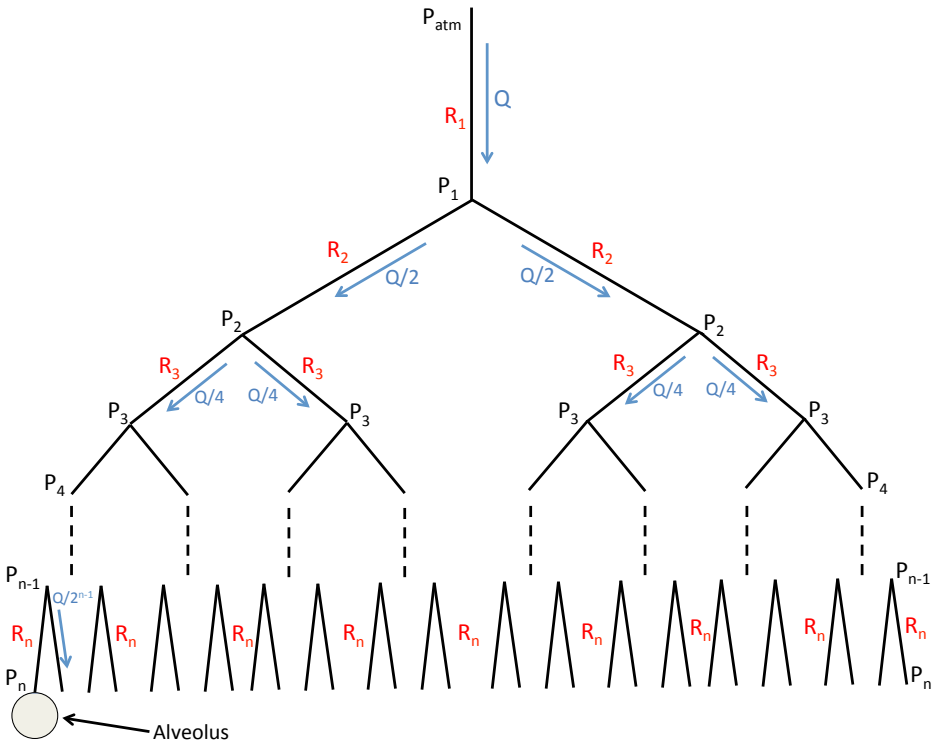

Figure A.1: Lung as a Resistive Tree

ΔP_i. For example, $\Delta P_1 = P_1 - P_{atm}$, $\Delta P_2 = P_2 - P_1$, and $\Delta P_n = P_n - P_{n-1}$.

The flux in the airway of every generation i and the pressure drop ΔP_i across it are related by the resistance R_i of the airway. For example, $\Delta P_2 = (Q/2)R_2$, $\Delta P_3 = (Q/4)R_3$, and so

$$\Delta P_i = Q\frac{R_i}{2^{i-1}}, \tag{A.1}$$

where i goes from 1 to n.
The summation of ΔP_i from 1 to n yields:

$$\sum_{i=1}^{n} \Delta P_i = P_n - P_{atm} = Q\sum_{i=1}^{n} \frac{R_i}{2^{i-1}}. \tag{A.2}$$

In equation (3.12), the effective resistance Ω relates the alveolar gauge pressure $(P_i - P_{atm})$ at an alveolus in generation i to the volumetric flux $(Q/2^{i-1})$ feeding into the alveolus. In other words, Ω is the resistance of the path that starts at the mouth and ends in the alveolus in generation i. If the alveolus is chosen to be in generation n, then:

$$\frac{P_n - P_{atm}}{\Omega} = \frac{Q}{2^{n-1}}. \tag{A.3}$$

Comparing equations (A.2) and (A.3), it can be concluded that the effective resistance of the path leading into the alveolus in generation n is given by:

$$\Omega = 2^{n-1}\sum_{i=1}^{n} \frac{R_i}{2^{i-1}}. \tag{A.4}$$

What still need to be found are the individual resistances R_i of the airways in the different generations. To do so, we refer to figure 1-5 in [135][1] to get the airways' dimensions in every generation. We then assume Poiseuille flow in every airway and express the resistance R_i as:

$$R_i = \frac{8\mu_a l_i}{\pi a_i^4}, \tag{A.5}$$

where μ_a is the dynamic viscosity of air, and l_i and a_i are the length and the radius of the airway in generation i. For example, if the alveolus is chosen to be in the last generation, the effective resistance[2] $\Omega = 0.65$ (N.sec/cm^5).

[1] Figure is not reproduced here because permission to reproduce was not requested.

[2] When solving the alveolar model numerically, the value of Ω affected the speed of the simulations. In cases where choosing a higher value of Ω did not affect the results, we chose to use the higher one (one or two orders of magnitude higher) to speed up the simulations.

Appendix B

Surfactant Transport Problem - Referential Description

Two coordinate transformations are applied to the surfactant transport problem. The motivation behind each transformation is described, and the method and final equations are presented.

Since surfactant transport only occurs in the hypophase, we introduce a spatial coordinate with a range equal to the hypophase thickness. Unlike the radial position r that spans the whole alveolus (air and hypophase), the new spatial variable q only spans the hypophase. It is defined below:

$$q = r - \Big(R(t) - h(t)\Big) \tag{B.1}$$

$$\left\{ \begin{array}{cc} At\ r = R(t) - h(t) & q = 0 \\ At\ r = R(t) & q = h(t) \end{array} \right\}.$$

Using the newly defined variable q, we note the following relations:

$$\frac{\partial C_s(r,t)}{\partial t}\Big|_{r\ fixed} = \frac{\partial \overline{C}_s(q,t)}{\partial t}\Big|_{q\ fixed} + \Big(\dot{h}(t) - \dot{R}(t)\Big)\frac{\partial \overline{C}_s(q,t)}{\partial q},$$

$$\frac{\partial C_s(r,t)}{\partial r} = \frac{\partial \overline{C}_s(q,t)}{\partial q},$$

$$\frac{\partial}{\partial r}\Big(r^2\frac{\partial C_s(r,t)}{\partial r}\Big) = \frac{\partial}{\partial q}\Big(\Big[q + R(t) - h(t)\Big]^2\frac{\partial \overline{C}_s(q,t)}{\partial q}\Big).$$

The equations of the surfactant transport problem can now be written as:

$$\frac{\partial \Gamma(t)}{\partial t} + \Gamma(t)\left(\frac{2R(t)^2}{(q+R(t)-h(t))^3}\frac{dR(t)}{dt}\Big|_{q=0}\right) = D_s \frac{\partial \overline{C}_s(q,t)}{\partial q}\Big|_{q=0}, \tag{B.2}$$

$$\begin{aligned}\frac{\partial \overline{C}_s(q,t)}{\partial t} - \Big(\dot{R}(t)-\dot{h}(t)\Big)\frac{\partial \overline{C}_s(q,t)}{\partial q} + \frac{R(t)^2}{(q+R(t)-h(t))^2}\frac{dR(t)}{dt}\frac{\partial \overline{C}_s(q,t)}{\partial q} \\ = \frac{D_s}{(q+R(t)-h(t))^2}\frac{\partial}{\partial q}\Big(\Big[q+R(t)-h(t)\Big]^2\frac{\partial \overline{C}_s(q,t)}{\partial q}\Big),\end{aligned} \tag{B.3}$$

$$D_s \frac{\partial \overline{C}_s(q,t)}{\partial q}\Big|_{q=0} = k_a \overline{C}_s(0,t)(\overline{\Gamma}-\Gamma(t)) - k_d\Gamma(t), \tag{B.4}$$

$$\frac{\partial \overline{C}_s(q,t)}{\partial q}\Big|_{q=h(t)} = 0. \tag{B.5}$$

This mapping is useful because it allows the presentation of surfactant bulk concentrations in the hypophase with the hypophase-gas interfaces superposed over each other ($q = 0$) over the course of respiration.

Next, we recast the surfactant transport problem in terms of a Lagrangian coordinate η. Unlike r and q, the new coordinate η ranges between two fixed values. It is defined below:

$$\eta = \frac{r^3 - b(t)^3}{3\hat{V}_0^{2/3}} = \frac{(q+b(t))^3 - b(t)^3}{3\hat{V}_0^{2/3}}, \tag{B.6}$$

where $b(t) = R(t) - h(t)$ and $\hat{V}_0 = R_0^3 - (R_0 - h_0)^3$.

$$\left\{ \begin{array}{cc} At\ r = R(t) - h(t) & \eta = 0 \\ At\ r = R(t) & \eta = \frac{1}{3}\hat{V}_0^{1/3} \end{array} \right\}.$$

Using the variable η, and the fact that the hypophase is an incompressible fluid with constant density (volume of hypophase is constant with time), we note the following relations:

$$\frac{\partial \overline{C}_s(q,t)}{\partial t}\Big|_{q\ fixed} = \frac{\partial \hat{C}_s(\eta,t)}{\partial t}\Big|_{\eta\ fixed} - \Big(\frac{R(t)^2}{(q+R(t)-h(t))^2}\frac{dR(t)}{dt} - (\dot{R}(t)-\dot{h}(t))\Big)\frac{\partial \overline{C}_s(q,t)}{\partial q},$$

$$\frac{\partial \overline{C}_s(q,t)}{\partial q} = \frac{(q+R(t)-h(t))^2}{\hat{V}_0^{2/3}}\frac{\partial \hat{C}_s(\eta,t)}{\partial \eta},$$

$$\frac{D_s}{(q+R(t)-h(t))^2}\frac{\partial}{\partial q}\Big(\Big[q+R(t)-h(t)\Big]^2\frac{\partial \overline{C}_s(q,t)}{\partial q}\Big)$$
$$=\frac{D_s}{\hat{V}_0^{4/3}}\frac{\partial}{\partial \eta}\left(\Big[3\eta\hat{V}_0^{2/3}+(R(t)-h(t))^3\Big]^{4/3}\frac{\partial \hat{C}_s(\eta,t)}{\partial \eta}\right).$$

The equations of the surfactant transport problem can now be written as:

$$\frac{\partial \Gamma(t)}{\partial t}+\Gamma(t)\left(\frac{2R(t)^2}{b(t)^3}\frac{dR(t)}{dt}\right)=\frac{D_s b(t)^2}{\hat{V}_0^{2/3}}\frac{\partial \hat{C}_s(\eta,t)}{\partial \eta}\Big|_{\eta=0}, \tag{B.7}$$

$$\frac{\partial \hat{C}_s(\eta,t)}{\partial t}=\frac{D_s}{\hat{V}_0^{4/3}}\frac{\partial}{\partial \eta}\left(\Big[3\eta\hat{V}_0^{2/3}+b(t)^3\Big]^{4/3}\frac{\partial \hat{C}_s(\eta,t)}{\partial \eta}\right), \tag{B.8}$$

$$\frac{D_s b(t)^2}{\hat{V}_0^{2/3}}\frac{\partial \hat{C}_s(\eta,t)}{\partial \eta}\Big|_{\eta=0}=k_a\hat{C}_s(0,t)(\overline{\Gamma}-\Gamma(t))-k_d\Gamma(t), \tag{B.9}$$

$$\frac{\partial \hat{C}_s(\eta,t)}{\partial \eta}\Big|_{\eta=\frac{1}{3}\hat{V}_0^{1/3}}=0. \tag{B.10}$$

This mapping leads to the elimination of the convective term in equation (3.24) as shown in equation (B.8) and a far more accurate computational method in the case of advection-dominated flow.

When analyzing surfactant bulk concentrations, either $C_s(r,t)$, $\overline{C}_s(q,t)$ or $\hat{C}_s(\eta,t)$ can be used.

Appendix C

Numerical Methods and Model Parameters

This appendix contains a short note on the numerical methods, and details on the different parameters used in the various parts of this dissertation. In many studied cases, the values of the parameters used were left out of the text, and included in this appendix. For the cases not shown in this appendix, all relevant information on parameter values can be found in text.

C.1 Numerical Methods

In chapter 2, the surfactant transport problem was solved using an implicit finite difference scheme (Backward Euler) on Matlab [136]. In the case of nonlinear terms such as the product of Γ and C_s in Langmuir kinetics (see equation (2.17) for example), a linearization procedure similar to the one presented in [130] was implemented.

In chapter 5, the surfactant transport problem was solved in the same way followed in chapter 2. The rest of the alveolar model equations were solved using an explicit finite difference scheme (Forward Euler) on Matlab.

C.2 Parameters of Chapter 2

In this section, we list the parameters used in chapter 2.

C.2.1 Parameters of subsection 2.2.1

The relevant parameters of subsection 2.2.1 are: $\omega = 1$ (rev/sec), $h_0 = 1$ (cm), and $C_{ref} = 1$ (g/cm^3). The initial surfactant concentration profile is uniform and equal to $C_s = 1$ (g/cm^3). The prescribed concentration at the subphase is given by $C_s(h_0, t) = 0.5\sin(t) + 1$ (g/cm^3).

In the case of slow diffusion, the diffusion coefficient $D_s = 0.001$ (cm^2/sec),and for fast diffusion $D_s = 10$ (cm^2/sec).

C.2.2 Parameters of subsection 2.2.3

In subsection 2.2.3, the adsorption and desorption coefficients and the maximum equilibrium surfactant concentration in a static system were all set to unity: $k_a = 1$ (cm^3/(g.sec)), $k_d = 1$ (1/sec), $\overline{\Gamma} = 1$ (g/cm^2). Also, $C_{ref} = 1$ (g/cm^3). In addition, the parameter used to normalize the time t is $T = 2\pi$.

C.2.3 Parameters of subsection 2.3.1

We list the parameter values used here: $\omega = 1$ (rev/sec), $\overline{\Gamma} = 1$ (g/cm^2) and $C_b = 1$ (g/cm^3). The variation in the area of the interface is given by $A(t) = -0.875\cos(t) + 2.125$ (cm^2). The parameter used to normalize the time t is $T = 2\pi$.

C.3 Parameters of Chapter 5

In this section, we list the parameters used in the various cases studied in chapter 5. We first present the parameters used in the base case studied in section 5.1. For all the other cases, most of the parameters are the same as those of the base case, but some are varied. We list the varied ones for each case. Before presenting the parameters, we show the input of the alveolar model used throughout the dissertation.

Pleural Pressure The pleural pressure is the input to the alveolar model. The shape of the measured physiological pleural pressure given in [137] is shown in figure C.1. We approximate the shape of the pleural pressure by a smooth sinusoidal curve also shown in figure C.1. This approximation has a very minor effect on results.

C.3.1 Parameters of section 5.1

Section 5.1 represented a base case of the results of the alveolar model. The values of the parameters used are tabulated in table C.1. For some of the parameters, we include more information in the text of this appendix.

$\overline{\gamma_O}$ and $\overline{\gamma_C}$

We assume that the values of $\overline{\gamma_O}$ and $\overline{\gamma_C}$ at the inlet of the alveolus are very close to those in air at room temperature.

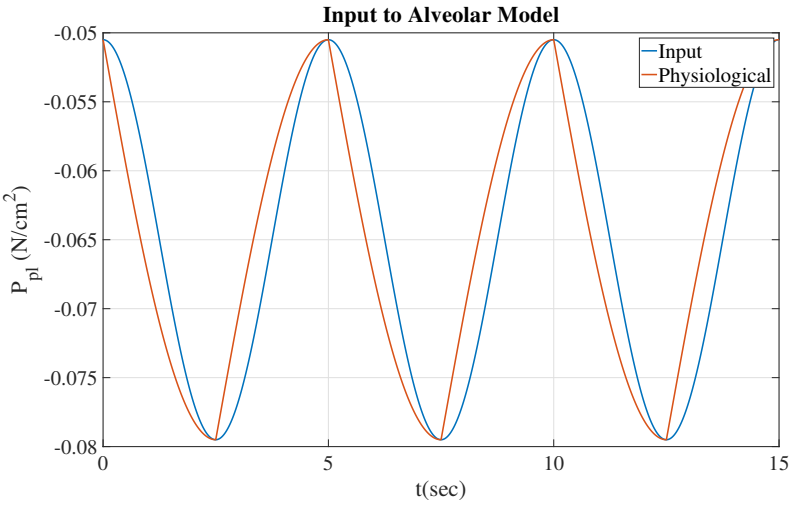

Figure C.1: Physiological pleural pressure is approximated by a simple sinusoidal curve.

Geometry

The alveolar geometry was obtained from an electron micrograph of the human lung (reader is referred to figure 13 in [9]). A single alveolus formed an ellipsoidal shell, with a major axis of $122 \pm 6.1\ \mu m$, a minor axis of $93 \pm 3.5\ \mu m$ and a wall thickness of $7\ \mu m$. The values of the alveolar radius and wall thickness were chosen to be of the same order of magnitude of those reported.

k_a and C_s

The values of k_a and C_s used in the base case were our personal choice. The surfactant bulk concentration profile was chosen to be uniform initially in all of chapter 5. The initial value of C_s was chosen to be of the same magnitude of those reported in [139]. The value of k_a was chosen to be less than those reported in the literature to show the effect of adsorption in a clearer way. Physiological values of both parameters were used in later parts of the dissertation.

ζ, D_{hO} and D_{hC}

The value of ζ is our personal choice. Values of D_{hO} and D_{hC} were chosen to be those of the diffusion coefficients of oxygen and carbon dioxide in a dilute aqueous solution respectively.

V_{bc}/τ

Instead of choosing separate values for V_{bc} and τ, we only choose values for the ratio $\frac{V_{bc}}{\tau}$. This is satisfactory because the two parameters only show up in the form of the mentioned ratio. Using the values available in literature, we find a range of acceptable values for this ratio. The blood flow speed in a capillary ranges between 0.1 and 10 mm/sec [140]. If we choose an average capillary with length of the same order of magnitude of the alveolar radius, say 0.1 mm, the range of the transit time τ is [0.01 - 1] (sec). The capillary volume of blood in the neighborhood of alveoli was reported to be 70 cm^3 in [112]. Because the number of alveoli can range between 274 and 790 million [12], we approximate the volume of blood in the neighborhood of one alveolus to be in the range $[70/(274 * 10^{-6})$ - $70/(790 * 10^{-6})]$ (cm^3). Using the lower and upper ends of the ranges of τ and V_{bc}, we find that the range of acceptable values of V_{bc}/τ is $[9 * 10^{-8}$ - $25 * 10^{-6}]$ (cm^3/sec).

Important Remark

For all the remaining results, the constitutive model given in section 3.5 was modified. Because the focus of this work is on surfactant dynamics and their effect on breathing, we decided to use a simple model for the alveolar wall. We chose to model it as a simple spring with a constitutive model given by:

$$\Sigma(t)e(t) = \Sigma_0 e_0 + S(R(t) - R_0), \tag{C.1}$$

where S is the stiffness, and Σ_0 is the value of $\Sigma(t)$ at R_0. The stiffness was chosen to be of the same order of magnitude of reported Young's modulus values [105]. Unless specified otherwise, $S = 0.1$ (N/cm^2), and $\Sigma_0 = 0.0012$ (N/cm^2). The value of Σ_0 was chosen to satisfy the mechanical equilibrium of the system.

The value of the ratio V_{bc}/τ was also modified from $9.5 * 10^{-7}$ to $3.6 * 10^{-7}$. All other parameters are the same as those given in table C.1 unless noted otherwise.

C.3.2 Parameters of subsection 5.2.1

To model the case of holding breath, only the pleural pressure was modified. It is shown in figure C.2.

C.3.3 Parameters of subsection 5.2.2

Only κ was changed from 0.9 to 0.0001 to suppress gas exchange between the alveolus and passing blood.

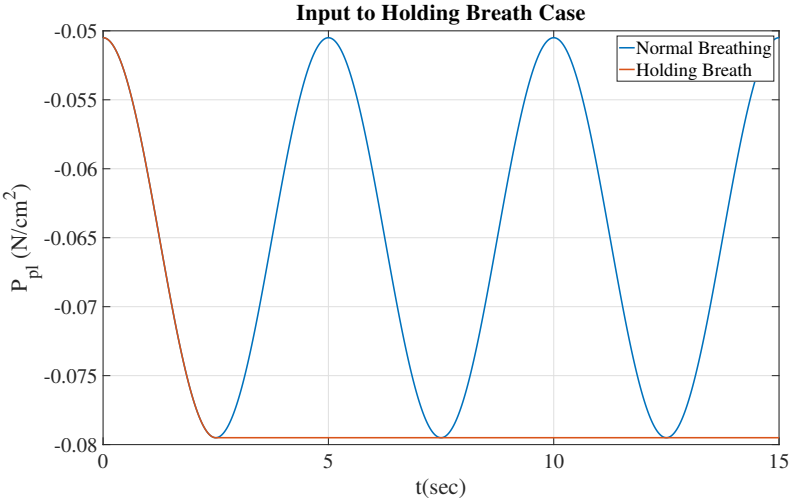

Figure C.2: Pleural pressure is kept constant at end of inhalation to model case of holding breath.

C.3.4 Parameters of subsection 5.2.3

For the case of breathing on the summit of mount Everest, P_{atm} was modified from 760 to 253 mmHg [126] and P_{bOi} was changed from 45 mmHg to 22 mmHg.

C.3.5 Parameters of subsection 5.2.4

In the case of no surfactants present in the hypophase, we set the value of σ to be constant at 70 (dyn/cm) at all times.

C.3.6 Parameters of subsection 5.3.1

In this section, only some surfactant properties were changed. Those are tabulated in table 5.1.

C.3.7 Parameters of subsection 5.3.2

In this section, only some surfactant properties were changed. Those are mentioned in subsection 5.3.2.

C.3.8 Parameters of subsection 5.3.3

In this case, ζ was chosen to be 0.1. Also, the stiffness S was modified to 0.2. κ was changed from 0.9 to 0.5, and the ratio V_{bc}/tau was chosen to be $3.39 * 10^{-7}$.

C.3.9 Parameters of section 5.5

In this section, all surfactant properties were modified. They are tabulated in tables 5.2 and 5.7. The initial surfactant concentration C_s was chosen to be 27 mg/cm^3 [139], and $\overline{\Gamma} = 3 * 10^{-7}$ (g/cm^2) [130]. Also, the initial stress was modified to $\Sigma_0 = 0.0312$(N/cm^2) to satisfy mechanical equilibrium initially for the case of CLS.

C.3.10 Parameters of section 5.6

In this section, the stiffness S of the alveolar wall was chosen to be $S = 0.051$ (N/cm^2). Surfactant A (SA) had the following properties:
$k_a = 90$ (ml/(g.sec)), $k_d = 7.5 * 10^{-4}$ (1/sec), $D_s = 1.6 * 10^{-8}$ (cm^2/sec), $\overline{\sigma} = 25$ (dyn/cm), $\overline{\Gamma} = 3 * 10^{-7}$ (g/cm^2), $\overline{\sigma}_{min} = 1$ (dyn/cm), $Y = 100$ (dyn/cm), $C_s = 0.0678$ (g/ml). Surfactant B (SB) had the same properties except for k_a and k_d:
$k_a = 30$ (ml/(g.sec)), $k_d = 2.5 * 10^{-4}$ (1/sec).

Base Case Parameter Values				
Parameter	Compartment	Value	Units	Source
Ω	Gas Mixture	See appendix A	N.sec/cm^5	See appendix A
$\overline{\gamma_O}$	Gas Mixture	0.2517	-	[138]; see text
$\overline{\gamma_C}$	Gas Mixture	0.000607	-	[138]; see text
$\overline{\gamma_N}$	Gas Mixture	0.7477	-	$1-\overline{\gamma_O}-\overline{\gamma_C}$
M_O	Gas Mixture	0.032	kg/mol	[138]
M_C	Gas Mixture	0.044	kg/mol	[138]
M_N	Gas Mixture	0.028	kg/mol	[138]
ρ_0	Gas Mixture	$1.0554 * 10^{-6}$	kg/cm^3	[138]
P_V	Gas Mixture	47	mmHg	[121]
P_{atm}	Gas Mixture	760	mmHg	[121]
R_0	Geometry	0.01	cm	See text
e_0	Geometry	10^{-3}	cm	See text
h_0	Geometry	5^{-5}	cm	[89]
μ_h	Hypophase	$6.92 * 10^{-8}$	N.sec/cm^2	[90]
D_s	Surfactant Transport	$1.6 * 10^{-8}$	cm^2/sec	[67]
C_s	Surfactant Transport	0.0678	g/ml	See text
k_a	Surfactant Transport	30	ml/(g.sec)	See text
k_d	Surfactant Transport	0.00025	1/sec	[67]
$\overline{\Gamma}$	Surfactant Transport	$3 * 10^{-7}$	g/cm^2	[130]
$\overline{\sigma}$	Surfactant Transport	25	dyn/cm	[22]
κ	Gas Exchange	0.9	-	[9]
ξ_O	Gas Exchange	$1.4 * 10^{-9}$	mol/(cm^3.mmHg)	[121]
ξ_C	Gas Exchange	$3.3 * 10^{-9}$	mol/(cm^3.mmHg)	[121]
ζ	Gas Exchange	1	-	See text
D_{wO}	Gas Exchange	$2.3 * 10^{-5}$	cm^2/sec	[107]
D_{wC}	Gas Exchange	$8.3 * 10^{-4}$	cm^2/sec	[107]
D_{hO}	Gas Exchange	$2.1 * 10^{-5}$	cm^2/sec	[116]; see text
D_{hC}	Gas Exchange	$1.92 * 10^{-5}$	cm^2/sec	[116]; see text
V_{bc}/τ	Blood Transport	$9.5 * 10^{-7}$	cm^3/sec	See text
P_{bOi}	Blood Transport	40	mmHg	[115]
P_{bCi}	Blood Transport	45	mmHg	[115]
C_{HB}	Blood Transport	$2.2 * 10^{-6}$	mol/cm^3	[113]
$P_{\frac{1}{2}bO}$	Blood Transport	26	mmHg	[113]
m	Blood Transport	2.5	-	[113]
$[H^+]$	Blood Transport	$10^{-10.4}$	mol/cm^3	[121]
K_1	Blood Transport	$0.12 * 10^{1.9}$	1/sec	[121]
K_{-1}	Blood Transport	$164 * 10^{7.9}$	cm^3/(mol.sec)	[121]

Table C.1: For each parameter, this table presents its corresponding compartment, value, unit and source.